ATLAS-CONF-2015-044
CMS-PAS-HIG-15-002

15th September 2015

Measurements of the Higgs boson production and decay rates and constraints on its couplings from a combined ATLAS and CMS analysis of the LHC pp collision data at $\sqrt{s}$ = 7 and 8 TeV

The ATLAS and CMS Collaborations

Abstract

Combined ATLAS and CMS measurements of the Higgs boson production and decay rates, as well as constraints on its couplings to vector bosons and fermions, are presented. The combination is based on the analysis of five production processes and of the $H \to ZZ, WW$, $\gamma\gamma, \tau\tau, bb$ and $\mu\mu$ decay modes. All results are reported assuming a value of 125.09 GeV for the Higgs boson mass, the result of the combined Higgs boson mass measurement by ATLAS and CMS. The analysis uses the LHC proton-proton collision datasets recorded by the ATLAS and CMS detectors in 2011 and 2012, corresponding to integrated luminosities per experiment of approximately 5 fb^{-1} at $\sqrt{s}$ = 7 TeV and 20 fb^{-1} at $\sqrt{s}$ = 8 TeV. The Higgs boson production and decay rates of the two experiments are combined within the context of two generic parameterisations: one based on ratios of cross sections and branching ratios and the other based on ratios of coupling modifiers, introduced within the context of a leading-order Higgs boson coupling framework. The combined signal yield relative to the Standard Model expectation is measured to be 1.09 ± 0.11 and the combination of the two experiments leads to observed significances of the VBF production process and of the $H \to \tau\tau$ decay at the level of 5.4σ and 5.5σ, respectively. Several interpretations of the results with more model-dependent parameterisations, derived from the generic ones, are also given. The data are consistent with the Standard Model predictions for all parameterisations considered.

Contents

1. Introduction

The elucidation of the mechanism of electroweak symmetry breaking has been one of the main goals driving the design of the ATLAS [1] and CMS [2] experiments at the CERN Large Hadron Collider (LHC). In the Standard Model (SM) of particle physics, this symmetry breaking is achieved through the introduction of a complex doublet scalar field [3–8]. This leads to the prediction of the existence of one physical neutral scalar particle, commonly known as the Higgs boson. Through Yukawa interactions, the Higgs scalar field can also account for fermion masses [9, 10]. While the SM does not predict the value of the Higgs boson mass, m_H, the production cross sections and decay branching ratios (BR) of the Higgs boson can be precisely calculated once the mass is known.

In 2012, the ATLAS and CMS Collaborations reported the observation of a new particle at a mass of approximately 125 GeV with Higgs boson-like properties [11, 12]. Subsequent publications from both experiments, summarised in Refs. [13–17], established that all measurements of the properties of the new particle, including its spin, parity, and coupling strengths to ordinary particles, are consistent with those expected for the SM Higgs boson within uncertainties. Recently ATLAS and CMS have published a combined measurement of the Higgs boson mass [18], using the $H \to \gamma\gamma$ and $H \to ZZ$ data from LHC Run 1, where Run 1 indicates the LHC data-taking period in 2011 and 2012 at pp centre-of-mass energies $\sqrt{s} = 7$ and 8 TeV. The combined mass is

$$m_H = 125.09 \pm 0.21(\text{stat.}) \pm 0.11(\text{syst.})\ \text{GeV}, \tag{1}$$

where the total uncertainty is still dominated by the statistical component. The Higgs boson mass is assumed to be $m_H = 125.09$ GeV in all analyses presented in this paper.

The results of the final ATLAS and CMS individual combinations based on the Run 1 data are reported in Refs. [13, 14]. This paper reports the first ATLAS and CMS combined measurements of the Higgs boson production and decay rates as well as constraints on its couplings to other SM particles. The main production modes studied are gluon fusion (ggF), vector boson fusion (VBF) and associated production with vector bosons (VH) or a pair of top quarks (ttH). The decay channels considered are decays to bosons, $H \to ZZ \to 4\ell$ (ZZ), $H \to WW \to \ell\nu\ell\nu$ (WW) and $H \to \gamma\gamma$ ($\gamma\gamma$), and to fermions, $H \to \tau\tau$ ($\tau\tau$), $H \to bb$ (bb) and $H \to \mu\mu$ ($\mu\mu$). Here and in the following, Z and W indicate both real and virtual vector bosons and ℓ refers to electrons and muons and their anti-particles.

All analyses entering the combination are based on the full Run 1 proton-proton collision data sets, corresponding to integrated luminosities per experiment of approximately 5 fb^{-1} at a centre-of-mass energy $\sqrt{s} = 7$ TeV (recorded in 2011) and 20 fb^{-1} at $\sqrt{s} = 8$ TeV (recorded in 2012) by the ATLAS and CMS detectors at the LHC.

In this paper, in the same way as for the combination results from the individual experiments, it is assumed that the studied particle is a single SM-like Higgs boson state, i.e. a CP-even scalar particle with the tensor structure of the SM interactions. The Higgs boson width, predicted to be approximately 4 MeV in the SM, is assumed to be small such that the narrow-width approximation is valid and that production and decay can be decomposed. These assumptions are corroborated by tests of spin and CP properties of the Higgs boson [16, 17] and by direct [14] and indirect (off-shell measurements [19, 20]) studies of its width. The Higgs boson signal modelling is based on the hypothesis of a SM Higgs boson in terms of its production and decay kinematics. Studies such as the measurements of differential production cross sections [21–24] support these assumptions, within the presently large statistical uncertainties. The inherent model dependence related to these hypotheses applies nevertheless to all results presented here;

it has a negligible effect for small deviations from the SM, but could be important for results substantially deviating from the SM predictions.

The results presented here for each experiment separately are expected to be slightly different with respect to those reported in Refs. [13, 14]. Some small variations in the results are due to evaluating them in the past at different values of the Higgs boson mass. Other differences are expected due to minor modifications to the signal parameterisation and to the handling of systematic uncertainties. These are introduced to implement a fully consistent and correlated treatment of the dominant signal theoretical uncertainties between the two experiments.

This paper is organised as follows. Section 2 briefly reviews the theoretical calculations of Higgs boson production and decay and the modelling of the Higgs boson signal in Monte Carlo (MC) simulation. The formalisms of signal strengths and coupling modifiers used for the interpretation of the data are also introduced in this section. Section 3 gives an overview of the analyses included in the combination, describes the statistical procedure used together with the treatment of systematic uncertainties, and summarises modifications to the individual analyses for the combination. Section 4 describes how the extracted signal can be parameterised in generic terms and reports the fit results for the combination of ATLAS and CMS and for each experiment using two generic parameterisations. In Section 5, the measured Higgs boson yields are compared with the SM predictions for different production processes and decay modes. In Section 6, the couplings of the Higgs boson are tested through fits to the observed data. These studies probe possible deviations from the SM predictions under various assumptions, motivated in many cases by beyond the SM (BSM) physics scenarios. Finally, a summary is presented in Section 7.

2. Higgs boson phenomenology and interpretation framework

This section briefly reviews Higgs boson phenomenology and introduces the most important aspects of the interpretation framework used to combine the measurements and to assess their compatibility with SM predictions. Specifically, the dominant production processes and major decay modes of the SM Higgs boson, along with the theoretical predictions for the cross sections and branching ratios are presented. The main features of MC generators used to simulate Higgs boson production and decay in each experiment are described. Finally, the formalisms of two widely used frameworks, based on signal strengths and coupling modifiers for the initial interpretation of the Higgs boson measurements at the LHC, are introduced.

2.1. Higgs boson production and decay

In the SM, Higgs boson production at the LHC mainly occurs through the following processes, listed in order of decreasing cross section at the Run 1 centre-of-mass energies:

- the gluon fusion process $gg \to H$ (ggF), as in Fig. 1a,
- the vector boson fusion process $qq \to qqH$ (VBF), as in Fig. 1b,
- associated production with a W boson, $qq, qg \to WH$ (WH), as in Fig. 2a,
- associated production with a Z boson, $pp \to ZH$ (ZH), which includes $gg \to ZH$ ($ggZH$), as in Figs. 2a, 2b and 2c,
- associated production with a pair of top quarks, $qq, gg \to ttH$ (ttH), as in Fig. 3.

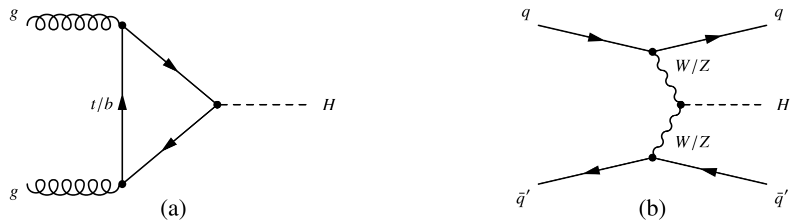

Figure 1: Leading-order Feynman diagrams for Higgs boson production via the (a) ggF and (b) VBF production processes.

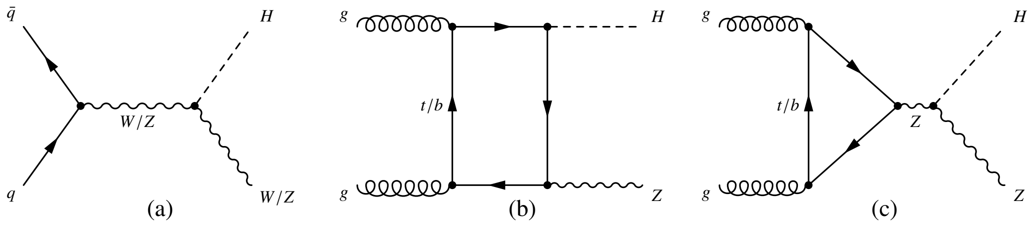

Figure 2: Leading-order Feynman diagrams of Higgs boson production via the (a) $q\bar{q} \to VH$ and (b,c) $gg \to ZH$ production processes.

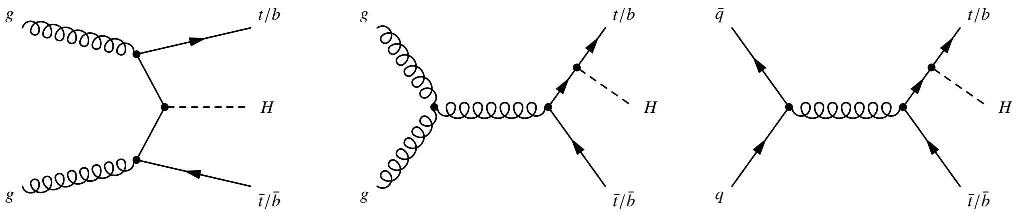

Figure 3: Leading-order Feynman diagrams of Higgs boson production via the $q\bar{q}/gg \to t\bar{t}H$ and $q\bar{q}/gg \to bbH$ processes.

The WH and ZH production processes are collectively referred to as the VH process. Other less important production processes in the SM that are not directly searched for, but are considered in the combination, are $qq, gg \to bbH$ (bbH), also shown in Fig. 3, and the production in association with a single top quark (tH) shown in Fig. 4. The latter proceeds through either the $qb \to tHq$ (tHq) (Figs. 4a and 4b) or $gb \to tHW$ (tHW) (Figs. 4c and 4d) process. The tH process is expected to have a negligible contribution in the SM but may become important in some BSM scenarios.

Leading-order Feynman diagrams of the Higgs boson decays considered in the combination are shown in Figs. 5 and 6. The decays to W and Z bosons (Fig. 5a) and to fermions (Fig. 5b) proceed through tree-level processes whereas the $H \to \gamma\gamma$ decay is mediated by W-boson or heavy quark loops (Fig. 6).

The theoretical calculations of the SM Higgs boson production cross sections and decay branching ratios have been reviewed and compiled by the LHC Higgs Cross Section Working Group in Refs. [25–27] and are summarised with their overall uncertainties in Tables 1 and 2 for a Higgs boson mass m_H = 125.09 GeV. The SM predictions of the branching ratios for $H \to gg$, cc and $Z\gamma$ are included for completeness. Though they are not explicitly searched for, they impact the combination through their contributions to the Higgs boson width and, at a small level, through their expected yield in certain categories.

Table 1: SM predictions for the Higgs boson production cross sections together with their theory uncertainties. The value of the Higgs boson mass is assumed to be $m_H = 125.09$ GeV and the predictions are obtained by linear interpolation from those at 125.0 and 125.1 GeV from Ref. [27] except for the tH cross section, which is obtained from Ref. [28]. The ZH cross section includes at NNLO(QCD) both the quark-initiated, i.e. $qq \to ZH$ or $qg \to ZH$, and the $gg \to ZH$ contributions. The contribution from the $ggZH$ production process, indicated in brackets, is given with a theoretical uncertainty assumed to be 30%. The uncertainties on the cross sections are evaluated as the quadratic sum of the uncertainties resulting from variations of QCD scales, parton distribution functions and α_s. The uncertainty on the tH cross section is calculated following the procedure of Ref. [29]. The order of the theory calculations for the different production processes is also indicated.

Production process	Cross section [pb] $\sqrt{s} = 7$ TeV	Cross section [pb] $\sqrt{s} = 8$ TeV	Order of calculation
ggF	15.0 ± 1.6	19.2 ± 2.0	NNLO(QCD)+NLO(EW)
VBF	1.22 ± 0.03	1.58 ± 0.04	NLO(QCD+EW)+~NNLO(QCD)
WH	0.577 ± 0.016	0.703 ± 0.018	NNLO(QCD)+NLO(EW)
ZH	0.334 ± 0.013	0.414 ± 0.016	NNLO(QCD)+NLO(EW)
$[ggZH]$	0.023 ± 0.007	0.032 ± 0.010	NLO(QCD)
bbH	0.156 ± 0.021	0.203 ± 0.028	5FS NNLO(QCD) + 4FS NLO(QCD)
ttH	0.086 ± 0.009	0.129 ± 0.014	NLO(QCD)
tH	0.012 ± 0.001	0.018 ± 0.001	NLO(QCD)
Total	17.4 ± 1.6	22.3 ± 2.0	

Table 2: SM predictions for the decay branching ratios of a Higgs boson with a mass of 125.09 GeV, together with their uncertainties. The predictions are obtained from Ref. [27]. Included are decay modes that are either directly studied or important for the combination due to their contributions to the Higgs boson width.

Decay channel	Branching ratio [%]
$H \to bb$	57.5 ± 1.9
$H \to WW$	21.6 ± 0.9
$H \to gg$	8.56 ± 0.86
$H \to \tau\tau$	6.30 ± 0.36
$H \to cc$	2.90 ± 0.35
$H \to ZZ$	2.67 ± 0.11
$H \to \gamma\gamma$	0.228 ± 0.011
$H \to Z\gamma$	0.155 ± 0.014
$H \to \mu\mu$	0.022 ± 0.001

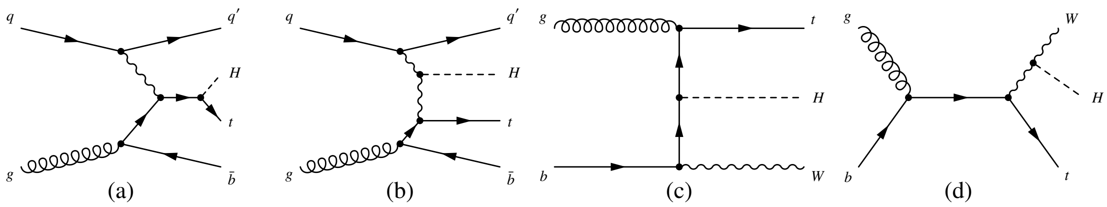

Figure 4: Leading-order Feynman diagrams of the Higgs boson production in association with a single top quark: (a,b) tHq and (c,d) tHW.

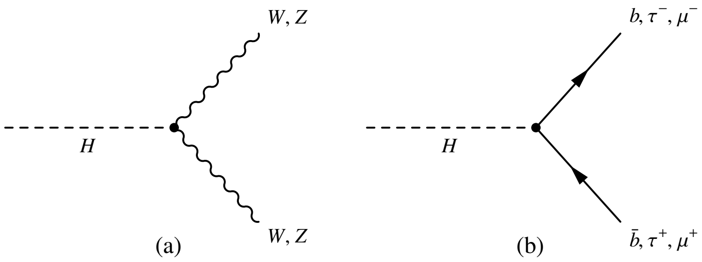

Figure 5: Leading-order Feynman diagrams of Higgs boson decays (a) to W and Z bosons and (b) to fermions.

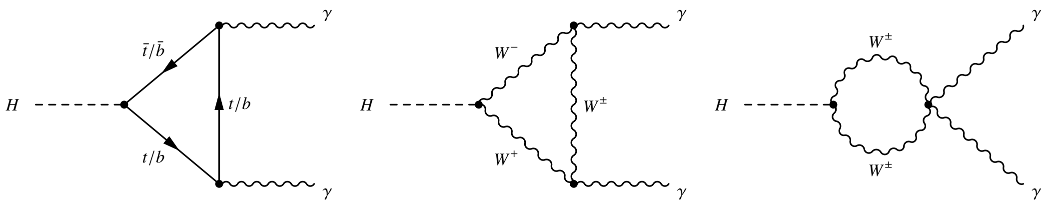

Figure 6: Leading-order Feynman diagrams of Higgs boson decays to a pair of photons.

2.2. Signal Monte Carlo simulation

All analyses use MC samples to model the Higgs boson production and decay kinematics, and to estimate acceptance and selection efficiency. Table 3 summarises the event generators used by ATLAS and CMS for the $\sqrt{s}$ = 8 TeV data analyses.

The main features of the signal simulation are recalled here; for more details, the reader is referred to the individual publications:

- for ggF and VBF both experiments use Powheg [30–34] for the event generation, interfaced either to Pythia8 [35] (ATLAS) or Pythia6.4 [36] (CMS) for the simulation of the parton shower, of the hadronisation, and of the underlying event, referred to in the following as UEPS (underlying event and parton shower).
- in the case of WH and ZH production, both experiments use leading-order (LO) event generators for all quark-initiated processes, namely Pythia8 in ATLAS and Pythia6.4 in CMS. A prominent exception is the more sensitive $H \to bb$ decay channel, for which ATLAS uses Powheg/Pythia8, while CMS uses Powheg/Herwig++ [37]. The $ggZH$ production process is also important to consider, even though it contributes only approximately 8% to the total ZH production cross

section in the SM. Owing to the harder expected p_T spectrum of the Higgs boson, this production process has a larger contribution for the most sensitive categories in the $H \to bb$ decay channel. Both experiments therefore include $ggZH$ production as a separate process in the VH analysis for the $H \to bb$ channel. ATLAS uses Powheg interfaced to Pythia8, while, in the case of CMS, given that the MC sample was not available at the time of the publication [38, 39], a reweighted $q\bar{q} \to ZH$ sample is used to model the $ggZH$ contribution, including next-to-leading order (NLO) effects [40–43]. For the other channels, the contribution from this process is only accounted for as a correction to the overall signal cross section.

- in the case of ttH production, ATLAS uses the NLO calculation of the HELAC-Oneloop package [44] interfaced to Powheg (this chain is often referred to as Powhel [45]), while CMS simulates this process with the LO Pythia6 program.

- within the SM, the contribution from tH production to analyses searching for ttH production is expected to be small, but in certain BSM scenarios it may become large through interference effects (see Section 2.4). For example for a negative value of the Higgs-top coupling with the same absolute strength as in the SM the tH total cross section becomes larger than that of the ttH process. The tH production processes are simulated in both experiments using MadGraph5_aMC@NLO interfaced to Herwig++ in the case of tHW production, while the tHq production process is simulated using MadGraph [46] interfaced to Pythia8 in ATLAS and MadGraph5_aMC@NLO [29] interfaced to Pythia6 in CMS.

- finally, bbH production contributes approximately 1% to the total Higgs boson cross section in the SM. It is simulated with Pythia, Pythia8 and MadGraph5_aMC@NLO for the categories most sensitive to this production process in the various channels. Given that the kinematic characteristics of bbH production are similar to those of the ggF process, the latter, after correcting approximately for the overall efficiency, is used to model the signal in all the other channels.

Table 3 summarises the choices of event generators for ATLAS and CMS. For the most precisely measured processes, namely ggF and VBF production for several decay channels, both experiments use the same event generator, interfaced, however, to different UEPS programs (Pythia8 for ATLAS and Pythia6.4 for CMS). For each process and decay, the cross section and branching ratio are normalised to the higher-order state-of-the-art theoretical calculations, namely the values given in Tables 1 and 2.

Furthermore, the transverse momentum (p_T) distribution of the Higgs boson for the ggF production process, that, in many cases, affects categorisation and selection efficiencies, is reweighted to match the calculation of HRes2.1 [47, 48], which includes next-to-next-to-leading-order (NNLO) perturbative QCD corrections and next-to-next-to-leading logarithmic (NNLL) QCD corrections. In addition, $gg \to H$ events with two or more jets are reweighted to match the transverse momentum distribution from Powheg MiNLO H+2-jet predictions [49]. This consistent treatment between the two experiments of the most prominent theoretical aspects of Higgs boson production and decay is quite important since all theoretical uncertainties in the various signal processes described in Table 3 are treated as correlated for the combination (see Section 3). The impact of using different generators for the less sensitive channels is negligible compared to their dominant sources of uncertainty.

Table 3: Summary of the event generators used to model the Higgs boson production processes and decay channels at $\sqrt{s}$ = 8 TeV in the ATLAS and CMS experiments.

Production process	Event generator ATLAS	Event generator CMS
ggF	POWHEG [30–34]	POWHEG
VBF	POWHEG	POWHEG
WH	PYTHIA8 [35]	PYTHIA6.4 [36]
ZH ($qq \to ZH$ or $qg \to ZH$)	PYTHIA8	PYTHIA6.4
$ggZH$ ($gg \to ZH$)	POWHEG	See text
ttH	POWHEL [44]	PYTHIA6.4
tHq ($qb \to tHq$)	MADGRAPH [46]	aMC@NLO [29]
tHW ($gb \to tHW$)	aMC@NLO	aMC@NLO
bbH	PYTHIA8	PYTHIA6, aMC@NLO

2.3. Signal strengths

The signal strength parameter μ, defined as the ratio between the measured Higgs boson rate and its SM expectation, has been extensively used to characterise the Higgs boson yields. However, the meaning of μ varies depending on the analysis. For a specific production and decay channel $i \to H \to f$, the signal strengths for the production, μ_i, and for the decay, μ^f, are defined as

$$\mu_i = \frac{\sigma_i}{(\sigma_i)_{\text{SM}}} \quad \text{and} \quad \mu^f = \frac{\text{BR}^f}{(\text{BR}^f)_{\text{SM}}}. \tag{2}$$

Here σ_i ($i = gg$F, VBF, WH, ZH, ttH) and BR^f ($f = ZZ, WW, \gamma\gamma, \tau\tau, bb$) are respectively the production cross section for $i \to H$ and the decay branching ratio for $H \to f$. The subscript "SM" refers to their respective SM predictions, so by definition, $\mu_i = 1$ and $\mu^f = 1$ in the SM. Since σ_i and BR^f cannot be separately measured without additional assumptions, only the product of μ_i and μ_f can be extracted experimentally, leading to a signal strength μ_i^f for the combined production and decay:

$$\mu_i^f = \frac{\sigma_i \cdot \text{BR}^f}{(\sigma_i)_{\text{SM}} \cdot (\text{BR}^f)_{\text{SM}}} = \mu_i \times \mu^f \tag{3}$$

The ATLAS and CMS data are combined and analysed using this signal strength formalism and the results are presented in Section 5. For all these signal strength fits, as well as for the generic parameterisation presented in Section 4.1, the parameterisations of the expected yields in each analysis category are done under the following assumptions: for the production processes, the bbH signal strength is assumed to be the same as for ggF, the tH signal strength is assumed to be the same as for ttH, and the $ggZH$ signal strength is assumed to be the same as for q-initiated ZH production; for the Higgs boson decays, the $H \to gg$ and $H \to cc$ signal strengths are assumed to be the same as for $H \to bb$ decays, and the $H \to Z\gamma$ signal strength is assumed to be the same as for $H \to \gamma\gamma$ decays. These assumptions are different from the ones made in the case of the fits using coupling modifiers described in Section 2.4.

2.4. Coupling modifiers

Based on a leading-order motivated framework [27] (κ-framework), coupling modifiers have been proposed to interpret the LHC data using specific modifications of the Higgs boson couplings related to new physics beyond the SM. Within the assumptions already mentioned in Section 1, the production and decay of the Higgs boson can be factorised, such that the cross section times BR of an individual channel $\sigma(i \to H \to f)$ contributing to a measured signal yield can be parameterised as:

$$\sigma_i \cdot \mathrm{BR}^f = \frac{\sigma_i(\vec{\kappa}) \cdot \Gamma^f(\vec{\kappa})}{\Gamma_\mathrm{H}}, \tag{4}$$

where Γ_H is the total width of the Higgs boson and Γ^f is the partial width of the Higgs boson decay to the final state f. A set of coupling modifiers, $\vec{\kappa}$, is introduced to parameterise potential deviations from the SM predictions of the Higgs boson couplings to SM bosons and fermions. For a given production process or decay mode denoted "j", a coupling modifier κ_j is defined such that:

$$\kappa_j^2 = \sigma_j/\sigma_j^{\mathrm{SM}} \quad \text{or} \quad \kappa_j^2 = \Gamma^j/\Gamma^j_{\mathrm{SM}}. \tag{5}$$

In the SM, all κ_j values are positive and equal to unity; here, by construction, the SM cross sections and branching ratios themselves include the best available higher-order QCD and EW corrections, as shown in Tables 1 and 2. This higher-order accuracy is not necessarily preserved for κ_j values different from unity, but the dominant higher-order QCD corrections factorise to a large extent from any rescaling of the coupling strengths and are therefore assumed to remain valid over the whole range of κ_j values considered in this paper. Individual coupling modifiers, corresponding to tree-level Higgs boson couplings to the different particles, are introduced, as well as effective coupling modifiers κ_g and κ_γ that describe ggF production and $H \to \gamma\gamma$ decay: this is possible because BSM particles which might be present in these loops are not expected to appreciably change the kinematics of the corresponding process. In contrast, the $gg \to ZH$ process, which occurs at leading order through box and triangular loop diagrams (see Figs. 2b and 2c) is not treated using an effective coupling modifier, because a tree-level $ggHZ$ contact interaction from new physics would likely show a kinematic structure very different from the SM and is expected to be highly suppressed [41, 50]. Any other possible BSM effects on the $gg \to ZH$ process are related to modifications of the HZZ and ttH interactions, which are best taken into account within the limitation of the framework, by resolving the loop in terms of the corresponding coupling modifiers, κ_Z and κ_t.

Different production processes and decay modes probe different coupling modifiers, as can be visualised from the Feynman diagrams in Section 2.1. Loop processes such as $gg \to H$ and $H \to \gamma\gamma$ can be studied through either the effective coupling modifiers, thereby providing sensitivity to potential BSM physics in the loops or the modifiers of the SM particles themselves. Interference contributions of different diagrams provide some sensitivity to relative signs between Higgs boson couplings to different particles. As discussed in Section 6.4, such effects are potentially largest for the $H \to \gamma\gamma$ decays, but could also be significant in the case of $ggZH$ and tH production. As an example, in the SM, the tH cross section is small, approximately 14% of the ttH cross section, because of the destructive interference between diagrams involving the couplings to the W boson and the top quark, as shown in Table 4, if one sets κ_t and κ_W to their SM value of unity. However, the interference becomes constructive for negative values of the product $\kappa_W \times \kappa_t$. In the specific case $\kappa_W \times \kappa_t = -1$, the tHW and tHq cross sections increase by a factor of 6 and 13, respectively, in which case the tH process becomes sensitive to the relative sign of the W-boson and top-quark couplings, despite its small SM cross section. As shown in Section 6.4, however, the sensitivity of the data presented here to most of these interference effects remains small.

Table 4: Higgs boson production cross sections σ_i, partial decay widths Γ^f and total decay width (in the absence of BSM decays) parameterised as a function of the κ coupling modifiers, including higher-order QCD and EW corrections to the inclusive cross sections, as described in Section 2.1. The numerical values are given for $\sqrt{s}$ = 8 TeV and m_H = 125.09 GeV (they are similar for $\sqrt{s}$ = 7 TeV). Contributions which are negligible or not relevant to the analyses presented in this paper are not shown.

Production	Loops	Interference	Multiplicative factor
$\sigma(ggF)$	✓	$b-t$	$\kappa_g^2 \sim 1.06 \cdot \kappa_t^2 + 0.01 \cdot \kappa_b^2 - 0.07 \cdot \kappa_t\kappa_b$
$\sigma(VBF)$	–	–	$\sim 0.74 \cdot \kappa_W^2 + 0.26 \cdot \kappa_Z^2$
$\sigma(WH)$	–	–	$\sim \kappa_W^2$
$\sigma(qq/qg \to ZH)$	–	–	$\sim \kappa_Z^2$
$\sigma(gg \to ZH)$	✓	$Z-t$	$\sim 2.27 \cdot \kappa_Z^2 + 0.37 \cdot \kappa_t^2 - 1.64 \cdot \kappa_Z\kappa_t$
$\sigma(ttH)$	–	–	$\sim \kappa_t^2$
$\sigma(gb \to WtH)$	–	$W-t$	$\sim 1.84 \cdot \kappa_t^2 + 1.57 \cdot \kappa_W^2 - 2.41 \cdot \kappa_t\kappa_W$
$\sigma(qb \to tHq)$	–	$W-t$	$\sim 3.4 \cdot \kappa_t^2 + 3.56 \cdot \kappa_W^2 - 5.96 \cdot \kappa_t\kappa_W$
$\sigma(bbH)$	–	–	$\sim \kappa_b^2$
Partial decay width			
Γ^{ZZ}	–	–	$\sim \kappa_Z^2$
Γ^{WW}	–	–	$\sim \kappa_W^2$
$\Gamma^{\gamma\gamma}$	✓	$W-t$	$\kappa_\gamma^2 \sim 1.59 \cdot \kappa_W^2 + 0.07 \cdot \kappa_t^2 - 0.66 \cdot \kappa_W\kappa_t$
$\Gamma^{\tau\tau}$	–	–	$\sim \kappa_\tau^2$
Γ^{bb}	–	–	$\sim \kappa_b^2$
$\Gamma^{\mu\mu}$	–	–	$\sim \kappa_\mu^2$
Total width for $\mathrm{BR_{BSM}} = 0$			
Γ_H	✓	–	$\kappa_H^2 \sim 0.57 \cdot \kappa_b^2 + 0.22 \cdot \kappa_W^2 + 0.09 \cdot \kappa_g^2 + 0.06 \cdot \kappa_\tau^2 + 0.03 \cdot \kappa_Z^2 + 0.03 \cdot \kappa_c^2 + 0.0023 \cdot \kappa_\gamma^2 + 0.0016 \cdot \kappa_{Z\gamma}^2 + 0.0001 \cdot \kappa_s^2 + 0.00022 \cdot \kappa_\mu^2$

Changes in the couplings will result in a variation of the Higgs boson width. A new modifier, κ_H, defined as $\kappa_H^2 = \sum_j \mathrm{BR}^j_{\mathrm{SM}}\kappa_j^2$, is introduced to characterise this variation. In case the only allowed decay channels of the Higgs boson are the same as in the SM, the relation $\kappa_H^2 = \Gamma_H/\Gamma_H^{\mathrm{SM}}$ holds. If instead BSM modifications of the decays are introduced, the width Γ_H can then be expressed as:

$$\Gamma_H = \frac{\kappa_H^2 \cdot \Gamma_H^{\mathrm{SM}}}{1 - \mathrm{BR_{BSM}}}, \tag{6}$$

where $\mathrm{BR_{BSM}}$ indicates the total branching ratio into BSM decays. Such BSM decays can be of three types: invisible decays into BSM particles, decays into BSM particles which are not detected as such, or modifications of the decays into SM particles in the case of channels that are not directly measured, for example $H \to cc$. Though direct and indirect experimental constraints on the Higgs boson width exist, they are either model-dependent or do not have enough precision to constrain the present fits and they are therefore not included in the combinations. Since Γ_H is not experimentally constrained in a model-independent way with sufficient precision at the LHC, only ratios of coupling strengths can be measured in the most generic model considered in the κ-framework.

In the SM, it is possible to derive the relation between the coupling modifiers, the production cross sections σ_i, and partial decay widths Γ^f. The approximate expressions are indicated in Table 4. In the context of this parameterisation, it is natural to vary the partial width Γ^g as κ_g. The current LHC data are insensitive to the coupling modifiers κ_c and κ_s, and have limited sensitivity to κ_μ. Thus, it is assumed that κ_c varies as κ_t, κ_s as κ_b, and κ_μ as κ_τ in the following. Other coupling modifiers (κ_u, κ_d and κ_e) are irrelevant for the combination as long as they are order of unity. These assumptions are not the same as the ones described for the signal strength framework (see Section 2.3), so the two parameterisations are only approximately equivalent. Given that the experimental observables are not sensitive to the absolute sign of the couplings, but only to the relative sign between different couplings through interference, the convention $\kappa_t > 0$ has been adopted in the following (except in the specific case of Section 6.4) without any loss of generality.

3. Combination procedure and experimental inputs

Individual analyses from ATLAS and CMS of the Higgs boson production and decay rates are combined using the method described in Section 3.2, based on a profile likelihood estimator. The combination performs simultaneous fits to the data from both experiments taking into account the correlations between systematic uncertainties within each experiment and between the two experiments. The analyses included in the combination, the statistical procedure used, the treatment of systematic uncertainties, and the changes made to the analyses for the combination are summarised in this section.

3.1. Overview of input analyses

Individual analyses included in the combination have been published separately by each experiment. Most of these analyses are performed according to a specific Higgs boson decay mode. They are $H \to \gamma\gamma$ [51, 52], $H \to ZZ$ [53, 54], $H \to WW$ [55–57], $H \to bb$ [38, 39], $H \to \tau\tau$ [58, 59] and $H \to \mu\mu$ [60, 61]. The ttH production has also been studied separately [28, 62–65] and the results are included in the combination. The $H \to \mu\mu$ analysis is only included in the combination fit for the specific parameterisation of the coupling analysis presented in Section 6.2. It provides a measurement of the coupling of the Higgs boson to a low-mass particle, but offers no relevant constraints for other parameterisations. The ATLAS [13] and CMS [14] individual combined publications take into account other results, such as upper limits on the $H \to Z\gamma$ decay [66, 67], constraints on the off-shell Higgs boson production [19, 20] and upper limits on invisible Higgs boson decays [68–70]. These results were not included in the individual combination for both experiments and are not considered further here.

Almost all input analyses are based on the concept of categorisation. For each decay mode, events are classified in different categories, based on their kinematic characteristics and their detailed properties. This categorisation increases the sensitivity of the analysis but also allows separation of the different production modes by exploiting exclusive selections which identify the decay products of the particles produced in association with the Higgs boson: W or Z boson decays, VBF jets and so on. Exclusive categories addressing the main production modes are defined for all processes with the exception of $H \to bb$ for which only the VH and ttH production modes are combined here. The ggF production is not used because of the overwhelming QCD background while the VBF mode has low sensitivity and is not included in this combination, although CMS recently published their first result in this specific channel [71].

The signal yield in a category k, $n_{\text{signal}}(k)$, can be expressed as a sum over all possible Higgs boson production processes i, with cross section σ_i, and decay channels f, with branching ratio BR^f:

$$\begin{aligned} n_{\text{signal}}(k) &= \mathcal{L}(k) \times \sum_i \sum_f \left\{\sigma_i \times A_i^f(k) \times \varepsilon_i^f(k) \times \text{BR}^f\right\}, \\ &= \mathcal{L}(k) \times \sum_i \sum_f \mu_i \mu^f \left\{\sigma_i^{\text{SM}} \times A_i^f(k) \times \varepsilon_i^f(k) \times \text{BR}_{\text{SM}}^f\right\} \end{aligned} \tag{7}$$

where $\mathcal{L}(k)$ represents the integrated luminosity, $A_i^f(k)$ the detector acceptance, and $\varepsilon_i^f(k)$ the overall selection and analysis efficiency for the signal category k. The symbols μ_i and μ^f are the production and decay signal strengths defined in Section 2.3, respectively. As Eq. 7 shows, the measurements considered in this paper are only sensitive to the products of the cross sections and branching ratios, $\sigma_i \times \text{BR}^f$. Additional information or assumptions are needed to determine the cross sections and branching ratios separately.

In the ideal case, each category would only select signal events from a given production process and decay channel. Most decay channels approach this ideal case, but, in the case of the production processes, the categories are much less pure and there is important cross-contamination in most channels.

3.2. Statistical treatment

The overall statistics methodology used in the combination to extract the parameters of interest in various parameterisations is that adopted also for the individual ATLAS and CMS combinations, as published in Refs. [13, 14]. It has been developed by the ATLAS and CMS Collaborations in the context of the LHC Higgs Combination Group and is described in Ref. [72]. Some details of this procedure are important for this combination and are briefly reviewed here.

The statistical treatment of the data is based on the standard LHC data modelling and handling toolkits, RooFit [73], RooStats [74] and HistFactory [75]. The parameters of interest $\vec{\alpha}$, e.g. signal strengths (μ), coupling modifiers (κ), production cross sections, branching ratios or ratios of the above quantities, are estimated with their corresponding confidence intervals via the profile likelihood ratio test statistic $\Lambda(\vec{\alpha})$ [76]. The latter depends on one or more parameters of interest, as well as on the nuisance parameters $\vec{\theta}$, which reflect various experimental or theoretical uncertainties.

$$\Lambda(\vec{\alpha}) = \frac{L(\vec{\alpha}, \hat{\hat{\vec{\theta}}}(\vec{\alpha}))}{L(\hat{\vec{\alpha}}, \hat{\vec{\theta}})} \tag{8}$$

The likelihood functions in the numerator and denominator of this equation are built using products of signal and background probability density functions (pdfs) in the discriminating variables. The pdfs are derived from simulation for the signal and from both data and simulation for the background, as described in Refs. [13, 14]. The vectors $\hat{\vec{\alpha}}$ and $\hat{\vec{\theta}}$ denote the unconditional maximum likelihood estimates of the parameter values, and $\hat{\hat{\vec{\theta}}}$ denotes the conditional maximum likelihood estimate for given fixed values of the parameters of interest $\vec{\alpha}$. Systematic uncertainties and their correlations are modelled by introducing nuisance parameters $\vec{\theta}$ described by likelihood functions associated with the estimate of the corresponding parameter. The choice of the parameters of interest depends on the parameterisation under consideration, with the remaining parameters treated as nuisance parameters. The profile likelihood ratios are defined accordingly.

For example, the parameterisation considered in Section 6.4 assumes that all fermion couplings are scaled by κ_F and all vector couplings are scaled by κ_V. The likelihood ratio is therefore a function of the two parameters of interest κ_F and κ_V:

$$\Lambda(\kappa_F, \kappa_V) = \frac{L(\kappa_F, \kappa_V, \hat{\hat{\vec{\theta}}}(\kappa_F, \kappa_V))}{L(\hat{\kappa}_F, \hat{\kappa}_V, \hat{\vec{\theta}})} \,. \tag{9}$$

Likelihood fits are carried out for the parameters of interest using the data or Asimov data sets for determining observed or expected results. An Asimov data set [76] is a pseudo-data distribution that is equal to the signal plus background expectation for given values of the parameters of interest and of all nuisance parameters and does not include statistical fluctuations. It is a representative dataset of a given parameterisation that yields a measurement that corresponds to the median of an ensemble of toys thrown from the same parameterisation. Two types of Asimov datasets can be constructed: pre-fit and post-fit. A pre-fit Asimov is meant to represent the expectations from the theory and all parameters are fixed to their best estimates without constraints from the fit to the data. A post-fit Asimov is representative of a given parameterisation with all nuisance parameters set to their unconditional maximum likelihood estimates. The best-fit results on a post-fit Asimov dataset are expected to give the same central values as those from the fit to the data, if the parameterisations used to generate the dataset and to fit it are the same. These fits are rather challenging, involving many parameters of interest and a very large number of nuisance parameters. All the fit results have been independently cross-checked at a very high level of precision by the two experiments, both for the combination and for the individual ones. In particular, fine likelihood scans of all the parameters of interest have been visually inspected to verify the convergence and stability of the fits.

For all results presented in this paper, the negative log-likelihood estimator $q(\vec{\alpha}) = -2\ln\Lambda(\vec{\alpha})$ is assumed to follow a χ^2 distribution (asymptotic approximation). The 68% (95%) confidence level (CL) intervals are defined by requiring that $q(\alpha_i) = 1.00$ (3.84), in the case of one-dimensional (1D) scans, and $q(\alpha_i) = 2.30$ (5.99), in the case of two-dimensional (2D) scans. For the derivation of the upper limit of $\mathrm{BR}_{\mathrm{BSM}}$ in section 6.1 the test statistic $\tilde{t}(\alpha)$ of Ref. [76] was used to account for the constraint $\alpha = \mathrm{BR}_{\mathrm{BSM}} \geq 0$. This is equivalent to the confidence intervals estimation according to Ref. [77]. The upper limit corresponds to $\tilde{t}(\alpha) = 3.84$. The p-values characterising the compatibility of a fit result with a given hypothesis are also computed in the asymptotic approximation. Table 20 in Appendix D summarises the observed p-values with respect to the predictions for the SM Higgs boson of all the fit results presented in this paper, while Table 12 in Section 5.2 reports the observed and expected significances for a number of production processes and decay channels with respect to the expectations in the absence of a SM Higgs boson.

3.3. Treatment of systematic uncertainties

The treatment of the systematic uncertainties is a crucial aspect of the combination of Higgs boson couplings. The details of the chosen methodology for treating systematic uncertainties, characterised by nuisance parameters are given in Ref. [72]. The combined ATLAS and CMS analysis incorporates approximately 4200 nuisance parameters. Most of these are statistical in nature, i.e. related to the finite size of the MC samples used to model the expected signals and backgrounds, but are treated as systematic uncertainties, as described below.

Nuisance parameters can be associated to one single analysis category or can be correlated between categories, channels and/or experiments. A very important and delicate part of this combination is the estimation of the correlations between the various sources of systematic uncertainty between the various channels and the two experiments. The correlations within each experiment are modelled following the procedure adopted for the individual combinations. The most important systematic uncertainties which are correlated between the two experiments are the signal theory systematic uncertainties, followed by certain background theory systematic uncertainties and finally by the experimental uncertainty related to the measurement of the integrated luminosity.

The main theoretical sources of uncertainties on the signal are the following: QCD scales, parton distribution functions (PDF), UEPS, and Higgs boson branching ratios. These uncertainties apply both to the inclusive cross sections and to the acceptance and selection efficiency in the various categories. The PDF uncertainties on the inclusive rates for different Higgs boson production processes are correlated between the two experiments for the same channel but are treated as uncorrelated between different channels, except in two cases:

- the WH and ZH production processes are assumed to be fully correlated;
- the ggF and ttH production processes, which are predicted to be anti-correlated at the level of 60%, are assumed to be fully anti-correlated.

A cross-check with the full correlation matrix, as given in Ref. [27], shows no differences larger than 1% for the generic models discussed in Section 4. Similarly, QCD scale and UEPS uncertainties are correlated between the two experiments in the same production channels and are treated as uncorrelated between different channels. The effects of correlations between Higgs boson branching ratios and partial decay widths have been determined to be negligible in general, and are ignored in the fits, except for the branching ratios to WW and ZZ which are treated as fully correlated. However, there are cases when measuring ratios, where such uncertainties become the dominant theory uncertainties, and in these cases (the measurements of ratios of branching ratios described in Section 4.2), the full BR correlation model specified in Ref. [27] has been applied. Other theory uncertainties on signal acceptance and selection efficiencies are also usually small. They are estimated and treated in very different ways by the two experiments and therefore are treated as uncorrelated between ATLAS and CMS.

Whereas the signal selection criteria are quite inclusive in most channels, this is not the case for the backgrounds which are often restricted to very limited regions of phase-space and often different between the two experiments. For these reasons, the ATLAS and CMS background modelling uncertainties cannot be easily correlated, even though this would seem natural in several channels where they represent significant contributions to the overall systematic uncertainty on the result. Obvious examples are those where the background estimates are entirely obtained from simulation, as is the case for the ZZ continuum background to the $H \to ZZ$ channel and for the ttW and ttZ backgrounds to the ttH multi-lepton channel. For these two cases, the background cross section uncertainties are treated as correlated between the two experiments. Other more complex examples are the WW continuum background to the $H \to WW$ channel, the $ttbb$ background to the ttH, $H \to bb$ channel, and the Wbb background to the WH, $H \to bb$ channel. In these cases, care has been taken to verify that the choice of not correlating the background modelling uncertainties between the two experiments has only a small impact on the measurements. The most significant impact has been found for the $ttbb$ background to the $ttH, H \to bb$ channel, for which the choice of different correlation models between the two experiments yields an impact on the signal strength measurement below 10% of the total uncertainty in this specific channel.

Finally, all experimental systematic uncertainties are treated independently between the two experiments, reflecting independent assessments of these uncertainties, except for the integrated luminosity uncertainties which are treated as partially correlated through the sub-dominant contribution arising from the knowledge of the beam currents in the LHC accelerator.

As already mentioned in Section 1, the Higgs boson mass is fixed and assumed to be the result of the combination of the ATLAS and CMS measurements [18], namely $m_H = 125.09$ GeV.

The various sources of uncertainties (statistical or systematic) or nuisance parameters which are floated in the fits can be broadly classified in four groups:

1. uncertainties (labelled as "stat" in the following), which are statistical in nature (except for the case of the finite size of MC simulation samples). These include in particular the statistical uncertainties on certain background control regions and certain fit parameters used to parameterise backgrounds measured from data;
2. theory uncertainties affecting the Higgs boson signal (labelled as "thsig" in the following);
3. theory uncertainties affecting background processes only (these are not correlated with any of the signal theory uncertainties and are labelled as "thbgd" in the following);
4. all other uncertainties (labelled as "expt" in the following), which include the experimental uncertainties and those related to the finite size of the MC simulation samples.

Some of the results are provided with a full breakdown of the uncertainties into these four categories. In most cases, the uncertainties are only split into their statistical and systematic (syst) components. In some cases, especially when considering ratios of cross sections or of coupling strengths, as in Section 4, the theory systematic uncertainties become very small, as signal normalisation uncertainties that are in general dominant, do not affect the measurements. In such cases, it should be noted that the precision with which these uncertainties can be quoted is typically of O(0.01) relative to the SM prediction.

3.4. Analysis modifications for the combination

There are some differences between the treatment of the data in the combined analysis and that in the published analyses from each experiment. The differences are larger for CMS than for ATLAS, mainly because the CMS analyses were published earlier, before the prescriptions for the interpretation of the data in terms of a Higgs boson signal had been refined. The main differences are the following:

- ATLAS now uses the Stewart-Tackmann prescription [78] for the jet bin uncertainties for the $H \to WW$ channel instead of the jet-veto-efficiency prescription of Ref. [79, 80];
- CMS now includes the bbH, tH and $ggZH$ production processes in the signal model for the channels for which they are relevant;
- CMS now adopts the signal cross-section calculations from Ref. [27] for all channels (in earlier analyses, less up-to-date prescriptions had been applied);

Table 5: Overview of the decay and production channels analysed in this paper. To show the relative importance of the various channels, the results from the combined analysis presented in this paper for m_H = 125.09 GeV (see Tables 10 and 11 in Section 5.2) are shown as observed signal strengths μ with their uncertainties (the expected uncertainties are shown in parentheses). Also shown are the observed statistical significances (the expected significances are shown in parentheses) except for the $H \to \mu\mu$ channel which has very low sensitivity. For most decay channels, only the most sensitive analyses are quoted as references, e.g. the ggF and VBF analyses for the $H \to WW$ decay channel or the VH analysis for the $H \to bb$ decay channel. The results are nevertheless close to those from the individual publications, in which, in addition, slightly different values for the Higgs boson mass were assumed and in which the signal modelling and signal uncertainties were slightly different, as discussed in the text.

Channel	References for individual publications		Signal strength [μ] from results in this paper (Section 5.2)		Signal significance [σ]	
	ATLAS	CMS	ATLAS	CMS	ATLAS	CMS
$H \to \gamma\gamma$	[51]	[52]	$1.15^{+0.27}_{-0.25}$	$1.12^{+0.25}_{-0.23}$	5.0	5.6
			$\left(^{+0.26}_{-0.24}\right)$	$\left(^{+0.24}_{-0.22}\right)$	(4.6)	(5.1)
$H \to ZZ \to 4\ell$	[53]	[54]	$1.51^{+0.39}_{-0.34}$	$1.05^{+0.32}_{-0.27}$	6.6	7.0
			$\left(^{+0.33}_{-0.27}\right)$	$\left(^{+0.31}_{-0.26}\right)$	(5.5)	(6.8)
$H \to WW$	[55, 56]	[57]	$1.23^{+0.23}_{-0.21}$	$0.91^{+0.24}_{-0.21}$	6.8	4.8
			$\left(^{+0.21}_{-0.20}\right)$	$\left(^{+0.23}_{-0.20}\right)$	(5.8)	(5.6)
$H \to \tau\tau$	[58]	[59]	$1.41^{+0.40}_{-0.35}$	$0.89^{+0.31}_{-0.28}$	4.4	3.4
			$\left(^{+0.37}_{-0.33}\right)$	$\left(^{+0.31}_{-0.29}\right)$	(3.3)	(3.7)
$H \to bb$	[38]	[39]	$0.62^{+0.37}_{-0.36}$	$0.81^{+0.45}_{-0.42}$	1.7	2.0
			$\left(^{+0.39}_{-0.37}\right)$	$\left(^{+0.45}_{-0.43}\right)$	(2.7)	(2.5)
$H \to \mu\mu$	[60]	[61]	-0.7 ± 3.6	0.8 ± 3.5		
			(± 3.6)	(± 3.5)		
ttH production	[28, 62, 63]	[65]	$1.9^{+0.8}_{-0.7}$	$2.9^{+1.0}_{-0.9}$	2.7	3.6
			$\left(^{+0.72}_{-0.66}\right)$	$\left(^{+0.88}_{-0.80}\right)$	(1.6)	(1.3)

- CMS now adopts a unified prescription for the treatment of the Higgs boson p_{T}, as described in Section 2.2;
- The cross sections for the dominant backgrounds have been adjusted to the same values in the cases where they are estimated from simulation (ZZ background for the $H \to ZZ$ channel and ttZ and ttW backgrounds for the ttH channels);
- Both experiments have adopted the same correlation scheme for some of the signal theory uncertainties: for example, the treatment of the PDF uncertainties on the signal production cross sections now follows a common scheme for all decay channels, as described in Section 3.3.

The total effect of these modifications is small, both on the expected and on the observed results. All measurements differ from the individual combined results by less than approximately 10% of the total uncertainty for CMS and by even less for ATLAS.

Table 5 gives an overview of the Higgs boson decay and production channels which are considered in the following. To provide a snapshot of the relative importance of the various channels, the results from the analysis presented in this paper (see Tables 10 and 11 in Section 5.2) are shown as measurements, separately for each experiment, of the overall signal-strength parameters μ for each of the six decay channels, and for the ttH production channel. The total observed and expected statistical significances for $m_H = 125.09$ GeV are also shown except for the $H \to \mu\mu$ channel which has very low sensitivity. These results are quite close to those published by the individual analyses in each experiment, which are quoted as references in the table. For several decay channels, these refer only to the most sensitive analyses, e.g. the VH analysis for the $H \to bb$ decay channel. Even though less sensitive, the ttH analyses have an impact on all the decay channels, and this is the main reason for quoting this production process specifically in this table. As stated above, the differences between the analysis in this paper and the published ones are also due in part to the different values assumed at the time for the Higgs boson mass and to the adjustments done to the various analyses, mostly in terms of signal modelling and of the treatment of signal theory uncertainties.

4. Generic parameterisations of experimental results

This section describes two generic parameterisations using ratios and presents their results. The first is based on ratios of cross sections and branching ratios, as described below. In this parameterisation, the dominant signal theoretical uncertainties on the inclusive cross sections for the various production processes do not affect the measured observables, in contrast to any measurements involving the μ parameters, as described in Section 2.3. This analysis leads to the most model-independent results presented in this paper and tests the compatibility of the measurements with the SM under minimal assumptions. The second parameterisation is derived from the one described in Section 2.4 and is based on ratios of coupling modifiers. Both of these parameterisations do not make assumptions on the Higgs boson total width, which can freely vary, provided the narrow width approximation is still valid. Furthermore, many theoretical and experimental systematic uncertainties cancel in these ratios.

Table 6: Parameters of interest in the two generic parameterisations described in Sections 4.1 and 4.2. For both parameterisations, the $gg \to H \to ZZ$ channel is chosen as a reference, expressed through the first row in the table. All other measurements are expressed as ratios of cross sections or branching ratios in the first column and of coupling modifiers in the second column. There are more parameters of interest in the case of the first parameterisation, because the ratios of cross sections for the WH ZH, and VBF processes can all be expressed as functions of two parameters λ_{WZ} and λ_{Zg} in the coupling parameterisation. The slightly different additional assumptions in each parameterisation are discussed in the text.

σ and BR ratio model	Coupling-strength ratio model
$\sigma(gg \to H \to ZZ)$	$\kappa_{\mathrm{gZ}} = \kappa_{\mathrm{g}} \cdot \kappa_{\mathrm{Z}}/\kappa_{\mathrm{H}}$
$\sigma_{V\mathrm{BF}}/\sigma_{gg\mathrm{F}}$	
$\sigma_{WH}/\sigma_{gg\mathrm{F}}$	
$\sigma_{ZH}/\sigma_{gg\mathrm{F}}$	$\lambda_{\mathrm{Zg}} = \kappa_{\mathrm{Z}}/\kappa_{\mathrm{g}}$
$\sigma_{ttH}/\sigma_{gg\mathrm{F}}$	$\lambda_{\mathrm{tg}} = \kappa_{\mathrm{t}}/\kappa_{\mathrm{g}}$
$\mathrm{BR}^{WW}/\mathrm{BR}^{ZZ}$	$\lambda_{\mathrm{WZ}} = \kappa_{\mathrm{W}}/\kappa_{\mathrm{Z}}$
$\mathrm{BR}^{\gamma\gamma}/\mathrm{BR}^{ZZ}$	$\lambda_{\gamma\mathrm{Z}} = \kappa_{\gamma}/\kappa_{\mathrm{Z}}$
$\mathrm{BR}^{\tau\tau}/\mathrm{BR}^{ZZ}$	$\lambda_{\tau\mathrm{Z}} = \kappa_{\tau}/\kappa_{\mathrm{Z}}$
$\mathrm{BR}^{bb}/\mathrm{BR}^{ZZ}$	$\lambda_{\mathrm{bZ}} = \kappa_{\mathrm{b}}/\kappa_{\mathrm{Z}}$

4.1. Parameterisation using ratios of cross sections and branching ratios

As discussed in Section 3.1, the measured Higgs boson rates are only sensitive to cross sections times branching ratios. Thus, from the rate measurements alone, the cross sections and decay branching ratios cannot be separately determined in a model-independent way. However, ratios of cross sections and of branching ratios can be extracted, without any additional assumptions beyond the general ones discussed in Section 1, from a combined fit to the data. This is achieved by normalising the yield of any specific channel $i \to H \to f$ to a reference process. In this paper, $gg \to H \to ZZ$ is chosen as the reference, because the combined value for $\sigma(gg \to H \to ZZ)$ has the smallest systematic and one of the smallest overall uncertainties.

The product of the cross section and the branching ratio of $i \to H \to f$ can then be expressed using the ratios as:

$$\sigma_i \cdot \mathrm{BR}^f = \sigma(gg \to H \to ZZ) \times \left(\frac{\sigma_i}{\sigma_{gg\mathrm{F}}}\right) \times \left(\frac{\mathrm{BR}^f}{\mathrm{BR}^{ZZ}}\right), \tag{10}$$

where $\sigma(gg \to H \to ZZ) = \sigma_{gg\mathrm{F}} \cdot \mathrm{BR}^{ZZ}$ under the narrow width approximation. With $\sigma(gg \to H \to ZZ)$ constraining the normalisation, the ratios in Eq. 10 can be determined separately, based on the five production processes (ggF, VBF, WH, ZH and ttH) and five decay modes ($H \to ZZ$, $H \to WW$, $H \to \gamma\gamma$, $H \to \tau\tau$ and $H \to bb$). The combined fit results can be presented as a function of nine parameters of interest: one reference cross section times branching ratio, $\sigma(gg \to H \to ZZ)$, four ratios of production cross sections, $\sigma_i/\sigma_{gg\mathrm{F}}$ and four ratios of branching ratios, $\mathrm{BR}^f/\mathrm{BR}^{ZZ}$ as shown in Table 6.

Expressing the measurements through ratios of cross sections and branching ratios has the advantage that the ratios are independent of the theoretical predictions on the inclusive production cross sections and

Table 7: Best-fit values of $\sigma(gg \to H \to ZZ)$, $\sigma_i/\sigma_{\mathrm{ggF}}$ and BR^f/BR^{ZZ} from the combined analysis of the $\sqrt{s} = 7$ and 8 TeV data. The cross-section ratios are given for $\sqrt{s} = 8$ TeV, assuming the SM values for $\sigma_i(7\ \mathrm{TeV})/\sigma_i(8\ \mathrm{TeV})$. The results are reported for the combination of ATLAS and CMS and also separately for each experiment, together with their total uncertainties and their breakdown into statistical and systematic components. The expected uncertainties on the measurements are also displayed (in parentheses). The SM predictions [27] are also shown with their total uncertainties.

Parameter	SM prediction	Best-fit value	Uncertainty Stat	Uncertainty Syst	Best-fit value	Uncertainty Stat	Uncertainty Syst	Best-fit value	Uncertainty Stat	Uncertainty Syst
		ATLAS+CMS			ATLAS			CMS		
$\sigma(gg \to H \to ZZ)$ (pb)	0.513 ± 0.057	$0.58^{+0.11}_{-0.10}$ $\left(^{+0.11}_{-0.10}\right)$	$^{+0.11}_{-0.10}$ $\left(^{+0.11}_{-0.09}\right)$	$^{+0.03}_{-0.02}$ $\left(^{+0.03}_{-0.02}\right)$	$0.76^{+0.19}_{-0.17}$ $\left(^{+0.16}_{-0.14}\right)$	$^{+0.19}_{-0.16}$ $\left(^{+0.16}_{-0.13}\right)$	$^{+0.05}_{-0.04}$ $\left(^{+0.04}_{-0.03}\right)$	$0.44^{+0.14}_{-0.11}$ $\left(^{+0.15}_{-0.13}\right)$	$^{+0.13}_{-0.11}$ $\left(^{+0.15}_{-0.13}\right)$	$^{+0.05}_{-0.03}$ $\left(^{+0.04}_{-0.03}\right)$
$\sigma_{\mathrm{VBF}}/\sigma_{\mathrm{ggF}}$	0.082 ± 0.009	$0.11^{+0.03}_{-0.03}$ $\left(^{+0.03}_{-0.02}\right)$	$^{+0.03}_{-0.02}$ $\left(^{+0.02}_{-0.02}\right)$	$^{+0.02}_{-0.01}$ $\left(^{+0.02}_{-0.01}\right)$	$0.08^{+0.03}_{-0.03}$ $\left(^{+0.04}_{-0.03}\right)$	$^{+0.03}_{-0.02}$ $\left(^{+0.04}_{-0.03}\right)$	$^{+0.02}_{-0.01}$ $\left(^{+0.02}_{-0.01}\right)$	$0.14^{+0.07}_{-0.05}$ $\left(^{+0.04}_{-0.03}\right)$	$^{+0.06}_{-0.05}$ $\left(^{+0.04}_{-0.03}\right)$	$^{+0.04}_{-0.02}$ $\left(^{+0.02}_{-0.01}\right)$
$\sigma_{WH}/\sigma_{\mathrm{ggF}}$	0.037 ± 0.004	$0.03^{+0.03}_{-0.03}$ $\left(^{+0.02}_{-0.02}\right)$	$^{+0.02}_{-0.02}$ $\left(^{+0.02}_{-0.02}\right)$	$^{+0.01}_{-0.01}$ $\left(^{+0.01}_{-0.01}\right)$	$0.05^{+0.04}_{-0.03}$ $\left(^{+0.03}_{-0.02}\right)$	$^{+0.03}_{-0.02}$ $\left(^{+0.03}_{-0.02}\right)$	$^{+0.02}_{-0.01}$ $\left(^{+0.02}_{-0.01}\right)$	$0.01^{+0.04}_{-0.04}$ $\left(^{+0.03}_{-0.02}\right)$	$^{+0.04}_{-0.03}$ $\left(^{+0.03}_{-0.02}\right)$	$^{+0.02}_{-0.02}$ $\left(^{+0.02}_{-0.01}\right)$
$\sigma_{ZH}/\sigma_{\mathrm{ggF}}$	0.022 ± 0.002	$0.07^{+0.04}_{-0.03}$ $\left(^{+0.02}_{-0.01}\right)$	$^{+0.03}_{-0.03}$ $\left(^{+0.01}_{-0.01}\right)$	$^{+0.02}_{-0.02}$ $\left(^{+0.01}_{-0.00}\right)$	$0.01^{+0.03}_{-0.01}$ $\left(^{+0.03}_{-0.01}\right)$	$^{+0.02}_{-0.01}$ $\left(^{+0.02}_{-0.01}\right)$	$^{+0.02}_{-0.01}$ $\left(^{+0.01}_{-0.01}\right)$	$0.13^{+0.08}_{-0.05}$ $\left(^{+0.02}_{-0.01}\right)$	$^{+0.06}_{-0.05}$ $\left(^{+0.02}_{-0.01}\right)$	$^{+0.04}_{-0.03}$ $\left(^{+0.01}_{-0.01}\right)$
$\sigma_{ttH}/\sigma_{\mathrm{ggF}}$	0.0067 ± 0.0010	$0.022^{+0.007}_{-0.006}$ $\left(^{+0.004}_{-0.004}\right)$	$^{+0.005}_{-0.005}$ $\left(^{+0.003}_{-0.003}\right)$	$^{+0.004}_{-0.003}$ $\left(^{+0.003}_{-0.002}\right)$	$0.013^{+0.007}_{-0.005}$ $\left(^{+0.006}_{-0.004}\right)$	$^{+0.005}_{-0.004}$ $\left(^{+0.005}_{-0.004}\right)$	$^{+0.004}_{-0.003}$ $\left(^{+0.004}_{-0.003}\right)$	$0.034^{+0.016}_{-0.012}$ $\left(^{+0.007}_{-0.005}\right)$	$^{+0.012}_{-0.010}$ $\left(^{+0.005}_{-0.004}\right)$	$^{+0.010}_{-0.006}$ $\left(^{+0.004}_{-0.004}\right)$
$\mathrm{BR}^{WW}/\mathrm{BR}^{ZZ}$	$8.10 \pm < 0.01$	$6.8^{+1.7}_{-1.3}$ $\left(^{+2.2}_{-1.7}\right)$	$^{+1.5}_{-1.2}$ $\left(^{+2.0}_{-1.6}\right)$	$^{+0.7}_{-0.5}$ $\left(^{+0.9}_{-0.7}\right)$	$6.5^{+2.2}_{-1.6}$ $\left(^{+3.5}_{-2.4}\right)$	$^{+2.0}_{-1.5}$ $\left(^{+3.3}_{-2.2}\right)$	$^{+0.9}_{-0.6}$ $\left(^{+1.3}_{-0.9}\right)$	$7.2^{+2.9}_{-2.1}$ $\left(^{+3.2}_{-2.2}\right)$	$^{+2.6}_{-1.8}$ $\left(^{+2.9}_{-2.0}\right)$	$^{+1.3}_{-0.9}$ $\left(^{+1.4}_{-1.0}\right)$
$\mathrm{BR}^{\gamma\gamma}/\mathrm{BR}^{ZZ}$	0.085 ± 0.001	$0.069^{+0.018}_{-0.015}$ $\left(^{+0.025}_{-0.019}\right)$	$^{+0.018}_{-0.014}$ $\left(^{+0.024}_{-0.019}\right)$	$^{+0.004}_{-0.003}$ $\left(^{+0.006}_{-0.004}\right)$	$0.063^{+0.024}_{-0.018}$ $\left(^{+0.040}_{-0.027}\right)$	$^{+0.023}_{-0.017}$ $\left(^{+0.039}_{-0.027}\right)$	$^{+0.008}_{-0.005}$ $\left(^{+0.011}_{-0.006}\right)$	$0.079^{+0.033}_{-0.023}$ $\left(^{+0.035}_{-0.025}\right)$	$^{+0.032}_{-0.023}$ $\left(^{+0.034}_{-0.024}\right)$	$^{+0.010}_{-0.006}$ $\left(^{+0.008}_{-0.005}\right)$
$\mathrm{BR}^{\tau\tau}/\mathrm{BR}^{ZZ}$	2.36 ± 0.05	$1.8^{+0.6}_{-0.5}$ $\left(^{+0.9}_{-0.7}\right)$	$^{+0.5}_{-0.4}$ $\left(^{+0.8}_{-0.6}\right)$	$^{+0.3}_{-0.2}$ $\left(^{+0.5}_{-0.3}\right)$	$2.2^{+1.1}_{-0.8}$ $\left(^{+1.5}_{-1.0}\right)$	$^{+0.9}_{-0.6}$ $\left(^{+1.3}_{-0.9}\right)$	$^{+0.6}_{-0.4}$ $\left(^{+0.8}_{-0.5}\right)$	$1.6^{+0.9}_{-0.6}$ $\left(^{+1.2}_{-0.9}\right)$	$^{+0.8}_{-0.5}$ $\left(^{+1.0}_{-0.7}\right)$	$^{+0.5}_{-0.3}$ $\left(^{+0.7}_{-0.4}\right)$
$\mathrm{BR}^{bb}/\mathrm{BR}^{ZZ}$	21.6 ± 1.0	$4.2^{+4.6}_{-2.6}$ $\left(^{+16.9}_{-9.1}\right)$	$^{+2.8}_{-2.0}$ $\left(^{+13.9}_{-7.9}\right)$	$^{+3.6}_{-1.7}$ $\left(^{+9.5}_{-4.4}\right)$	$9.7^{+10.2}_{-5.8}$ $\left(^{+29.4}_{-11.8}\right)$	$^{+7.4}_{-4.4}$ $\left(^{+24.3}_{-10.5}\right)$	$^{+7.0}_{-3.8}$ $\left(^{+16.7}_{-5.4}\right)$	$3.7^{+4.1}_{-2.4}$ $\left(^{+29.4}_{-11.9}\right)$	$^{+3.1}_{-1.9}$ $\left(^{+23.4}_{-10.4}\right)$	$^{+2.7}_{-1.6}$ $\left(^{+17.7}_{-5.9}\right)$

decay branching ratios of the Higgs boson. In particular, they are not subject to the dominant signal theoretical uncertainties on the inclusive cross sections for the various production processes. These measurements will therefore remain valid, for example when improved theoretical calculations of Higgs boson production cross sections will become available. The remaining theoretical uncertainties are reduced to those related to the acceptances and selection efficiencies in the various categories, for which SM Higgs boson production and decay kinematics are assumed in the simulations, based on the MC generators discussed in Section 2.2. This is the most generic parameterisation considered, and from the results in terms of their central values and the full error covariance matrix, it is possible, assuming the asymptotic approximation, to derive other results of signal strength parameterisations with different constraints, such as those quoted in Section 5.

Table 7 shows the results of the fit to the data with a breakdown of the statistical and total systematic uncertainties, while the complete breakdown into the four components of the uncertainties is shown in Table 17 in Appendix A. The results are shown for the combination of ATLAS and CMS and also separately for each experiment. They are illustrated also in Fig. 7, where the fit result for each parameter is normalised to the corresponding SM prediction. Also shown in Fig. 7 are the theory uncertainties on

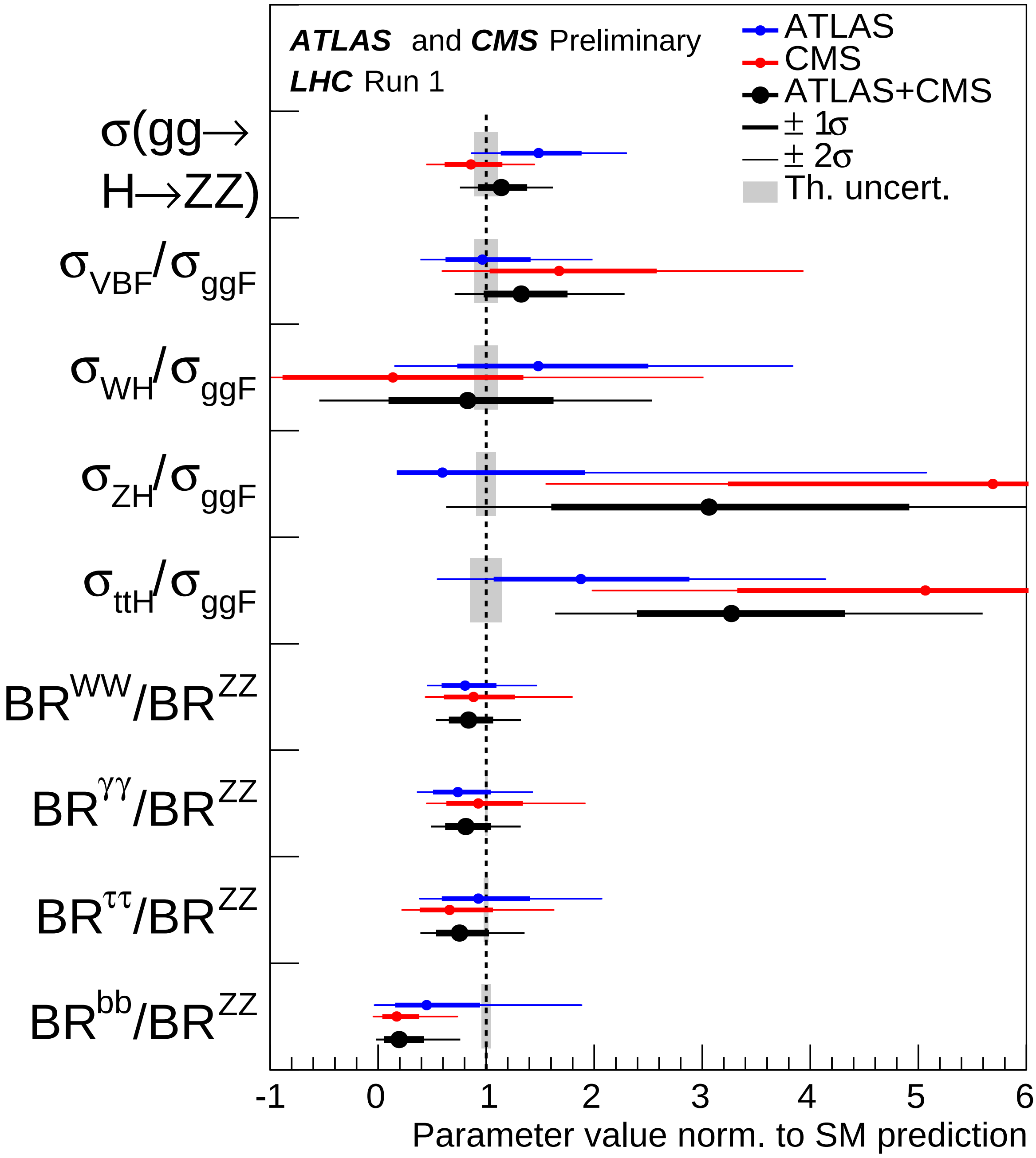

Figure 7: Best-fit values of the $\sigma(gg \to H \to ZZ)$ cross section and of ratios of cross sections and branching ratios, as obtained from the generic parameterisation described in the text and as tabulated in Table 7 for the combination of ATLAS and CMS measurements. Also shown for completeness are the results for each experiment. The error bars indicate the 1σ (thick lines) and 2σ (thin lines) intervals. In this figure, the fit results are normalised to the SM predictions for the various parameters and the shaded bands indicate the theory uncertainties on these predictions.

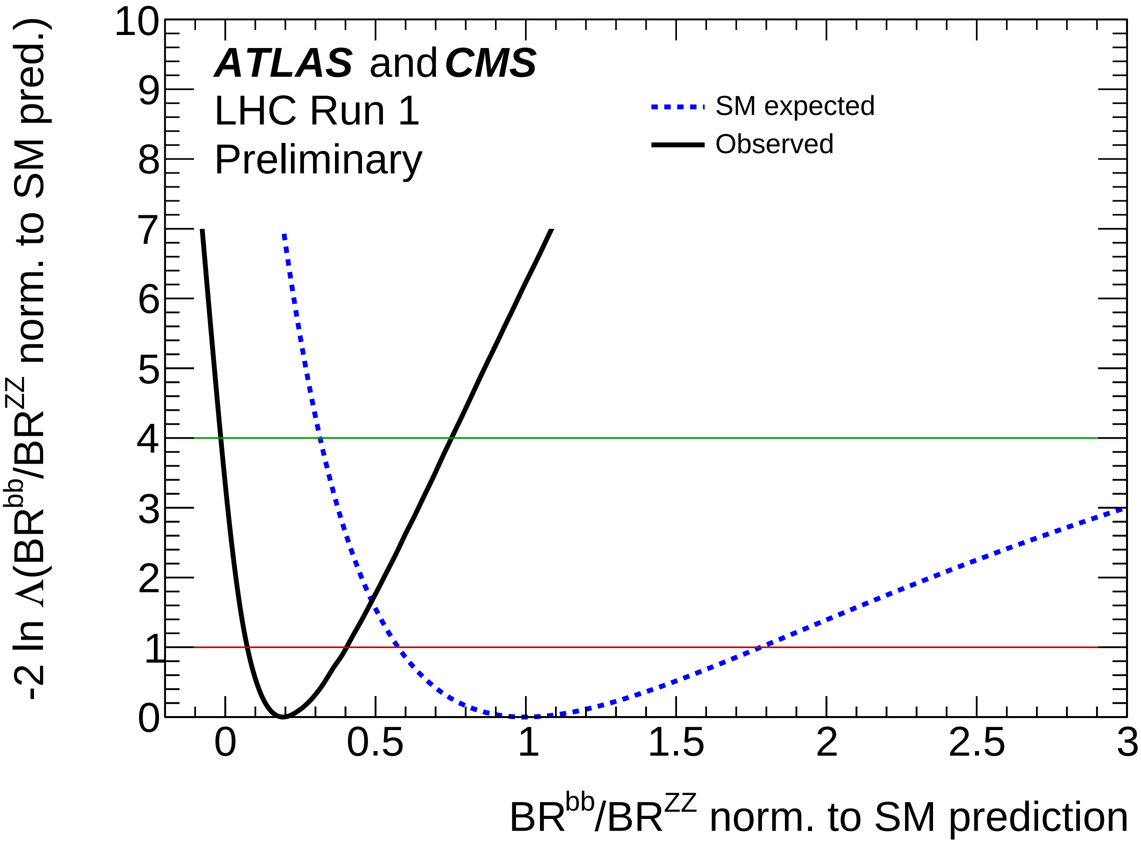

Figure 8: Observed (solid line) and expected (dashed line) negative log-likelihood scan of the $\mathrm{BR}^{bb}/\mathrm{BR}^{ZZ}$ parameter. All the other ratios of cross sections and branching ratios in the parameterisation are profiled. The red (green) horizontal line indicates the value of the profile likelihood ratio corresponding to a 1σ (2σ) confidence interval for the parameter of interest, assuming the asymptotic χ^2 distribution for the test statistic.

the SM predictions for the fitted parameters (they are very small, and therefore barely visible, for the ratios of branching ratios). In the various fits, the combination of 7 and 8 TeV data is carried out under the assumption that the ratios of the production cross sections with respect to the SM predictions are the same at $\sqrt{s}$ = 7 and 8 TeV. The total relative uncertainty on $\sigma(gg \to H \to ZZ)$ is approximately 19%, with its main contribution coming from the statistical uncertainty. The total relative systematic uncertainty is only $\sim$ 4%. Table 18 and Fig. 26 in Appendix A show the results obtained when choosing the $H \to WW$ channel as an alternative reference process. This yields a somewhat smaller total uncertainty of approximately 15% on $\sigma(gg \to H \to WW)$, but with a much larger contribution of $\sim$ 11% from the systematic uncertainties. The ratio of cross sections $\sigma_{\mathrm{VBF}}/\sigma_{gg\mathrm{F}}$ and the ratios of BRs, $\mathrm{BR}^{WW}/\mathrm{BR}^{ZZ}$ and $\mathrm{BR}^{\gamma\gamma}/\mathrm{BR}^{ZZ}$, are measured with a relative uncertainty of approximately 30%, while the $\mathrm{BR}^{\tau\tau}/\mathrm{BR}^{ZZ}$ ratio of BRs is measured with a relative accuracy of approximately 40%.

The p-value of the compatibility between the data and the SM predictions is 16%. The most precise measurements are all consistent with the SM predictions within less than 2σ, however the production cross-section ratio $\sigma_{ttH}/\sigma_{gg\mathrm{F}}$ relative to the SM ratio is measured to be $3.3^{+1.0}_{-0.9}$, corresponding to an excess compared to the SM prediction of approximately 2.3σ. This excess is mainly due to the multi-lepton categories. The ratio $\sigma_{ZH}/\sigma_{gg\mathrm{F}}$ relative to the SM ratio is measured to be $3.2^{+1.8}_{-1.4}$ with the observed

Table 8: Best-fit values of $\kappa_{gZ} = \kappa_g \cdot \kappa_Z/\kappa_H$ and of the ratios of coupling modifiers, as defined in the most generic model studied in the context of the κ-framework, from the combined analysis of the $\sqrt{s} = 7$ and 8 TeV data. The results are shown for the ATLAS+CMS combination and also separately for each experiment, together with their total uncertainties and their breakdown into statistical and systematic components. The total uncertainties on λ_{tg} and λ_{WZ}, for which a negative solution is allowed, are calculated around the overall best-fit value, while the uncertainty breakdown is performed in the positive range. The full ATLAS+CMS 68% CL limits are $\lambda_{WZ} = [-0.97, -0.82] \cup [0.80, 0.98]$ and $\lambda_{tg} = [-2.00, -1.55] \cup [1.47, 2.08]$.

Parameter	ATLAS+CMS Best-fit value	ATLAS+CMS Uncertainty Stat	ATLAS+CMS Uncertainty Syst	ATLAS Best-fit value	ATLAS Uncertainty Stat	ATLAS Uncertainty Syst	CMS Best-fit value	CMS Uncertainty Stat	CMS Uncertainty Syst
$\kappa_{gZ} = \kappa_g \cdot \kappa_Z/\kappa_H$	$1.10^{+0.11}_{-0.11}$ $\left(^{+0.11}_{-0.11}\right)$	$^{+0.09}_{-0.09}$ $\left(^{+0.09}_{-0.09}\right)$	$^{+0.07}_{-0.06}$ $\left(^{+0.06}_{-0.05}\right)$	$1.20^{+0.16}_{-0.15}$ $\left(^{+0.16}_{-0.15}\right)$	$^{+0.14}_{-0.14}$ $\left(^{+0.14}_{-0.13}\right)$	$^{+0.08}_{-0.06}$ $\left(^{+0.07}_{-0.06}\right)$	$0.99^{+0.14}_{-0.13}$ $\left(^{+0.15}_{-0.14}\right)$	$^{+0.12}_{-0.12}$ $\left(^{+0.13}_{-0.12}\right)$	$^{+0.07}_{-0.06}$ $\left(^{+0.07}_{-0.06}\right)$
$\lambda_{Zg} = \kappa_Z/\kappa_g$	$1.26^{+0.23}_{-0.19}$ $\left(^{+0.20}_{-0.17}\right)$	$^{+0.18}_{-0.16}$ $\left(^{+0.15}_{-0.14}\right)$	$^{+0.15}_{-0.12}$ $\left(^{+0.12}_{-0.10}\right)$	$1.06^{+0.26}_{-0.21}$ $\left(^{+0.28}_{-0.23}\right)$	$^{+0.21}_{-0.18}$ $\left(^{+0.23}_{-0.20}\right)$	$^{+0.14}_{-0.11}$ $\left(^{+0.16}_{-0.11}\right)$	$1.47^{+0.44}_{-0.34}$ $\left(^{+0.27}_{-0.23}\right)$	$^{+0.34}_{-0.28}$ $\left(^{+0.22}_{-0.19}\right)$	$^{+0.29}_{-0.19}$ $\left(^{+0.17}_{-0.12}\right)$
$\lambda_{tg} = \kappa_t/\kappa_g$	$1.76^{+0.32}_{-0.29}$ $\left(^{+0.29}_{-0.39}\right)$	$^{+0.21}_{-0.20}$ $\left(^{+0.20}_{-0.21}\right)$	$^{+0.23}_{-0.20}$ $\left(^{+0.21}_{-0.24}\right)$	$1.39^{+0.34}_{-0.33}$ $\left(^{+0.38}_{-0.54}\right)$	$^{+0.25}_{-0.24}$ $\left(^{+0.28}_{-0.28}\right)$	$^{+0.23}_{-0.22}$ $\left(^{+0.26}_{-0.33}\right)$	$-2.25^{+0.51}_{-0.55}$ $\left(^{+0.42}_{-0.64}\right)$	$^{+0.39}_{-0.36}$ $\left(^{+0.31}_{-0.33}\right)$	$^{+0.39}_{-0.30}$ $\left(^{+0.29}_{-0.46}\right)$
$\lambda_{WZ} = \kappa_W/\kappa_Z$	$0.89^{+0.10}_{-0.09}$ $\left(^{+0.12}_{-0.10}\right)$	$^{+0.09}_{-0.08}$ $\left(^{+0.11}_{-0.09}\right)$	$^{+0.04}_{-0.04}$ $\left(^{+0.05}_{-0.04}\right)$	$0.92^{+0.14}_{-0.12}$ $\left(^{+0.18}_{-0.15}\right)$	$^{+0.13}_{-0.11}$ $\left(^{+0.16}_{-0.13}\right)$	$^{+0.05}_{-0.04}$ $\left(^{+0.07}_{-0.06}\right)$	$-0.85^{+0.13}_{-0.15}$ $\left(^{+0.17}_{-0.14}\right)$	$^{+0.13}_{-0.11}$ $\left(^{+0.15}_{-0.13}\right)$	$^{+0.07}_{-0.06}$ $\left(^{+0.07}_{-0.07}\right)$
$\lambda_{\gamma Z} = \kappa_\gamma/\kappa_Z$	$0.89^{+0.11}_{-0.10}$ $\left(^{+0.13}_{-0.12}\right)$	$^{+0.11}_{-0.09}$ $\left(^{+0.13}_{-0.11}\right)$	$^{+0.04}_{-0.03}$ $\left(^{+0.04}_{-0.03}\right)$	$0.88^{+0.16}_{-0.14}$ $\left(^{+0.20}_{-0.17}\right)$	$^{+0.15}_{-0.13}$ $\left(^{+0.19}_{-0.17}\right)$	$^{+0.04}_{-0.03}$ $\left(^{+0.06}_{-0.04}\right)$	$0.91^{+0.17}_{-0.14}$ $\left(^{+0.18}_{-0.16}\right)$	$^{+0.16}_{-0.13}$ $\left(^{+0.17}_{-0.15}\right)$	$^{+0.05}_{-0.04}$ $\left(^{+0.05}_{-0.04}\right)$
$\lambda_{\tau Z} = \kappa_\tau/\kappa_Z$	$0.85^{+0.14}_{-0.12}$ $\left(^{+0.17}_{-0.15}\right)$	$^{+0.12}_{-0.10}$ $\left(^{+0.14}_{-0.13}\right)$	$^{+0.07}_{-0.06}$ $\left(^{+0.09}_{-0.08}\right)$	$0.97^{+0.22}_{-0.18}$ $\left(^{+0.27}_{-0.23}\right)$	$^{+0.18}_{-0.15}$ $\left(^{+0.23}_{-0.19}\right)$	$^{+0.11}_{-0.09}$ $\left(^{+0.14}_{-0.12}\right)$	$0.78^{+0.20}_{-0.17}$ $\left(^{+0.23}_{-0.20}\right)$	$^{+0.16}_{-0.15}$ $\left(^{+0.19}_{-0.17}\right)$	$^{+0.10}_{-0.08}$ $\left(^{+0.12}_{-0.11}\right)$
$\lambda_{bZ} = \kappa_b/\kappa_Z$	$0.56^{+0.18}_{-0.18}$ $\left(^{+0.25}_{-0.22}\right)$	$^{+0.12}_{-0.11}$ $\left(^{+0.21}_{-0.18}\right)$	$^{+0.10}_{-0.11}$ $\left(^{+0.14}_{-0.11}\right)$	$0.61^{+0.24}_{-0.24}$ $\left(^{+0.36}_{-0.29}\right)$	$^{+0.20}_{-0.18}$ $\left(^{+0.31}_{-0.24}\right)$	$^{+0.14}_{-0.15}$ $\left(^{+0.18}_{-0.14}\right)$	$0.47^{+0.26}_{-0.17}$ $\left(^{+0.38}_{-0.37}\right)$	$^{+0.17}_{-0.15}$ $\left(^{+0.32}_{-0.25}\right)$	$^{+0.15}_{-0.16}$ $\left(^{+0.20}_{-0.17}\right)$

excess mainly due to the CMS $H \to ZZ$ two jet categories. The ratio of branching ratios $\mathrm{BR}^{bb}/\mathrm{BR}^{ZZ}$ relative to the SM ratio is measured to be $0.19^{+0.21}_{-0.12}$. In this parameterisation, the high values found for the production cross-section ratios for the ZH and ttH processes induce a low value for the $H \to bb$ decay branching ratio because the $H \to bb$ decay channel does not contribute to the observed excesses. The likelihood scan of the $\mathrm{BR}^{bb}/\mathrm{BR}^{ZZ}$ parameter is very asymmetric, as shown in Fig. 8, resulting in an overall deficit compared to the SM prediction of approximately 2.5σ (this deviation is anti-correlated with the ones quoted above for the $\sigma_{ttH}/\sigma_{gg\mathrm{F}}$ and $\sigma_{ZH}/\sigma_{gg\mathrm{F}}$ production cross-section ratios).

4.2. Parameterisation using ratios of coupling modifiers

The parameterisation using the Higgs boson coupling modifiers is based on the κ-framework described in Section 2.4. The cross section times branching ratio for the $gg \to H \to ZZ$ channel is parameterised as a function of $\kappa_{gZ} = \kappa_g \cdot \kappa_Z/\kappa_H$, where κ_g is the effective coupling modifier of the Higgs boson to the gluon in ggF production through the dominant loops involving top and bottom quarks. The combined input channels span also here five Higgs boson production processes and five decay channels. Four of the decay channels, namely $H \to ZZ$, $H \to WW$, $H \to \tau\tau$, and $H \to bb$, probe single coupling modifiers to a gauge boson or a fermion through their respective ratios to the $H \to ZZ$ branching ratio, $\lambda_{Zg} = \kappa_Z/\kappa_g$, $\lambda_{WZ} = \kappa_W/\kappa_Z$, $\lambda_{\tau Z} = \kappa_\tau/\kappa_Z$ and $\lambda_{bZ} = \kappa_b/\kappa_Z$. The remaining decay channel, $H \to \gamma\gamma$, which occurs through loops involving predominantly the top quark and the W boson, is described by an effective coupling

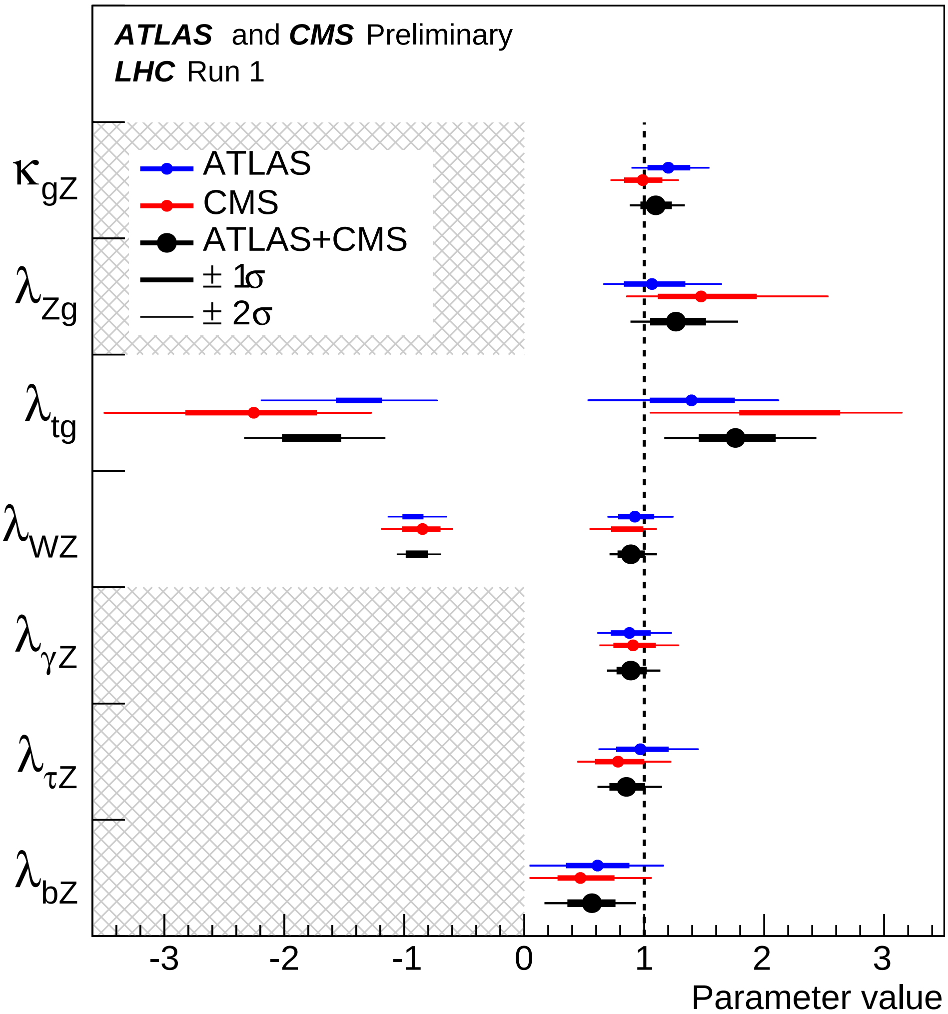

Figure 9: Best-fit values of ratios of Higgs boson coupling modifiers, as obtained from the generic parameterisation described in the text and as tabulated in Table 8 for the combination of ATLAS and CMS measurements. Also shown for completeness are the results for each experiment. The error bars indicate the 1σ (thick lines) and 2σ (thin lines) intervals. The hatched areas indicate the parameters which are assumed to be positive without loss of generality.

modifier through the ratio $\lambda_{\gamma Z} = \kappa_\gamma/\kappa_Z$. Finally, the measurements of the ttH production process are parameterised as a function of $\lambda_{tg} = \kappa_t/\kappa_g$. In this parameterisation, $\lambda_{Zg} = \kappa_Z/\kappa_g$ and $\lambda_{WZ} = \kappa_W/\kappa_Z$ are also probed by the VBF, WH and ZH production processes.

Table 6 compares the measured observables of the two generic parameterisations described in Section 4. The first line makes explicit the choice of the $gg \to H \to ZZ$ channel as a reference, while $\lambda_{Zg} = \kappa_Z/\kappa_g$ is related to the ratio of cross sections between the ZH and ggF production processes. As stated above, once $\lambda_{WZ} = \kappa_W/\kappa_Z$ is also specified, then the VBF, WH and ZH production cross sections are fully defined. This explains the smaller number of independent parameters of interest in the coupling modifier ratio parameterisation. The two parameterisations described in this section are not equivalent because of the approximations inherent to each one of them which are summarised in Sections 2.3 and 2.4. These are due in part to the early stage of these measurements, which do not experimentally constrain all possible

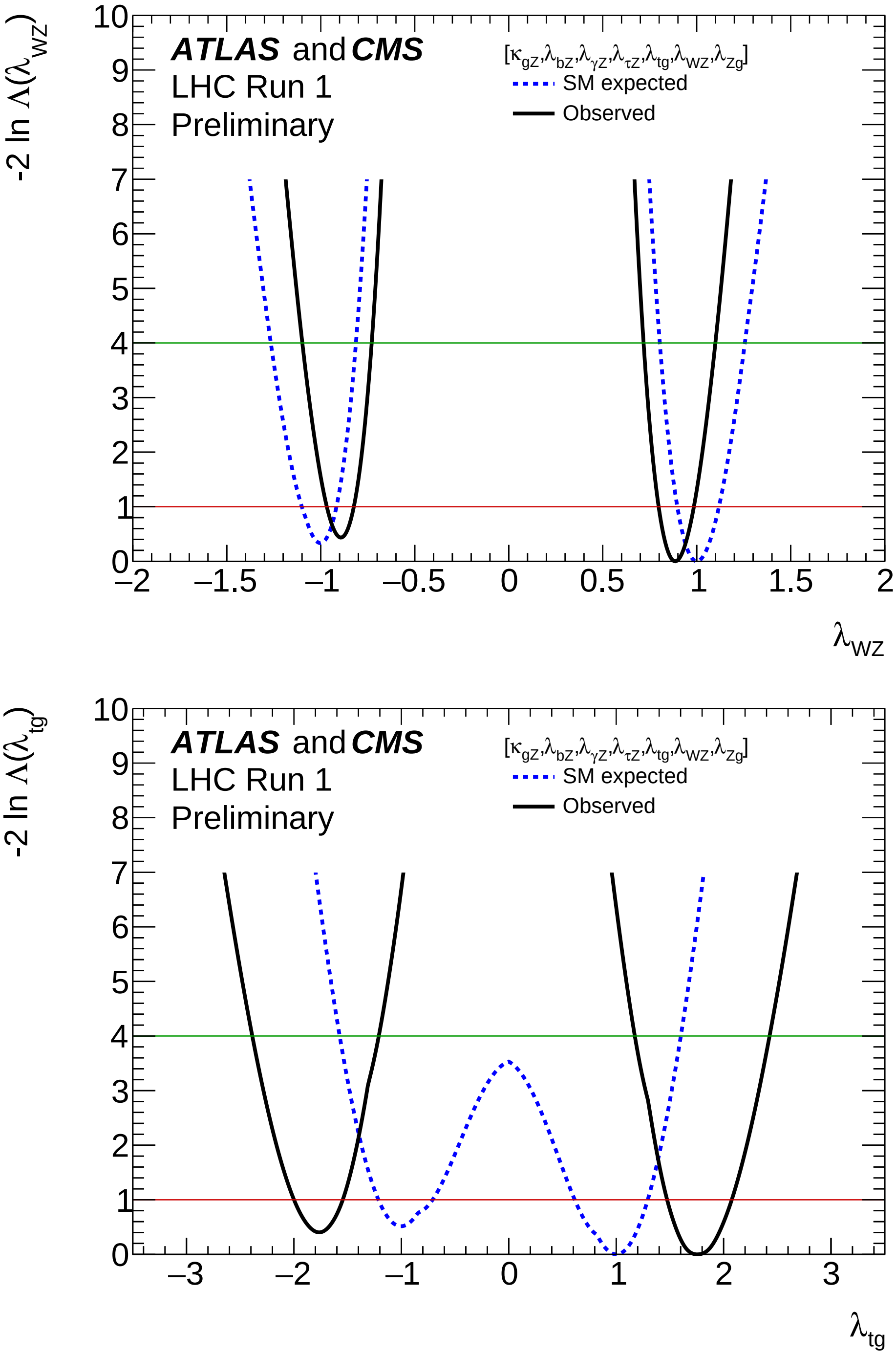

Figure 10: Negative log-likelihood scans for λ_{WZ} and λ_{tg}, the two parameters of Fig. 9 which are of interest in the negative range in the the generic parameterisation of ratios of Higgs boson coupling modifiers described in the text.

Higgs boson production processes and decay channels, in particular those which are expected to be small in the SM but might be enhanced if new physics beyond the SM would be present.

Table 8 shows the results of the fit to the data with a breakdown of the statistical and total systematic uncertainties, while the complete breakdown into the four components of the uncertainties is shown in Table 19 in Appendix A. The assumptions that the coupling modifiers are the same at the two centre-of-mass energies is assumed to be valid in this case as in the parameterisation of the ratios of cross sections and branching ratios. These tables only show the values and uncertainties for positive values of all the parameters, while Fig. 9 illustrates the complete ranges of allowed values with their total uncertainties, including the negative ranges allowed for λ_{WZ} and λ_{tg}, the two parameters chosen to illustrate possible interference effects due to $ggZH$ or tH production. Figure 10 shows the likelihood scan results for these two parameters in the case of the combination of ATLAS and CMS, both for the observed and expected results. In both cases, the best-fit values correspond to the positive sign, but the sensitivity to the interference terms remains small at this stage. As described in Section 2.4, these are responsible for the small asymmetry between the likelihood curves for the positive and negative values of these parameters of interest. The p-value of the compatibility between the data and the SM predictions is 13%. As for the first generic parameterisation, all results are consistent with the SM predictions within less than 2σ except for λ_{bZ} and λ_{tg} which reflect similar tensions to those described in Section 4.1 for the measurement of the ratios of the bb and ZZ decay branching ratios and of the ttH and ggF production cross sections.

5. Measurements of signal strengths

In Section 4.1, the fit results from a generic parameterisation, expressed mostly as ratios of cross sections and of branching ratios, have been shown. This section probes more specific parameterisations with additional assumptions. In the following, results from the fits are presented starting with the most restrictive parameterisation as a function of a single parameter of interest, which has historically been the approach to assess the sensitivity of the experimental data to the presence of a Higgs boson. The results are obtained from the combined fits to the $\sqrt{s}$ = 7 and 8 TeV data under the premise that the signal strengths are the same at the two energies.

5.1. Global signal strength

The simplest and most restrictive signal strength parameterisation is to assume that the μ_i and μ^f values are the same for all production processes and decay channels. In this case, the SM predictions of signal yields in all categories are scaled by a global signal strength μ. Such a parameterisation provides the simplest test of the compatibility of the experimental data with the SM predictions. A fit to the combined ATLAS and CMS data at $\sqrt{s}$ = 7 and 8 TeV with μ as the parameter of interest results in the best-fit value:

$$\mu = 1.09^{+0.11}_{-0.10} = 1.09^{+0.07}_{-0.07}\,(\text{stat})\,^{+0.04}_{-0.04}\,(\text{expt})\,^{+0.03}_{-0.03}\,(\text{thbgd})^{+0.07}_{-0.06}\,(\text{thsig}),$$

where the breakdown of the uncertainties into their four main components is done as described in Section 3.3. The overall systematic uncertainty of $^{+0.09}_{-0.08}$ is larger than the statistical uncertainty and its largest component is the theoretical uncertainty on the ggF cross section. This result is consistent with the SM expectation of $\mu = 1$ within less than 1σ and the p-value of the compatibility between the data and the SM predictions is 34%. This result is shown in Table 9, together with that from each experiment, including

Table 9: Measured (meas.) global signal strengths μ together with their total observed and expected (exp.) uncertainties, and with the breakdown of these uncertainties into their four components as defined in Section 3.3. The results are shown for the combination of ATLAS and CMS and separately for each experiment. These results are derived assuming that the Higgs boson production cross sections and branching ratios are the same as in the SM.

	Best-fit μ	Uncertainty				
		Total	Stat	Expt	Thbgd	Thsig
ATLAS and CMS (meas.)	1.09	$^{+0.11}_{-0.10}$	$^{+0.07}_{-0.07}$	$^{+0.04}_{-0.04}$	$^{+0.03}_{-0.03}$	$^{+0.07}_{-0.06}$
ATLAS and CMS (exp.)	–	$^{+0.11}_{-0.10}$	$^{+0.07}_{-0.07}$	$^{+0.04}_{-0.04}$	$^{+0.03}_{-0.03}$	$^{+0.06}_{-0.06}$
ATLAS (meas.)	1.20	$^{+0.15}_{-0.14}$	$^{+0.10}_{-0.10}$	$^{+0.06}_{-0.06}$	$^{+0.04}_{-0.04}$	$^{+0.08}_{-0.07}$
CMS (meas.)	0.98	$^{+0.14}_{-0.13}$	$^{+0.10}_{-0.09}$	$^{+0.06}_{-0.05}$	$^{+0.04}_{-0.04}$	$^{+0.08}_{-0.07}$

Table 10: Measured signal strengths μ and their total uncertainties for different Higgs boson production processes. The results are shown for the combination of ATLAS and CMS and separately for each experiment, for the combined $\sqrt{s}$ = 7 and 8 TeV data. These results are derived assuming that the Higgs boson branching ratios are the same as in the SM.

Production process	ATLAS+CMS	ATLAS	CMS
μ_{ggF}	$1.03^{+0.17}_{-0.15}$	$1.25^{+0.24}_{-0.21}$	$0.84^{+0.19}_{-0.16}$
μ_{VBF}	$1.18^{+0.25}_{-0.23}$	$1.21^{+0.33}_{-0.30}$	$1.13^{+0.37}_{-0.34}$
μ_{WH}	$0.88^{+0.40}_{-0.38}$	$1.25^{+0.56}_{-0.52}$	$0.46^{+0.57}_{-0.54}$
μ_{ZH}	$0.80^{+0.39}_{-0.36}$	$0.30^{+0.51}_{-0.46}$	$1.35^{+0.58}_{-0.54}$
μ_{ttH}	$2.3^{+0.7}_{-0.6}$	$1.9^{+0.8}_{-0.7}$	$2.9^{+1.0}_{-0.9}$

the breakdown of the uncertainties into their four main components. Also shown for the combination of ATLAS and CMS are the expected uncertainties and their breakdown.

5.2. Signal strengths of individual production processes and decay channels

The global signal strength is the most precisely measured Higgs boson coupling-related observable, but this simple parameterisation is very model dependent, since all Higgs boson production and decay measurements are combined with the assumption that all their ratios are the same as in the SM. The compatibility of the measurements with the SM can be tested in a less model-dependent way, by relaxing these assumptions separately for the production cross sections and the decay branching ratios.

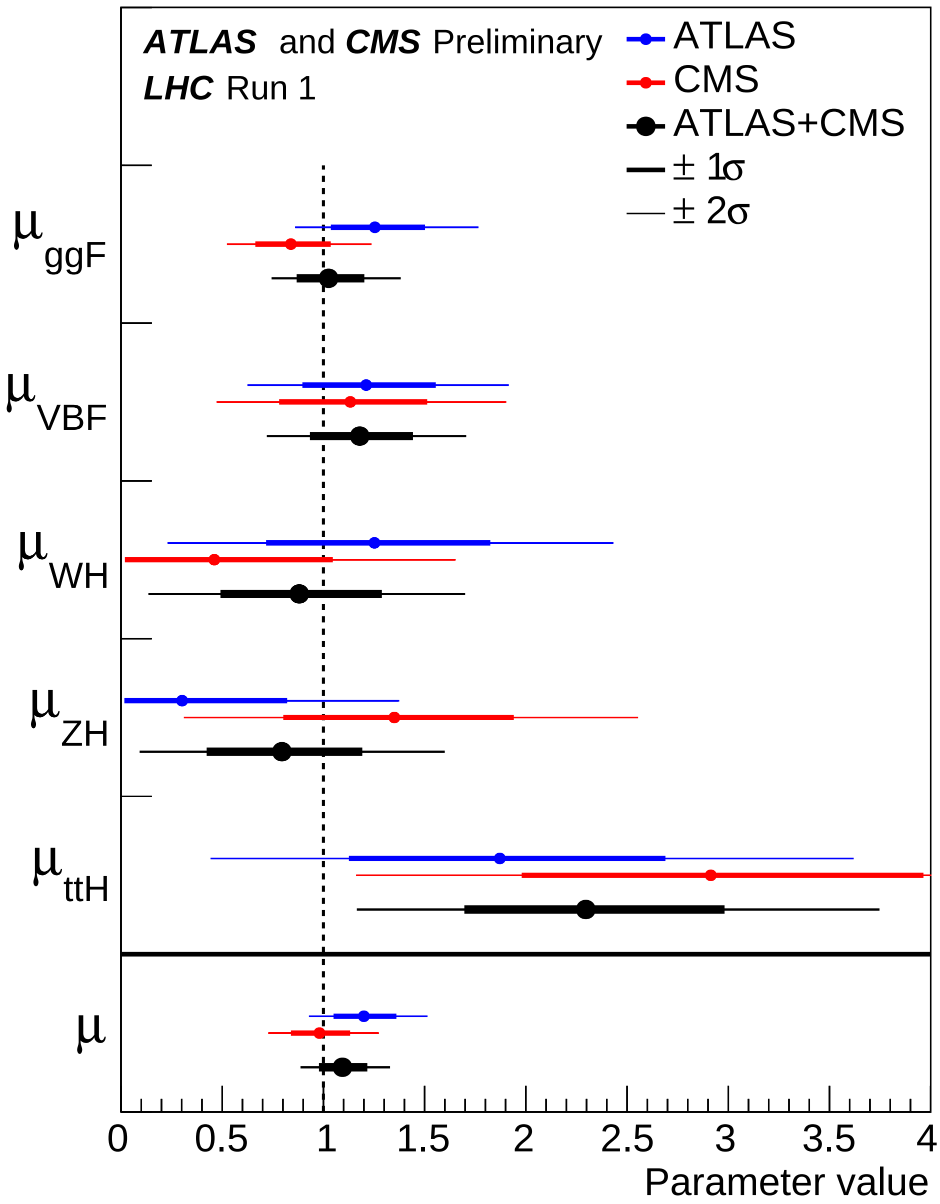

Figure 11: Best-fit results for the production signal strengths for the combination of ATLAS and CMS. Also shown for completeness are the results for each experiment. The error bars indicate the 1σ (thick lines) and 2σ (thin lines) intervals. The measurements of the global signal strength μ are also shown.

Table 11: Measured signal strengths μ and their total uncertainties for different Higgs boson decay channels. The results are shown for the combination of ATLAS and CMS and separately for each experiment, for the combined $\sqrt{s} = 7$ and 8 TeV data. These results are derived assuming that the Higgs boson production process cross sections at $\sqrt{s} = 7$ and 8 TeV are the same as in the SM.

Decay channel	ATLAS+CMS	ATLAS	CMS
$\mu^{\gamma\gamma}$	$1.16^{+0.20}_{-0.18}$	$1.15^{+0.27}_{-0.25}$	$1.12^{+0.25}_{-0.23}$
μ^{ZZ}	$1.31^{+0.27}_{-0.24}$	$1.51^{+0.39}_{-0.34}$	$1.05^{+0.32}_{-0.27}$
μ^{WW}	$1.11^{+0.18}_{-0.17}$	$1.23^{+0.23}_{-0.21}$	$0.91^{+0.24}_{-0.21}$
$\mu^{\tau\tau}$	$1.12^{+0.25}_{-0.23}$	$1.41^{+0.40}_{-0.35}$	$0.89^{+0.31}_{-0.28}$
μ^{bb}	$0.69^{+0.29}_{-0.27}$	$0.62^{+0.37}_{-0.36}$	$0.81^{+0.45}_{-0.42}$

Table 12: Measured and expected significances for the observation of Higgs boson production processes and decay channels for the combination of ATLAS and CMS. Not included here are the ggF production process and the $H \to ZZ$, $H \to WW$, and $H \to \gamma\gamma$ decay channels, which have been already clearly observed. All results are obtained constraining the decays to their SM values when considering the production modes, and constraining the production modes to their SM values when studying the decays.

Production process	Measured significance (σ)	Expected significance (σ)
VBF	5.4	4.7
WH	2.4	2.7
ZH	2.3	2.9
VH	3.5	4.2
ttH	4.4	2.0
Decay channel		
$H \to \tau\tau$	5.5	5.0
$H \to bb$	2.6	3.7

Assuming the SM values for the Higgs boson branching ratios, namely $\mu^f = 1$ in Eq. 7, the five main Higgs boson production processes are explored with independent signal strengths: $\mu_{gg\mathrm{F}}$, μ_{VBF}, μ_{WH}, μ_{ZH} and μ_{ttH}. A combined analysis of the ATLAS and CMS data is performed with these five signal strengths as the parameters of interest and the results are shown in Table 10 for the combined $\sqrt{s} = 7$ and 8 TeV datasets. The signal strengths at the two energies are assumed to be the same for each production process. Figure 11 illustrates these results with their total uncertainties. The p-value of the compatibility between the data and the SM predictions is 24%.

Similarly to the production case, Higgs boson decays can be studied with five independent signal strengths, one for each decay channel included in the combination, assuming that the Higgs boson production cross sections are the same as in the SM. Unlike the production, these decay-based signal strengths are independent of the collision centre-of-mass energy and therefore the $\sqrt{s} = 7$ and 8 TeV datasets can be combined without additional assumptions. Table 11 and Fig. 12 show the best-fit results for the combination of ATLAS and CMS and separately for each experiment. The p-value of the compatibility between the data and the SM predictions is 60%.

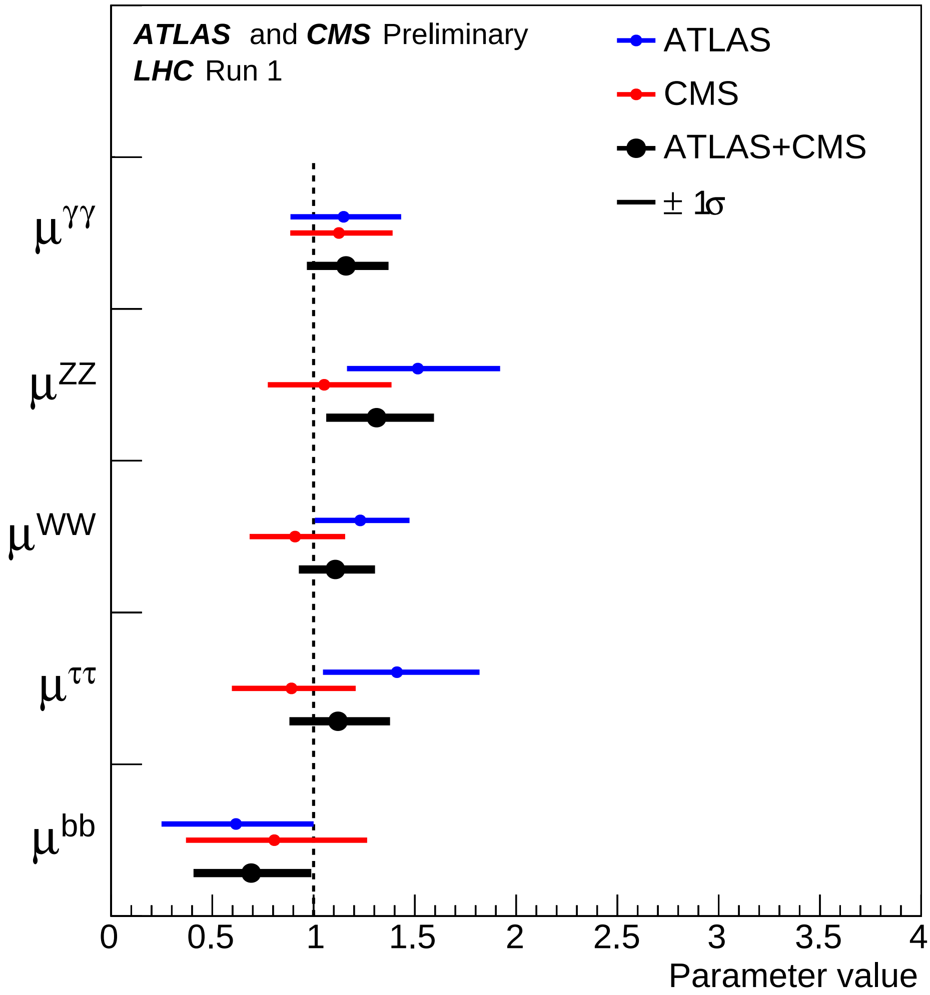

Figure 12: Best-fit results for the decay signal strengths for the combination of ATLAS and CMS. Also shown for completeness are the results for each experiment. The error bars indicate the 1σ intervals.

The rather large measured value of the combined μ_{ttH} leads to a tension between the observed ggF signal strength and that for ttH production in cases such as the fit of the decay signal strengths, for which the production cross sections are constrained to their SM values. This is mitigated to a certain extent by a non-negligible pull of the gluon PDF nuisance parameter used for the Higgs boson signal, which is anti-correlated between ggF and ttH production. This pull reduces the SM prediction of $\sigma_{gg\mathrm{F}}$ and, as a consequence, the decay signal strengths of the channels mainly sensitive to ggF production are enhanced for the combination of ATLAS and CMS. In the case of the $H \to \gamma\gamma$ decay channel, which is mostly sensitive to ggF production and for which the measurements of the two experiments are much closer to each other than their overall uncertainty, this effect is most visible, but corresponds to only $\sim 10\%$ of the total uncertainty. This explains the slightly larger measured combined value of $\mu^{\gamma\gamma}$ compared to that of the individual experiments.

From the combined likelihood scans it is possible to evaluate the significances for the observation of the different production processes and decay channels. The combination of the data from the two experiments increases the sensitivity by approximately a factor of $\sqrt{2}$, since the theoretical uncertainties on the Higgs boson signal are not relevant for this evaluation and all the other significant uncertainties are uncorrelated between the two experiments. The results are reported in Table 12 for all production processes and decay channels, except those which have already been clearly observed, namely the ggF production process and the $H \to ZZ$, $H \to WW$, and $H \to \gamma\gamma$ decay channels. The combined significances for the observation of the VBF production process and of the $H \to \tau\tau$ decay are above 5σ, and the combined significance for the VH production process is above 3σ. The combined significance for the ttH process is 4.4σ, whereas only 2.0σ is expected, owing to the measured excess of 2.3σ with respect to the SM prediction.

5.3. Boson- and fermion-mediated production processes

The Higgs boson production processes can be associated with Higgs boson couplings to either fermions (ggF and ttH) or vector bosons (VBF, WH and ZH). Potential deviations of these couplings from the SM can be tested for each decay channel f using two signal strength parameters, μ_F^f for the fermion-mediated production processes and μ_V^f for the vector-boson-mediated production processes. When calculated separately, however, for each Higgs boson decay channel, the branching ratio cancels in the ratio of μ_V^f/μ_F^f that can be combined. Two fits are performed for the combination of ATLAS and CMS, and also separately for each experiment. The first one is an overall 10-parameter fit of μ_F^f and μ_V^f for each of the five decay channels, while the second one is a 6-parameter fit of μ_V/μ_F and of μ_F^f for each of the five decay channels.

Figure 13 shows the 68% CL contours for the 10-parameter fit of the five decay modes included in the combination of the ATLAS and CMS measurements (while Fig. 28 in Appendix C shows both the 68% and 95% contours for the results of this fit). These results are obtained combining the $\sqrt{s} = 7$ and 8 TeV data, assuming that μ_F^f and μ_V^f are the same at the two energies. The SM expectation of $\mu_F^f = 1$ and $\mu_V^f = 1$ is within the 68% CL contours of all these measurements. Combinations of these contours would require assumptions about the branching ratios and are therefore not performed. Table 13 reports the best-fit values and the total uncertainties for all the parameters of each one of the two fits, together with the expected uncertainties for the combination of ATLAS and CMS. The p-values of the compatibility between the data and the SM predictions are 88% and 72%, for the 10-parameter and 6-parameter fits respectively. In particular, the 6-parameter fit, without any additional assumptions about the Higgs boson branching ratios, yields: $\mu_V/\mu_F = 1.06^{+0.35}_{-0.27}$, in agreement with the SM.

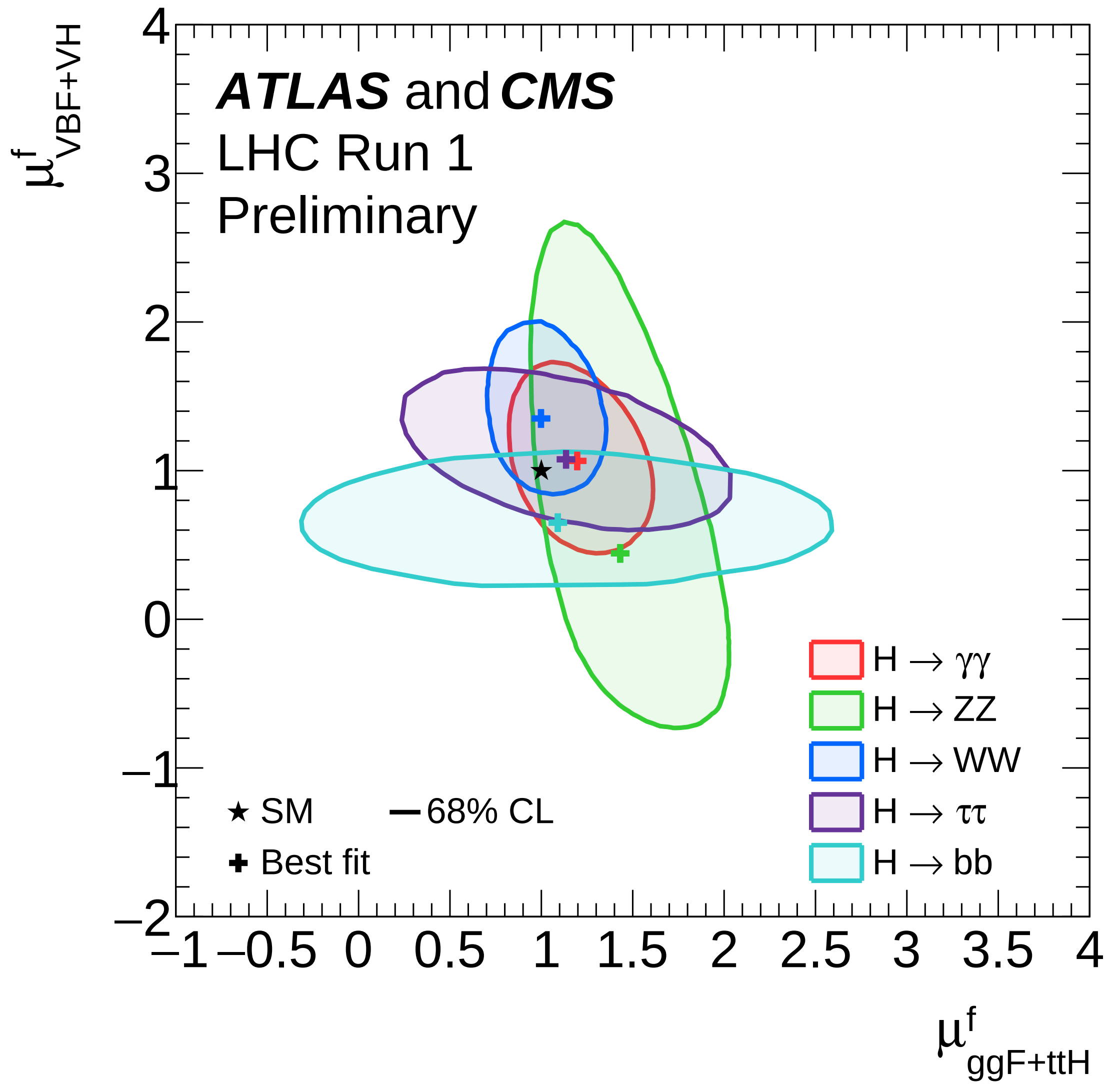

Figure 13: Likelihood contours in the $(\mu^{f}_{ggF+ttH}, \mu^{f}_{\mathrm{VBF}+VH})$ plane for the combination of ATLAS and CMS, shown for the five decay channels, $H \to ZZ$, $H \to WW$, $H \to \gamma\gamma$, $H \to \tau\tau$, and $H \to bb$. The results are shown as 68% CL contours, together with the best-fit values to the data and the SM expectation. Figure 28 in Appendix C shows both the 68% and 95% contours for the results of these fits.

Table 13: Results of the 10-parameter fit of $\mu_F^f = \mu_{ggF+ttH}^f$ and $\mu_V^f = \mu_{VBF+VH}^f$ for each of the five decay channels, and of the 6-parameter fit of the global ratio $\mu_V/\mu_F = \mu_{VBF+VH}/\mu_{ggF+ttH}$ together with μ_F^f for each of the five decay channels. The results are shown for the combination of ATLAS and CMS, together with their measured and expected uncertainties, and the measured results are also shown separately for each experiment.

Parameter	ATLAS+CMS Measured	ATLAS+CMS Expected uncertainty	ATLAS Measured	CMS Measured
10-parameter fit of μ_F^f and μ_V^f				
$\mu_V^{\gamma\gamma}$	$1.05^{+0.44}_{-0.41}$	$^{+0.42}_{-0.38}$	$0.69^{+0.64}_{-0.58}$	$1.37^{+0.62}_{-0.56}$
μ_V^{ZZ}	$0.48^{+1.37}_{-0.91}$	$^{+1.16}_{-0.84}$	$0.26^{+1.60}_{-0.91}$	$1.44^{+2.32}_{-2.30}$
μ_V^{WW}	$1.38^{+0.41}_{-0.37}$	$^{+0.38}_{-0.35}$	$1.56^{+0.52}_{-0.46}$	$1.08^{+0.65}_{-0.58}$
$\mu_V^{\tau\tau}$	$1.12^{+0.37}_{-0.35}$	$^{+0.38}_{-0.36}$	$1.29^{+0.58}_{-0.53}$	$0.87^{+0.49}_{-0.45}$
μ_V^{bb}	$0.65^{+0.30}_{-0.29}$	$^{+0.32}_{-0.30}$	$0.50^{+0.39}_{-0.37}$	$0.85^{+0.47}_{-0.44}$
$\mu_F^{\gamma\gamma}$	$1.19^{+0.28}_{-0.25}$	$^{+0.25}_{-0.23}$	$1.31^{+0.37}_{-0.34}$	$1.01^{+0.34}_{-0.31}$
μ_F^{ZZ}	$1.44^{+0.38}_{-0.34}$	$^{+0.29}_{-0.25}$	$1.73^{+0.51}_{-0.45}$	$0.97^{+0.54}_{-0.42}$
μ_F^{WW}	$1.00^{+0.23}_{-0.20}$	$^{+0.21}_{-0.19}$	$1.10^{+0.29}_{-0.26}$	$0.85^{+0.28}_{-0.25}$
$\mu_F^{\tau\tau}$	$1.10^{+0.61}_{-0.58}$	$^{+0.56}_{-0.53}$	$1.72^{+1.24}_{-1.13}$	$0.91^{+0.69}_{-0.64}$
μ_F^{bb}	$1.09^{+0.93}_{-0.89}$	$^{+0.91}_{-0.86}$	$1.51^{+1.15}_{-1.08}$	$0.10^{+1.83}_{-1.86}$
6-parameter fit of global μ_V/μ_F and to μ_F^f				
μ_V/μ_F	$1.06^{+0.35}_{-0.27}$	$^{+0.34}_{-0.26}$	$0.91^{+0.41}_{-0.30}$	$1.29^{+0.67}_{-0.46}$
$\mu_F^{\gamma\gamma}$	$1.13^{+0.24}_{-0.21}$	$^{+0.21}_{-0.19}$	$1.18^{+0.33}_{-0.29}$	$1.03^{+0.30}_{-0.26}$
μ_F^{ZZ}	$1.29^{+0.29}_{-0.25}$	$^{+0.24}_{-0.20}$	$1.54^{+0.44}_{-0.36}$	$1.00^{+0.33}_{-0.27}$
μ_F^{WW}	$1.08^{+0.22}_{-0.19}$	$^{+0.19}_{-0.17}$	$1.26^{+0.29}_{-0.25}$	$0.85^{+0.25}_{-0.22}$
$\mu_F^{\tau\tau}$	$1.07^{+0.35}_{-0.28}$	$^{+0.32}_{-0.27}$	$1.50^{+0.66}_{-0.49}$	$0.75^{+0.39}_{-0.29}$
μ_F^{bb}	$0.65^{+0.37}_{-0.28}$	$^{+0.45}_{-0.34}$	$0.67^{+0.58}_{-0.42}$	$0.64^{+0.54}_{-0.36}$

6. Constraints on Higgs boson couplings

In Section 4.2, the fit results from the most generic parameterisation in the context of the κ-framework have been shown. This section probes more specific parameterisations with additional assumptions. In the following, results from a few selected parameterisations, with increasingly restrictive assumptions, are presented. The results are obtained from the combined fits to the $\sqrt{s}$ = 7 and 8 TeV data under the premise that the coupling modifiers are the same at the two energies.

6.1. Parameterisations allowing contributions from BSM particles in loops and in decays

As discussed in Sections 2 and 3, the rates of the Higgs boson production in the various decay channels are inversely proportional to the Higgs boson width, which is sensitive to invisible or undetected Higgs boson decays which are predicted by many BSM theories. To directly measure the individual coupling modifiers, an assumption on the Higgs boson width is necessary. Two scenarios are considered in this section: the first one assumes that the Higgs boson does not have any BSM decays, i.e., $\mathrm{BR}_{\mathrm{BSM}} = 0$, while the second one leaves $\mathrm{BR}_{\mathrm{BSM}}$ free, but assumes that $\kappa_{\mathrm{W}} \leq 1$ and $\kappa_{\mathrm{Z}} \leq 1$ (this assumption is denoted as $\kappa_V \leq 1$ in the following) and that $\mathrm{BR}_{\mathrm{BSM}} \geq 0$. These latter constraints are compatible with a wide range of BSM physics models. BSM physics may manifest itself in the loop-induced processes of $gg \to H$ production and $H \to \gamma\gamma$ decay. These processes are particularly sensitive to loop contributions from new heavy particles, carrying electric or colour charge, or both, and such new physics can be probed using the effective coupling modifiers κ_g and κ_γ. Furthermore, potential deviations from the SM of the tree-level couplings to ordinary particles are parameterised with their respective coupling modifiers. The parameters of interest of the fits to the data are thus the seven independent coupling modifiers, κ_γ, κ_g, κ_W, κ_Z, κ_b, κ_t and κ_τ, one for each SM particle involved in the production processes and decay channels studied, plus $\mathrm{BR}_{\mathrm{BSM}}$ in the case of the second fit.

Table 14 and Figure 14 show the results of the fits for the two scenarios discussed above in terms of the scaling of the total width of the Higgs boson, assuming either $\kappa_V \leq 1$ or $\mathrm{BR}_{\mathrm{BSM}} = 0$. In the former case, the least model-dependent upper limit of 0.34 at 95% CL is obtained for $\mathrm{BR}_{\mathrm{BSM}}$, for an expected limit of 0.35. The corresponding negative log-likelihood scan is shown in Fig. 15. The p-value of the compatibility between the data and the SM predictions in the assumption of $\mathrm{BR}_{\mathrm{BSM}} = 0$ is 11%.

Another fit, motivated for example by BSM physics scenarios containing new heavy particles which may contribute to loop processes in Higgs boson production or decay, assumes that all the couplings to SM particles are the same as in the SM, that there are no BSM decays ($BR_{BSM} = 0$), and that only the gluon-gluon production and $\gamma\gamma$ decay loops may be affected by the presence of additional particles. The results of this fit, which has only the effective coupling modifiers κ_γ and κ_g as free parameters, with all the other coupling modifiers fixed to their SM value of unity, is shown in Fig. 16. The point $\kappa_\gamma = 1$ and $\kappa_g = 1$ lies within the 68% CL contour and the p-value of the compatibility between the data and the SM predictions is 82%.

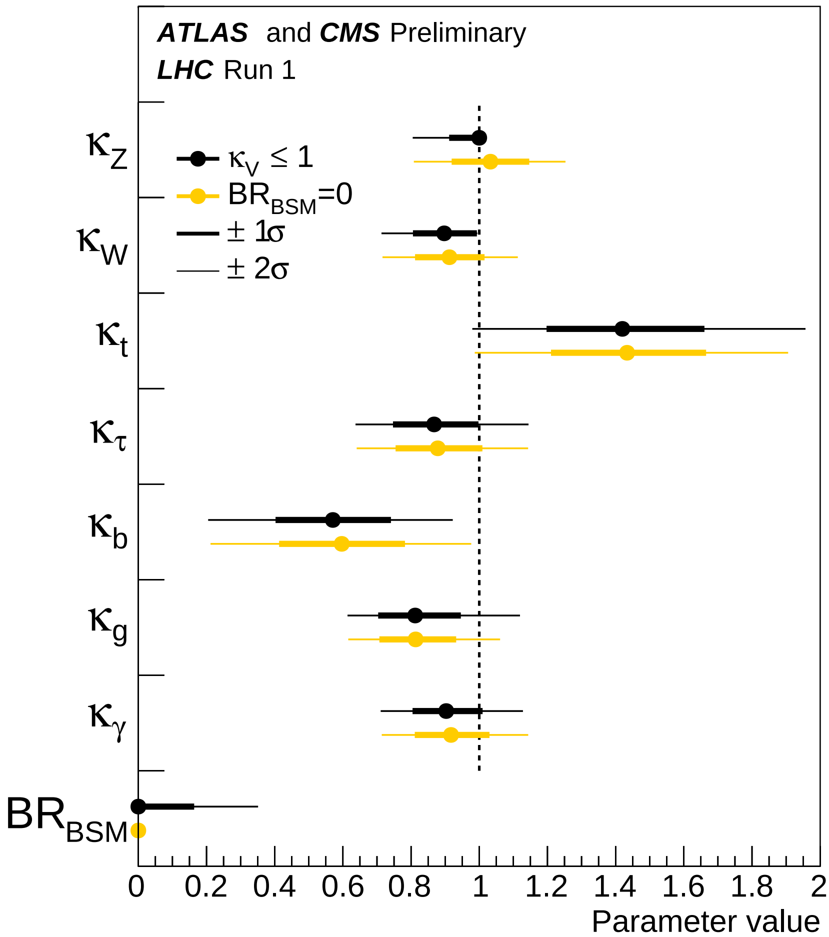

Figure 14: Fit results for the two parameterisations allowing BSM loop couplings, with $\kappa_V \leq 1$, where κ_V stands for κ_Z or κ_W, or without additional BSM contributions to the Higgs boson width, i.e. $\mathrm{BR}_{\mathrm{BSM}} = 0$. The measured results for the combination of ATLAS and CMS are reported together with their uncertainties. The error bars indicate the 1σ (thick lines) and 2σ (thin lines) intervals. The uncertainties are not indicated when the parameters are constrained and hit a boundary, namely $\kappa_V = 1$ or $\mathrm{BR}_{\mathrm{BSM}} = 0$.

Table 14: Fit results for the two parameterisations allowing BSM loop couplings, with $\kappa_V \leq 1$, where κ_V stands for κ_Z or κ_W, or without additional BSM contributions to the Higgs boson width, i.e. $\mathrm{BR}_{\mathrm{BSM}} = 0$. The measured results for the combination of ATLAS and CMS are reported together with their measured and expected uncertainties, as well as the measured results for each experiment. The uncertainties are not indicated when the parameters are constrained and hit a boundary, namely $\kappa_V = 1$ or $\mathrm{BR}_{\mathrm{BSM}} = 0$.

Parameter	ATLAS+CMS Measured	ATLAS+CMS Expected uncertainty	ATLAS Measured	CMS Measured
Parameterisation assuming $\mathrm{BR}_{\mathrm{BSM}} = 0$				
κ_Z	$1.03^{+0.11}_{-0.11}$	${}^{+0.10}_{-0.11}$	$1.00^{+0.14}_{-0.14}$	$1.07^{+0.17}_{-0.18}$
κ_W	$0.91^{+0.10}_{-0.10}$	${}^{+0.10}_{-0.11}$	$0.92^{+0.13}_{-0.13}$	$0.90^{+0.15}_{-0.15}$
κ_t	$1.43^{+0.23}_{-0.22}$	${}^{+0.26}_{-0.32}$	$1.31^{+0.30}_{-0.32}$	$1.56^{+0.34}_{-0.32}$
κ_τ	$0.88^{+0.13}_{-0.12}$	${}^{+0.16}_{-0.15}$	$0.97^{+0.19}_{-0.17}$	$0.82^{+0.19}_{-0.17}$
κ_b	$0.60^{+0.18}_{-0.18}$	${}^{+0.25}_{-0.24}$	$0.61^{+0.26}_{-0.26}$	$0.61^{+0.27}_{-0.26}$
κ_g	$0.81^{+0.11}_{-0.10}$	${}^{+0.17}_{-0.14}$	$0.94^{+0.18}_{-0.15}$	$0.70^{+0.15}_{-0.13}$
κ_γ	$0.92^{+0.11}_{-0.10}$	${}^{+0.12}_{-0.12}$	$0.88^{+0.15}_{-0.14}$	$0.96^{+0.17}_{-0.15}$
Parameterisation assuming $\kappa_V \leq 1$				
κ_Z	$1.00_{-0.08}$	-0.11	$1.00_{-0.14}$	$1.00_{-0.12}$
κ_W	$0.90^{+0.09}_{-0.09}$	-0.11	$0.92^{+0.08}_{-0.13}$	$0.86^{+0.14}_{-0.13}$
κ_t	$1.42^{+0.23}_{-0.22}$	${}^{+0.27}_{-0.32}$	$1.31^{+0.34}_{-0.32}$	$1.53^{+0.35}_{-0.31}$
κ_τ	$0.87^{+0.12}_{-0.11}$	${}^{+0.14}_{-0.15}$	$0.97^{+0.21}_{-0.17}$	$0.80^{+0.18}_{-0.16}$
κ_b	$0.57^{+0.16}_{-0.16}$	${}^{+0.19}_{-0.23}$	$0.61^{+0.24}_{-0.26}$	$0.55^{+0.24}_{-0.23}$
κ_g	$0.81^{+0.13}_{-0.10}$	${}^{+0.17}_{-0.14}$	$0.94^{+0.23}_{-0.15}$	$0.70^{+0.16}_{-0.13}$
κ_γ	$0.90^{+0.10}_{-0.09}$	${}^{+0.10}_{-0.12}$	$0.88^{+0.15}_{-0.14}$	$0.93^{+0.15}_{-0.13}$
$\mathrm{BR}_{\mathrm{BSM}}$	$0.00^{+0.16}$	$+0.18$	$0.00^{+0.26}$	$0.00^{+0.23}$

6.2. Parameterisation assuming SM structure of the loops and no BSM decays

Given that the effective coupling modifiers κ_g and κ_γ are measured to be consistent with the SM expectations, it is assumed in this section that there are no new particles in these loops. The effective coupling modifiers are expressed in terms of those of the SM particles in the loops, as indicated in Table 4. This leads to a parameterisation with six free coupling modifiers: κ_W, κ_Z, κ_t, κ_b, κ_τ and κ_μ; the results of the $H \to \mu\mu$ analysis are included for this specific case. In this more constrained fit, it is also assumed that $\mathrm{BR}_{\mathrm{BSM}} = 0$ and that $\kappa_j \geq 0$.

Figure 17 and Table 15 show the results of the fit for the combination of ATLAS and CMS and separately for each experiment. From the comparison of these results with those of the fitted decay signal strengths (Table 11) or with the global signal strength $\mu = 1.09 \pm 0.11$ (Section 5.1), one notices that this fit results in lower values of the coupling modifiers than the SM expectation. This is a consequence of the low value of κ_b, as measured by the combination of ATLAS and CMS and by each experiment. A low value of κ_b reduces the total Higgs boson width through the dominant Γ^{bb} partial decay width, and, as a consequence, the measured values of all the coupling modifiers are reduced. The p-value of the compatibility between

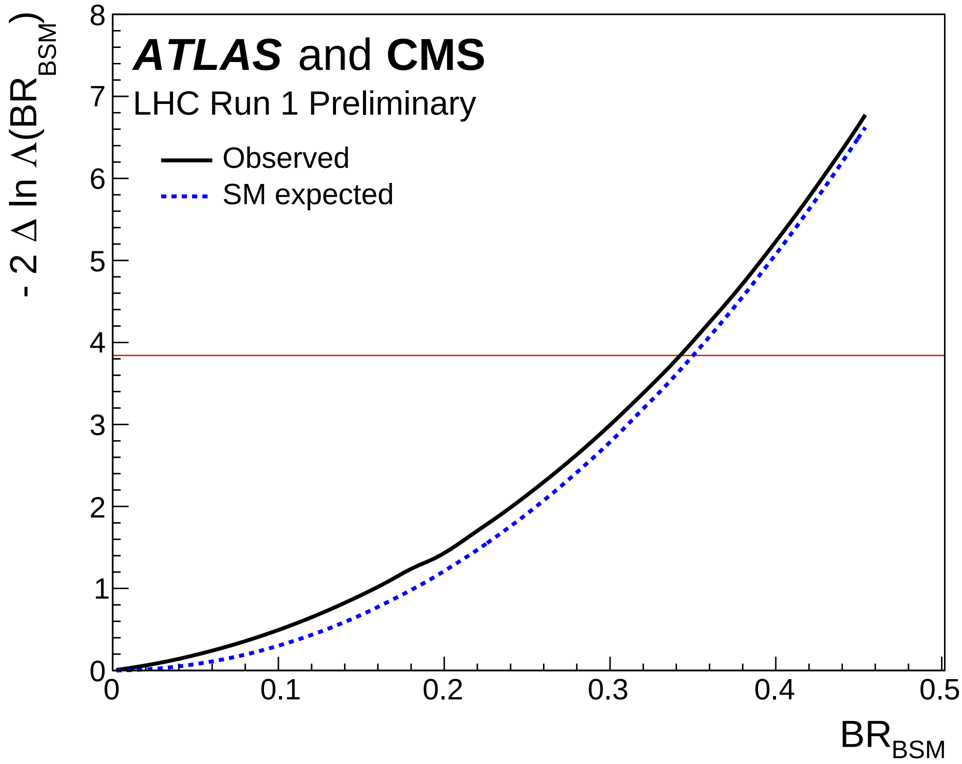

Figure 15: Observed and expected negative log-likelihood scan of BR_{BSM}, shown for the combination of ATLAS and CMS in the case of the parameterisation allowing non-SM loop couplings with additional BSM contributions to the Higgs boson width. This corresponds to the constraint $\kappa_V \leq 1$ in Fig. 14. The red horizontal line at 3.84 indicates the log-likelihood variation corresponding to the 95% CL upper limit, as discussed in Section 3.2.

the data and the SM predictions is 65%.

A different view of the relation between the fitted coupling modifiers and the SM predictions is presented in Fig. 18 which shows the same results as those of Fig. 17, expressed this time as reduced coupling modifiers defined as:

$$y_{V,i} = \sqrt{\kappa_{V,i} \frac{g_{V,i}}{2v}} = \sqrt{\kappa_{V,i}} \frac{m_{V,i}}{v}, \tag{11}$$

for the weak vector bosons with mass m_V, where $g_{V,i}$ is the absolute Higgs boson coupling strength and v is the vacuum expectation value of the Higgs field, and:

$$y_{F,i} = \kappa_{F,i} \frac{g_{F,i}}{\sqrt{2}} = \kappa_{F,i} \frac{m_{F,i}}{v}, \tag{12}$$

for fermions as a function of their mass m_F, assuming a SM Higgs boson with a mass of 125.09 GeV. The linear scaling of the reduced coupling modifiers as a function of the particle masses indicates qualitatively the consistency of the measurements with the SM. The same plot is shown in Fig. 27 in Appendix B, which also shows at the bottom the ratios of the reduced coupling modifiers to the SM predictions.

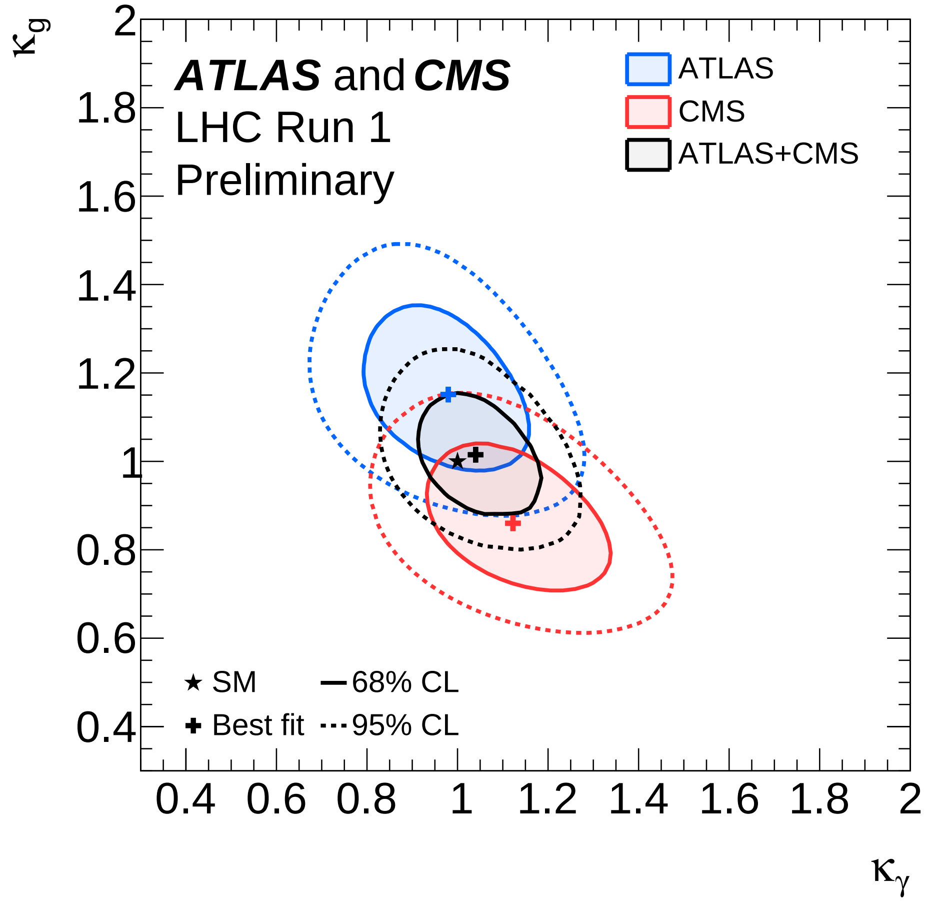

Figure 16: Negative log-likelihood contours at 68% and 95% CL of κ_γ versus κ_g for the combination of ATLAS and CMS and for each experiment separately, for the parameterisation constraining all the other coupling modifiers to their SM values and assuming $\mathrm{BR}_{\mathrm{BSM}} = 0$.

6.3. Parameterisations related to the fermion sector

Common coupling modifications for up-type fermions versus down-type fermions or for leptons versus quarks are predicted by many extensions of the SM. One such class of theoretically well motivated models is the 2HDM [81]. For example in the Minimal Supersymmetric Model [82] the coupling modifiers of neutral Higgs bosons to up- and down-type fermions may differ by a common scaling factor.

The ratios of the coupling modifiers are tested in the most generic parameterisation proposed in Ref. [27], in which the total Higgs boson width is also allowed to vary. The parameter of interest is $\lambda_{du} = \kappa_d/\kappa_u$, for the up- and down-type fermion symmetry test, and $\lambda_{lq} = \kappa_l/\kappa_q$ for the lepton and quark symmetry test, where both are allowed to be positive or negative. The other free parameters are, assuming that the coupling modifiers of the W and Z bosons are the same, $\kappa_W = \kappa_Z = \kappa_V$ and κ_H. In this parameterisation, the loops are resolved in terms of their expected SM contributions.

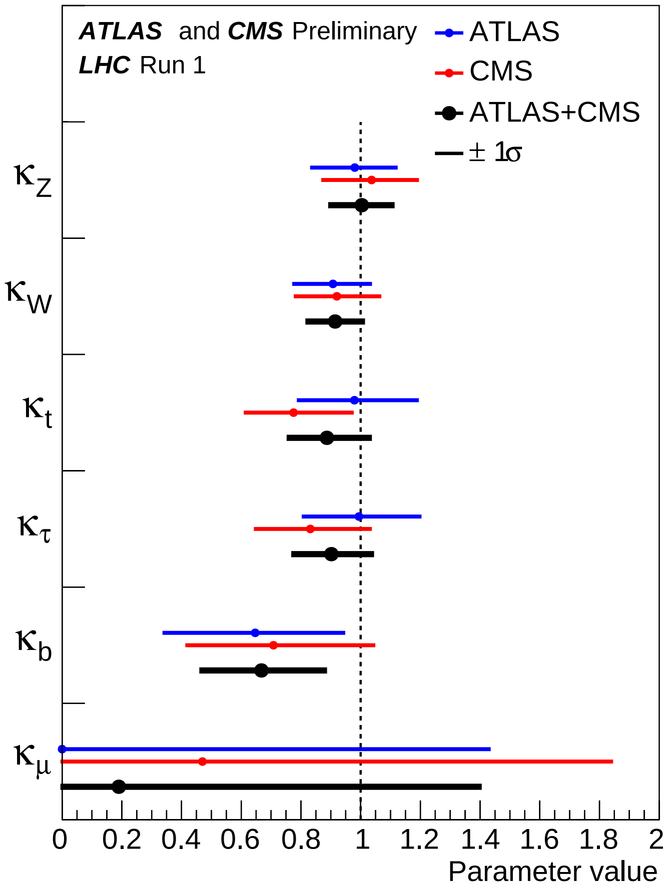

Figure 17: Best-fit values of parameters for the combination of ATLAS and CMS and separately for each experiment, for the parameterisation assuming the absence of BSM particles in the loops, $\mathrm{BR_{BSM}} = 0$, and $\kappa_j \geq 0$. The uncertainties are not indicated when the parameters are constrained and hit a boundary, namely $\kappa_j = 0$.

6.3.1. Probing the up- and down-type fermion symmetry

The parameterisation for this test has as free parameters $\lambda_{du} = \kappa_d/\kappa_u$, $\lambda_{Vu} = \kappa_V/\kappa_u$ and $\kappa_{uu} = \kappa_u \cdot \kappa_u/\kappa_H$. The up-type fermion couplings are mainly probed by the ggF production process, the $H \to \gamma\gamma$ decay channel and to a certain extent by the ttH production process. The down-type fermion couplings are mainly probed by the $H \to bb$ and $H \to \tau\tau$ decays and a small sensitivity to the relative sign comes from the interference between top and bottom quarks in the gluon fusion loop.

The results of the fit are reported in Fig. 19 and in Table 16. The corresponding likelihood scan for the λ_{du} parameter and for the combination of ATLAS and CMS is shown in Fig. 20. The p-value of the compatibility between the data and the SM predictions is 67%.

6.3.2. Probing the lepton and quark symmetry

The parameterisation for this test is very similar to that in Section 6.3.1 which probes the up- and down-type fermion symmetry. In this case, the free parameters are $\lambda_{lq} = \kappa_l/\kappa_q$, $\lambda_{Vq} = \kappa_V/\kappa_q$ and $\kappa_{qq} = \kappa_q \cdot \kappa_q/\kappa_H$.

Table 15: Fit results for the parameterisation assuming the absence of BSM particles in the loops, $\mathrm{BR}_{\mathrm{BSM}} = 0$, and $\kappa_j \geq 0$. The measured results with their measured and expected uncertainties are reported for the combination of ATLAS and CMS, together with the measured results with their uncertainties for each experiment. The uncertainties are not indicated when the parameters are constrained and hit a boundary, namely $\kappa_j = 0$.

Parameter $\kappa_j \geq 0$	ATLAS+CMS Measured	ATLAS+CMS Expected uncertainty	ATLAS Measured	CMS Measured
κ_Z	$1.00^{+0.10}_{-0.11}$	$^{+0.10}_{-0.10}$	$0.98^{+0.14}_{-0.14}$	$1.04^{+0.15}_{-0.16}$
κ_W	$0.91^{+0.09}_{-0.09}$	$^{+0.09}_{-0.09}$	$0.91^{+0.12}_{-0.13}$	$0.92^{+0.14}_{-0.14}$
κ_t	$0.89^{+0.15}_{-0.13}$	$^{+0.14}_{-0.13}$	$0.98^{+0.21}_{-0.18}$	$0.78^{+0.20}_{-0.16}$
κ_τ	$0.90^{+0.14}_{-0.13}$	$^{+0.15}_{-0.14}$	$0.99^{+0.20}_{-0.18}$	$0.83^{+0.20}_{-0.18}$
κ_b	$0.67^{+0.22}_{-0.20}$	$^{+0.23}_{-0.22}$	$0.65^{+0.29}_{-0.30}$	$0.71^{+0.34}_{-0.29}$
κ_μ	$0.2^{+1.2}_{-0.2}$	$^{+0.9}_{-1.0}$	$0.0^{+1.4}$	$0.5^{+1.4}_{-0.5}$

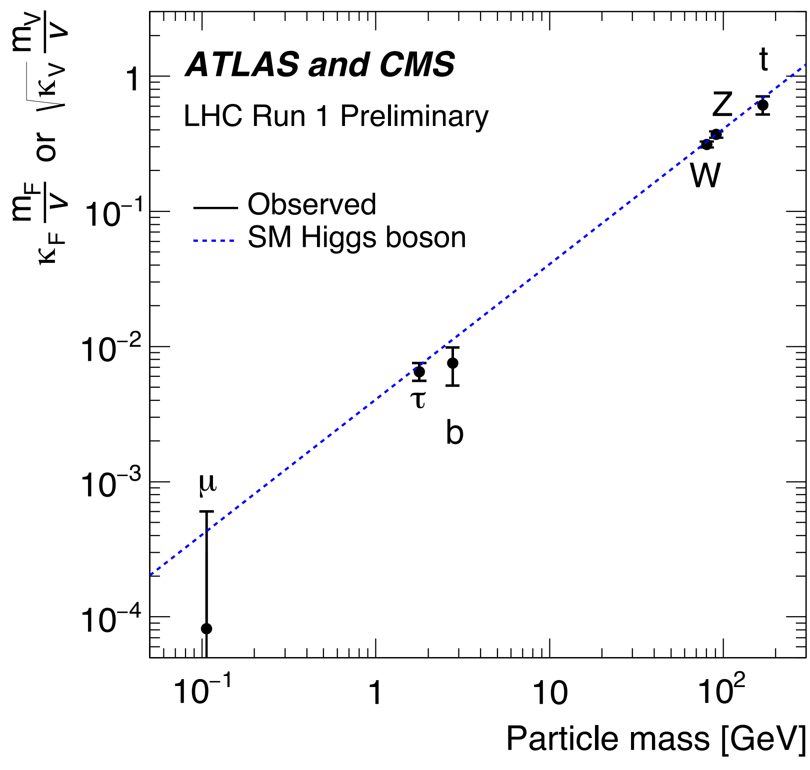

Figure 18: Fit results for the combination of ATLAS and CMS in the case of the parameterisation with reduced coupling modifiers $y_{V,i} = \sqrt{\kappa_{V,i} \frac{g_{V,i}}{2v}} = \sqrt{\kappa_{V,i}} \frac{m_{V,i}}{v}$ for the weak vector bosons, and $y_{F,i} = \kappa_{F,i} \frac{g_{F,i}}{\sqrt{2}} = \kappa_{F,i} \frac{m_{F,i}}{v}$ for the fermions, as a function of the particle mass. The dashed line indicates the predicted dependence on the particle mass for the SM Higgs boson.

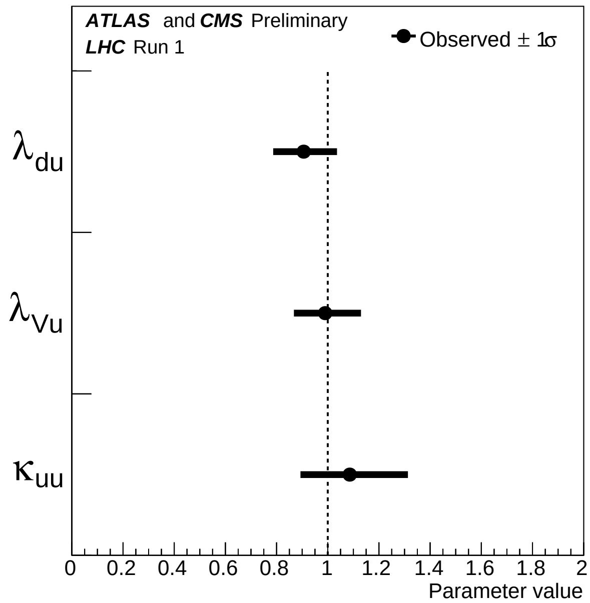

Figure 19: 1σ intervals for combined results of the λ_{du}, λ_{Vu} and κ_{uu} parameters from fits with the most general parameterisation testing the up- and down-fermion coupling ratios. The negative range for λ_{du} is not shown because no values are allowed in the 68% CL interval, as can be seen in Fig. 20.

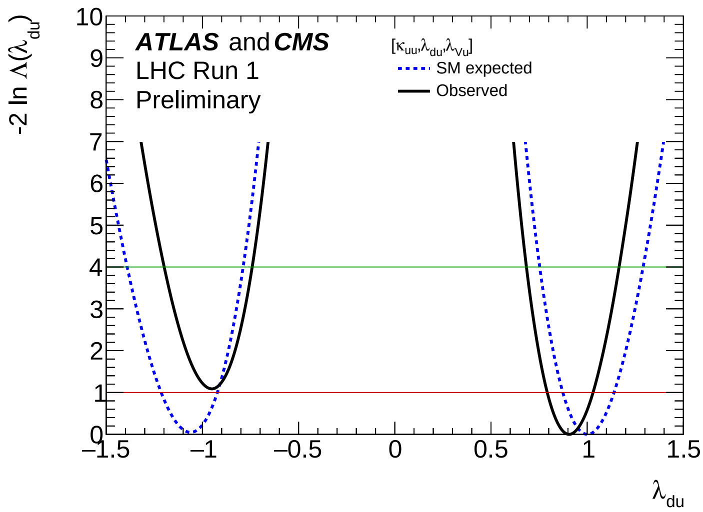

Figure 20: Negative log-likelihood scan of the λ_{du} parameter, probing the ratios of coupling modifiers for up-type versus down-type fermions for the combination of ATLAS and CMS, while profiling the other two parameters λ_{Vu} and κ_{uu}. Both observed (solid) and expected (dotted) curves are shown.

The quark couplings are mainly probed by the ggF process, the $H \to \gamma\gamma$ and $H \to bb$ decays, and to a lesser extent by the ttH process. The lepton couplings are probed by the $H \to \tau\tau$ decays and the results are expected to be insensitive to the relative sign of the couplings because there is no sizeable lepton-quark interference in any of the relevant Higgs boson production and decay processes.

The results of the fit of the λ_{lq} parameter in terms of 1σ intervals are reported in Fig. 21 and in Table 16.

Table 16: Summary of fit results for the two parameterisations probing the ratios of coupling modifiers for up-type versus down-type fermions and for leptons versus quarks. The measured results are reported for the combination of ATLAS and CMS, together with the measured and expected uncertainties.

Parameter	ATLAS+CMS	
	Measured	Expected uncertainty
λ_{du}	$0.91^{+0.12}_{-0.11}$	$[-1.21, -0.92] \cup [0.87, 1.14]$
λ_{Vu}	$0.99^{+0.13}_{-0.12}$	$^{+0.20}_{-0.12}$
κ_{uu}	$1.09^{+0.22}_{-0.19}$	$^{+0.20}_{-0.27}$
$\lvert\lambda_{lq}\rvert$	$1.06^{+0.15}_{-0.14}$	$^{+0.16}_{-0.14}$
λ_{Vq}	$1.09^{+0.14}_{-0.13}$	$^{+0.13}_{-0.11}$
κ_{qq}	$0.94^{+0.17}_{-0.15}$	$^{+0.18}_{-0.16}$

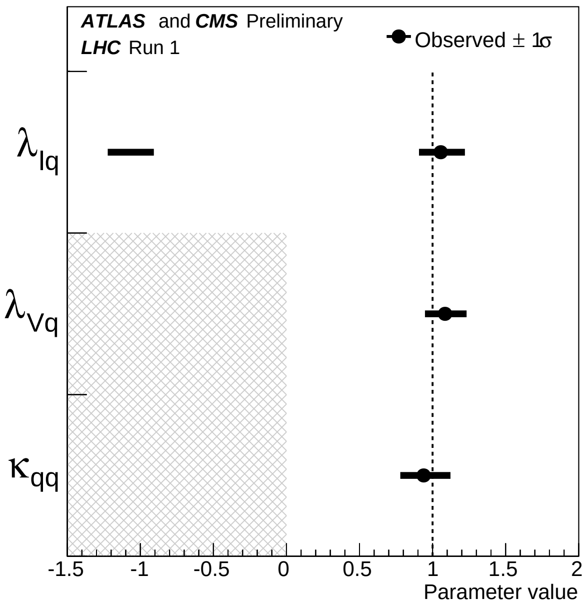

Figure 21: 1σ intervals for combined results of the λ_{lq}, λ_{Vq} and κ_{qq} parameters from fits with the most general parameterisation testing the lepton and quark coupling ratios. The hatched areas indicate the parameters which are assumed to be positive without loss of generality.

The corresponding likelihood scan for the combination is shown in Fig. 22. The p-value of the compatibility between the data and the SM predictions is 78%.

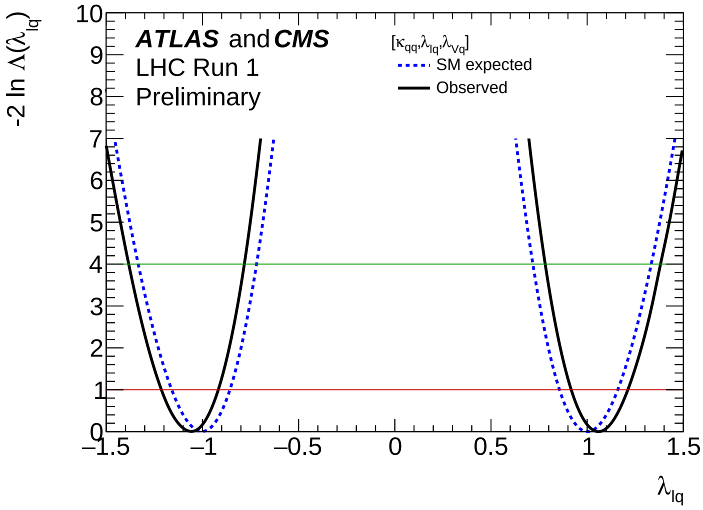

Figure 22: Negative log-likelihood scan of the λ_{lq} parameter, profiling the other two parameters λ_{Vq} and κ_{qq}. Both observed (solid) and expected (dotted) curves are shown.

6.4. Fermion and vector boson couplings

The last and most constrained parameterisation studied in this paper is motivated by the intrinsic difference between the Higgs boson couplings to vector bosons, which originate from the breaking of the electroweak symmetry, and the Yukawa couplings to the fermions. Similarly to Section 6.2, it is assumed in this section that there are no new particles in the loops (ggF production process and $H \to \gamma\gamma$ decay channel) and that there are no BSM decays, i.e. $\mathrm{BR}_{\mathrm{BSM}} = 0$. Vector and fermion coupling modifiers, κ_V and κ_F, are defined, such that $\kappa_Z = \kappa_W = \kappa_V$ and $\kappa_t = \kappa_\tau = \kappa_b = \kappa_F$. These definitions can either be applied globally, yielding two parameters, or separately for each of the five decay channels, yielding ten parameters κ_V^f and κ_F^f (following the notation related to Higgs boson decays used for the signal strength parameterisation). Two fits are then performed: a 2-parameter global fit as a function of κ_V and κ_F and a 10-parameter fit yielding the best-fit values of κ_V^f and κ_F^f for each decay channel while profiling all the other parameters.

Even though the SM values of κ_V and κ_F are assumed to be unity, new physics could in principle manifest itself through negative values of these parameters. However, as explained in Section 2.4 and shown explicitly in Table 4, the Higgs boson production cross sections and partial decay widths are only sensitive to products of coupling modifiers and not to their absolute sign. In addition, any sensitivity to the relative sign between κ_V and κ_F can only occur through interference terms, either in the $H \to \gamma\gamma$ decays, through the $t - W$ interference in the $\gamma\gamma$ decay loop, or in $ggZH$ or tH production, as explained in Section 2.4. Without any loss of generality, one can therefore assume that one of the two modifiers can be negative, namely κ_F, for historical reasons in this specific case (note that throughout the rest of this paper, the general assumption has been the opposite, namely that κ_t is positive).

In a first step, assuming that in all cases κ_F and κ_V are both positive, likelihood scans are carried out for the two global coupling modifiers and for those of each decay channel. The results of these scans are shown in Fig. 23 (top), while Fig. 23 (bottom) presents again, on an enlarged scale, the results of the scan carried out for the global coupling modifiers, as well as those obtained for each experiment. The most precise determination of κ_F^f and κ_V^f is obtained from the $H \rightarrow WW$ decay channel because it is the only one which at the same time provides significant constraints on both parameters, through the ggF and VBF categories. The combination of all decay modes brings significant additional constraints. All results are in agreement with the SM prediction of $\kappa_F^f = 1$ and $\kappa_V^f = 1$. It is also clear that the combination of ATLAS and CMS provides significantly stronger constraints on any contributions from BSM physics than those from the individual experiments. The p-value of the compatibility between the data and the SM predictions is 59%.

In a second step, it is interesting to examine the case when the relative sign between the values of κ_F^f and κ_V^f can be also negative, as shown in Fig. 24 for the combination of ATLAS and CMS and for each individual decay channel as well as for their global combination. The individual decay channels are clearly compatible with each other only for positive values of κ_F^f. The incompatibility between the channels for negative values of κ_F^f arises mostly from the $H \rightarrow \gamma\gamma$, $H \rightarrow WW$ and $H \rightarrow ZZ$ channels. However, the best-fit values for most of the individual channels correspond to negative values of κ_F^f, which is in contrast with the best-fit value of the global fit to all channels which yields $\kappa_F \geq 0$, a result which is mostly driven by the large asymmetry between positive and negative coupling modifier ratio in the case of $H \rightarrow \gamma\gamma$ decays.

These two features (global minimum for $\kappa_F^f \geq 0$) and individual channel minima for $\kappa_F^f \leq 0$) have a different origin. Concerning the global minimum, Fig. 25 (a-e) shows from the likelihood scans of κ_F^f for each decay channel that none of the decay channels alone has any significant sensitivity to the relative sign of the two coupling modifiers. However, the channel most sensitive to the relative sign of the couplings is the $H \rightarrow \gamma\gamma$ decay channel: because of the $t - W$ interference in the $\gamma\gamma$ loop, the $H \rightarrow \gamma\gamma$ partial width would be much larger if the sign of $\kappa_F^{\gamma\gamma}$ were opposite to that of $\kappa_V^{\gamma\gamma}$. When combining the $H \rightarrow \gamma\gamma$ decay channel with all the other channels, the overall sensitivity to the sign is at the level of almost 5σ, as can be seen from Fig. 25 (f).

The fact that four out of five individual channels present minima for $\kappa_F^f \leq 0$ is much less significant, as shown by the likelihood curves in Fig. 25 (a-e). The $H \rightarrow bb$ decay channel has the largest expected sensitivity, mainly owing to the contribution of the $ggZH$ process and the best-fit value of κ_F^{bb} is positive. In all other decay modes, the small sensitivity is due to the tH process, and the excess observed in the combination of the two experiments for the ttH production process induces a preference for a relative negative sign between the two coupling modifiers, which increases significantly the tH cross section and thereby provides a better fit to the data. The only visible difference between the two minima at positive and negative values of κ_F^f is observed for the $H \rightarrow WW$ channel. The difference in size between the $H \rightarrow WW$ contours in the region $\kappa_F^f \geq 0$ between Figs 23 (top), where it is explicitly assumed that $\kappa_F^f \geq 0$, and Fig. 24 is due to the fact that the negative log-likelihood contours are evaluated using as a reference the minima obtained from different likelihood fits.

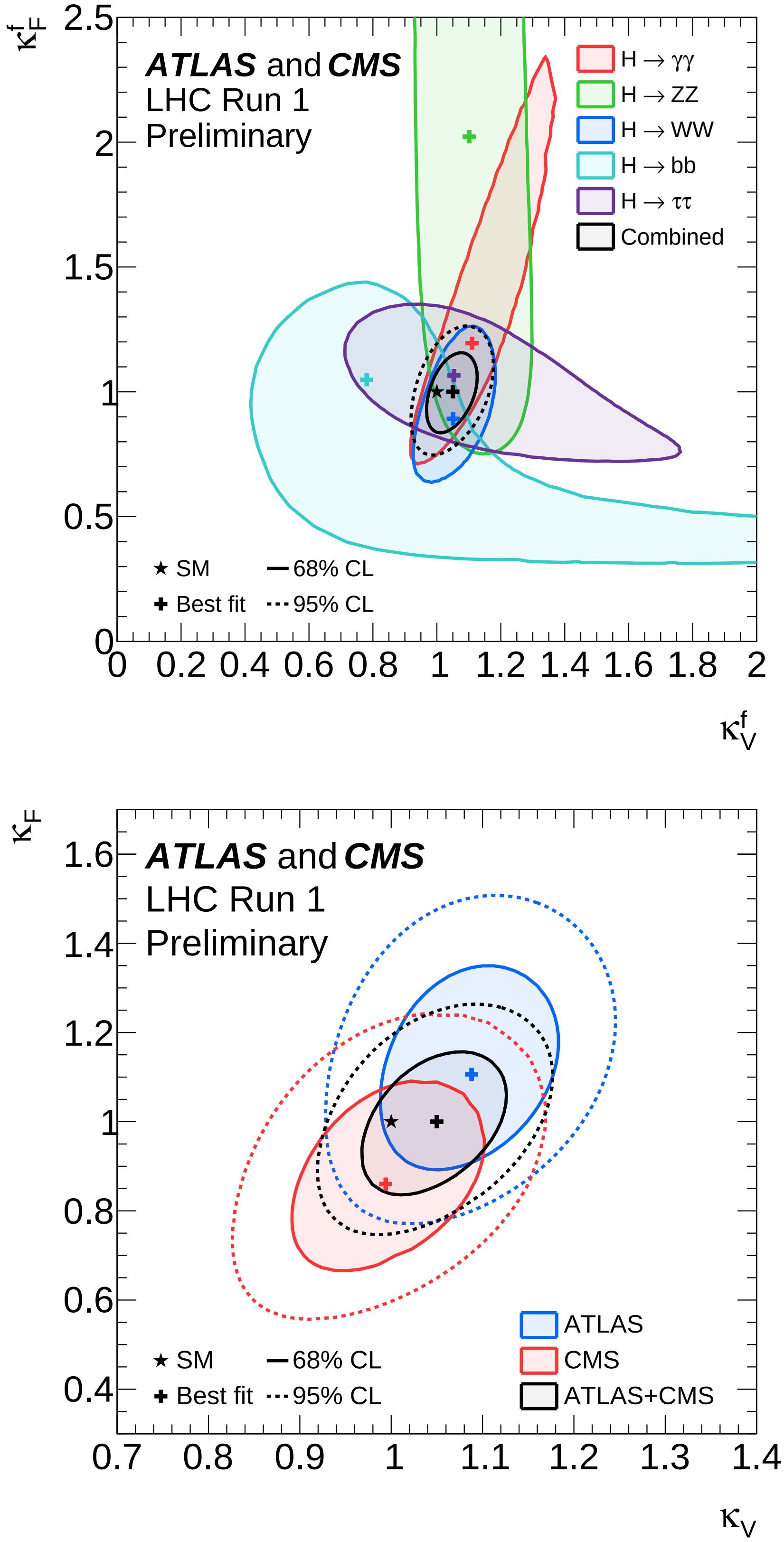

Figure 23: Top: negative log-likelihood contours of κ_F^f versus κ_V^f for the combination of ATLAS and CMS and for the individual decay channels as well as for their global combination (κ_F versus κ_V shown in black), assuming that all coupling modifiers are positive. Bottom: negative log-likelihood contours of κ_F versus κ_V on an enlarged scale for the combination of ATLAS and CMS and for the global fit of all channels. Also shown are the contours obtained for each experiment.

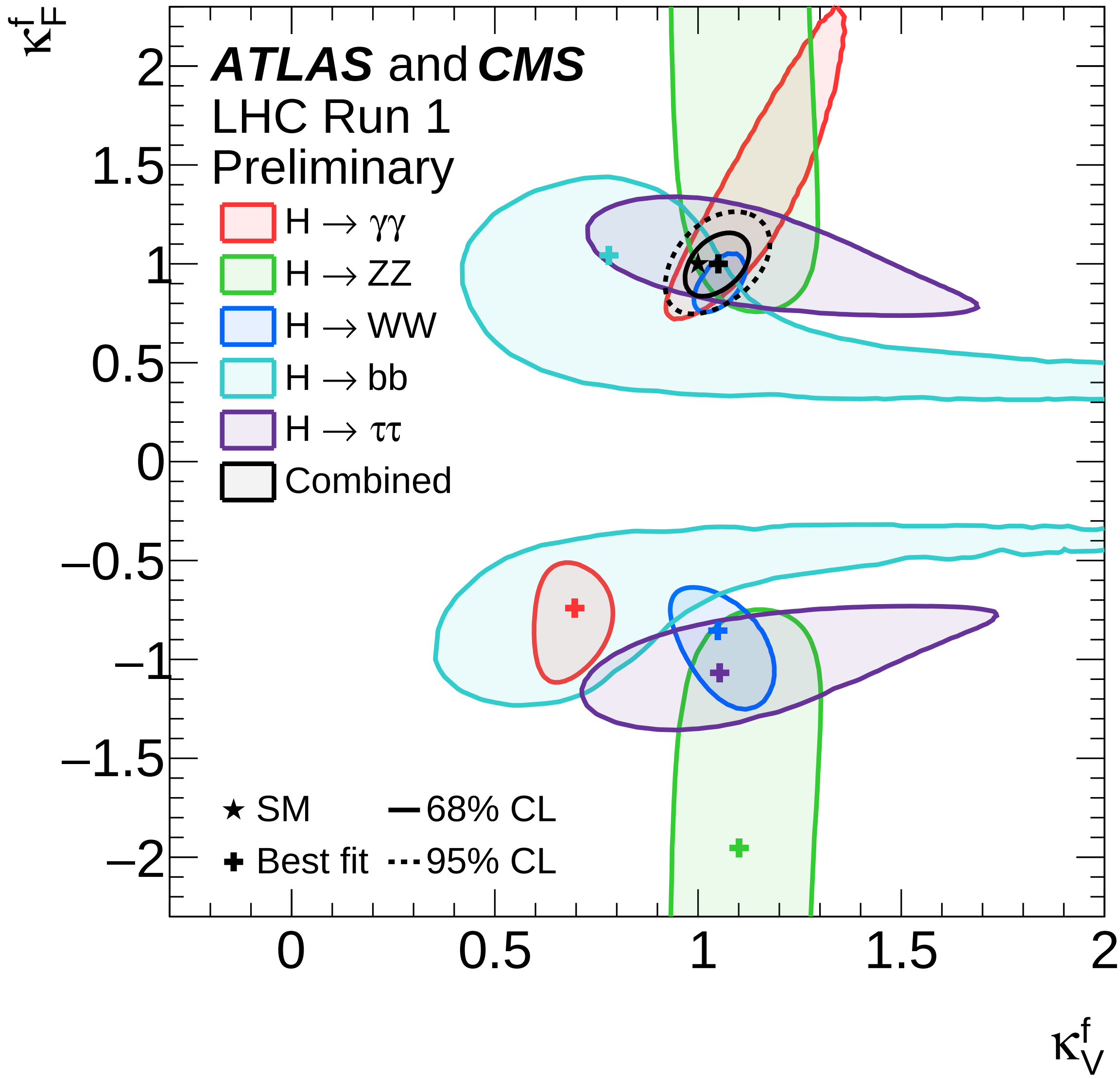

Figure 24: Negative log-likelihood contours of κ_F^f versus κ_V^f for the combination of ATLAS and CMS and for the individual decay channels, as well as for their global combination (κ_F versus κ_V shown in black), without any assumptions on the sign of the coupling modifiers. The other two quadrants (not shown) are symmetric with respect to the point (0,0).

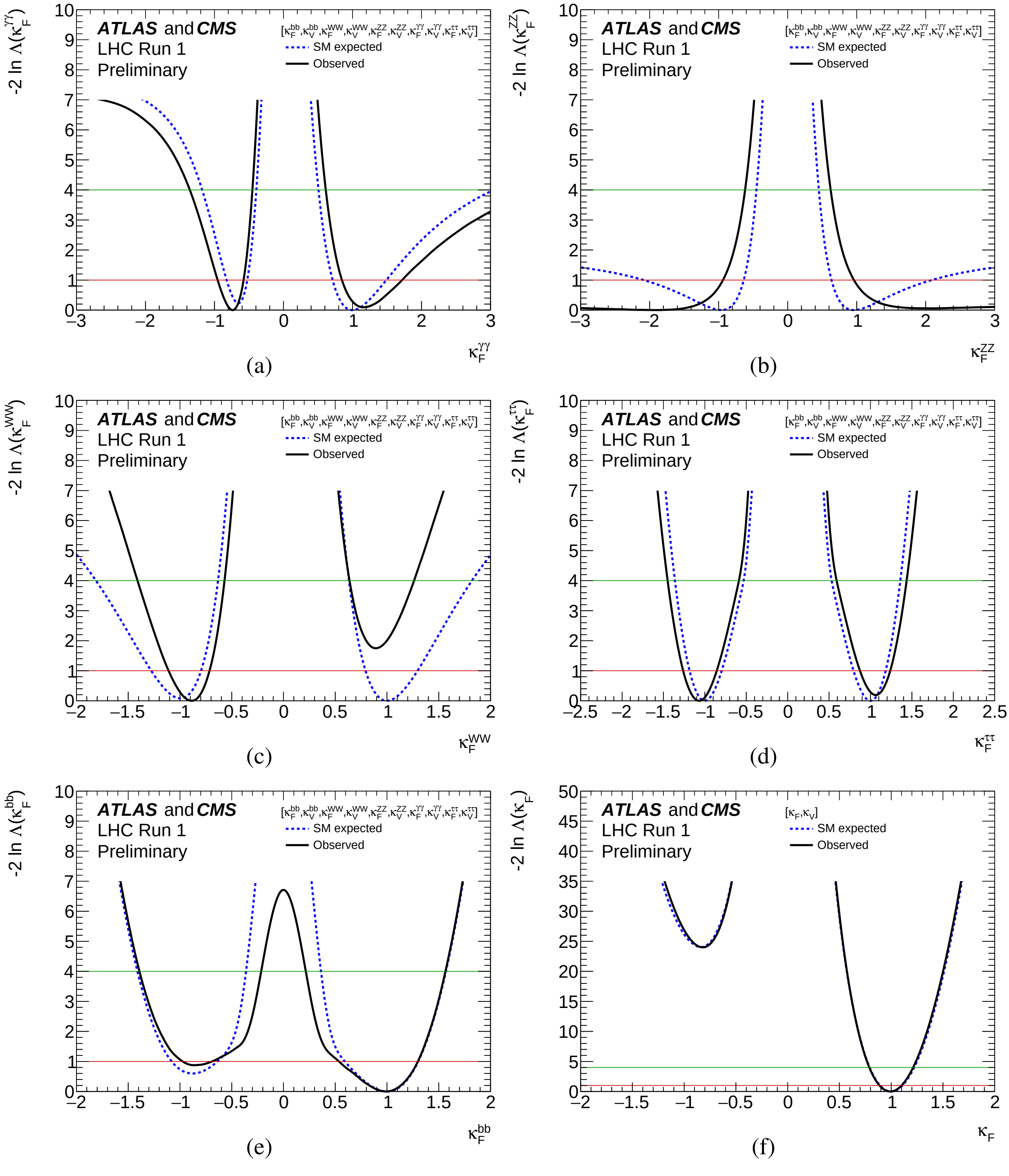

Figure 25: Negative log-likelihood scans for the five κ_F^f parameters, corresponding to each individual decay channel, and for the global κ_F parameter, corresponding to the combination of all decay channels: (a) $\kappa_F^{\gamma\gamma}$, (b) κ_F^{ZZ}, (c) κ_F^{WW}, (d) $\kappa_F^{\tau\tau}$, (e) κ_F^{bb}, and (f) κ_F.

7. Summary

Combined ATLAS and CMS measurements of the Higgs boson production and decay rates have been performed and constraints on its couplings to vector bosons and fermions have been derived. The combination is based on the analysis of five production processes, ggF, VBF, WH, ZH and ttH, and of six decay channels, $H \to ZZ, WW, \gamma\gamma, \tau\tau, bb$ and $\mu\mu$. All results are reported assuming a value of 125.09 GeV for the Higgs boson mass, the result of the combined Higgs boson mass measurement by the two experiments. The analysis uses the LHC proton-proton collision datasets recorded by the ATLAS and CMS detectors in 2011 and 2012, corresponding to integrated luminosities per experiment of approximately 5 fb^{-1} at $\sqrt{s} = 7$ TeV and 20 fb^{-1} at $\sqrt{s} = 8$ TeV.

The Higgs boson production and decay rates of the two experiments are combined within the context of two generic parameterisations: one based on ratios of cross sections and branching ratios and the other based on ratios of coupling modifiers, introduced within the context of a leading-order Higgs boson coupling framework. The combined signal yield relative to the Standard Model expectation is measured to be 1.09 ± 0.11 and the combination of the two experiments leads to observed significances of the VBF production process and of the $H \to \tau\tau$ decay at the level of 5.4σ and 5.5σ, respectively. Several interpretations of the results with more model-dependent parameterisations, derived from the generic ones, are also given. The data are consistent with the Standard Model predictions for all parameterisations considered.

References

[1] ATLAS Collaboration, *The ATLAS Experiment at the CERN Large Hadron Collider*, JINST **3** (2008) S08003.

[2] CMS Collaboration, *The CMS experiment at the CERN LHC*, JINST **3** (2008) S08004.

[3] F. Englert and R. Brout, *Broken Symmetry and the Mass of Gauge Vector Mesons*, Phys. Rev. Lett. **13** (1964) 321.

[4] P. W. Higgs, *Broken symmetries, massless particles and gauge fields*, Phys. Lett. **12** (1964) 132.

[5] P. W. Higgs, *Broken Symmetries and the Masses of Gauge Bosons*, Phys. Rev. Lett. **13** (1964) 508.

[6] G. S. Guralnik, C. R. Hagen, and T. W. B. Kibble, *Global conservation laws and massless particles*, Phys. Rev. Lett. **13** (1964) 585.

[7] P. W. Higgs, *Spontaneous symmetry breakdown without massless bosons*, Phys. Rev. **145** (1966) 1156.

[8] T. W. B. Kibble, *Symmetry breaking in non-Abelian gauge theories*, Phys. Rev. **155** (1967) 1554.

[9] Y. Nambu and G. Jona-Lasinio, *Dynamical Model of Elementary Particles Based on an Analogy with Superconductivity. I*, Phys. Rev. **122** (1961) 345.

[10] M. Gell-Mann and M. Levy, *The axial vector current in beta decay*, Nuovo Cim. **16** (1960) 705.

[11] ATLAS Collaboration, *Observation of a new particle in the search for the Standard Model Higgs boson with the ATLAS detector at the LHC*, Phys. Lett. **B716** (2012) 1, `arXiv:1207.7214 [hep-ex]`.

[12] CMS Collaboration, *Observation of a new boson at a mass of 125 GeV with the CMS experiment at the LHC*, Phys. Lett. **B716** (2012) 30, `arXiv:1207.7235 [hep-ex]`.

[13] ATLAS Collaboration, *Measurements of the Higgs boson production and decay rates and coupling strengths using pp collision data at* $\sqrt{s} = 7$ *and* 8 *TeV in the ATLAS experiment*, `arXiv:1507.04548 [hep-ex]`.

[14] CMS Collaboration, *Precise determination of the mass of the Higgs boson and tests of compatibility of its couplings with the standard model predictions using proton collisions at 7 and 8 TeV*, Accepted for publication in *Eur. Phys. J. C*, 2014.

[15] CMS Collaboration, *Study of the Mass and Spin-Parity of the Higgs Boson Candidate Via Its Decays to Z Boson Pairs*, Phys. Rev. Lett. **110** no. 8, (2013) 081803, `arXiv:1212.6639 [hep-ex]`.

[16] ATLAS Collaboration, *Evidence for the spin-0 nature of the Higgs boson using ATLAS data*, Phys. Lett. **B726** (2013) 120, `arXiv:1307.1432 [hep-ex]`.

[17] CMS Collaboration, *Constraints on the spin-parity and anomalous HVV couplings of the Higgs boson in proton collisions at 7 and 8 TeV*, Accepted for publication in *Phys. Rev. D*, 2014.

[18] ATLAS and CMS Collaborations, *Combined Measurement of the Higgs Boson Mass in pp Collisions at* $\sqrt{s} = 7$ *and* 8 *TeV with the ATLAS and CMS Experiments*, PRL **114** (2015) 191803, `arXiv:1503.07589 [hep-ex]`.

[19] ATLAS Collaboration, *Determination of the off-shell Higgs boson signal strength in the high-mass ZZ and WW final states with the ATLAS detector*, arXiv:1503.01060 [hep-ex].

[20] CMS Collaboration, *Constraints on the Higgs boson width from off-shell production and decay to Z-boson pairs,*, Phys. Lett. **B736** (2014) 64, arXiv:1405.3455 [hep-ex].

[21] ATLAS Collaboration, *Measurements of fiducial and differential cross sections for Higgs boson production in the diphoton decay channel at $\sqrt{s}$ = 8 TeV with ATLAS*, JHEP **1409** (2014) 112, arXiv:1407.4222 [hep-ex].

[22] ATLAS Collaboration, *Fiducial and differential cross sections of Higgs boson production measured in the four-lepton decay channel in pp collisions at $\sqrt{s}$=8 TeV with the ATLAS detector*, Phys. Lett. **B738** (2014) 234, arXiv:1408.3226 [hep-ex].

[23] CMS Collaboration, *Measurement of differential cross sections for Higgs boson production in the diphoton decay channel in pp collisions at $\sqrt{s}$ = 8 TeV*, Submitted for publication in *Eur. Phys. J. C*, arXiv:1508.07819 [hep-ex].

[24] CMS Collaboration, *Measurement of inclusive and differential fiducial cross sections for Higgs boson production in the H-to-4l decay channel in p-p collisions at 7 TeV and 8 TeV*, CMS Physics Analysis Summary CMS-PAS-HIG-14-028, 2015. http://cdsweb.cern.ch/record/2040210.

[25] S. Dittmaier et al., *Handbook of LHC Higgs Cross Sections: 1. Inclusive Observables*, arXiv:1101.0593 [hep-ph].

[26] S. Dittmaier et al., *Handbook of LHC Higgs Cross Sections: 2. Differential Distributions*, arXiv:1201.3084 [hep-ph].

[27] S. Heinemeyer et al., *Handbook of LHC Higgs Cross Sections: 3. Higgs Properties*, arXiv:1307.1347 [hep-ph].

[28] ATLAS Collaboration, *Search for $H \to \gamma\gamma$ produced in association with top quarks and constraints on the Yukawa coupling between the top quark and the Higgs boson using data taken at 7 TeV and 8 TeV with the ATLAS detector*, Phys. Lett. **B740** (2015) 222, arXiv:1409.3122 [hep-ex].

[29] J. Alwall, R. Frederix, S. Frixione, V. Hirschi, F. Maltoni, et al., *The automated computation of tree-level and next-to-leading order differential cross sections, and their matching to parton shower simulations*, JHEP **1407** (2014) 079, arXiv:1405.0301 [hep-ph].

[30] P. Nason, *A New method for combining NLO QCD with shower Monte Carlo algorithms*, JHEP **0411** (2004) 040, arXiv:hep-ph/0409146 [hep-ph].

[31] S. Frixione, P. Nason, and C. Oleari, *Matching NLO QCD computations with Parton Shower simulations: the POWHEG method*, JHEP **0711** (2007) 070, arXiv:0709.2092 [hep-ph].

[32] S. Alioli, P. Nason, C. Oleari, and E. Re, *NLO Higgs boson production via gluon fusion matched with shower in POWHEG*, JHEP **0904** (2009) 002, arXiv:0812.0578 [hep-ph].

[33] S. Alioli, P. Nason, C. Oleari, and E. Re, *A general framework for implementing NLO calculations in shower Monte Carlo programs: the POWHEG BOX*, JHEP **1006** (2010) 043, arXiv:1002.2581 [hep-ph].

[34] E. Bagnaschi, G. Degrassi, P. Slavich, and A. Vicini, *Higgs production via gluon fusion in the POWHEG approach in the SM and in the MSSM*, JHEP **1202** (2012) 088, arXiv:1111.2854 [hep-ph].

[35] T. Sjostrand, S. Mrenna, and P. Z. Skands, *A Brief Introduction to PYTHIA 8.1*, Comput. Phys. Commun. **178** (2008) 852, arXiv:0710.3820 [hep-ph].

[36] T. Sjostrand, S. Mrenna, and P. Z. Skands, *PYTHIA 6.4 Physics and Manual*, JHEP **0605** (2006) 026, arXiv:hep-ph/0603175 [hep-ph].

[37] M. Bahr, S. Gieseke, M. Gigg, D. Grellscheid, K. Hamilton, et al., *Herwig++ Physics and Manual*, Eur. Phys. J. **C58** (2008) 639, arXiv:0803.0883 [hep-ph].

[38] ATLAS Collaboration, *Search for the $b\bar{b}$ decay of the Standard Model Higgs boson in associated $(W/Z)H$ production with the ATLAS detector*, JHEP **1501** (2015) 069, arXiv:1409.6212 [hep-ex].

[39] CMS Collaboration, *Search for the standard model Higgs boson produced in association with a W or a Z boson and decaying to bottom quarks*, Phys. Rev. D **89** (2014) 012003, arXiv:1310.3687 [hep-ex].

[40] L. Altenkamp, S. Dittmaier, R. V. Harlander, H. Rzehak, and T. J. E. Zirke, *Gluon-induced Higgs-strahlung at next-to-leading order QCD*, J. High Energy Phys. **02** (2013) 078, arXiv:1211.5015 [hep-ph].

[41] M. M. C. Englert and M. Spannowsky, *Gluon-initiated associated production boosts Higgs physics*, Phys. Rev. **D89** (2014) 013013, arXiv:1310.4828 [hep-ph].

[42] G. Luisoni, P. Nason, C. Oleari, and F. Tramontano, *$HW^{\pm}/HZ + 0$ and 1 jet at NLO with the POWHEG BOX interfaced to GoSam and their merging within MiNLO*, J. High Energy Phys. **10** (2013) 083, arXiv:1306.2542 [hep-ph].

[43] G. Ferrera, M. Grazzini, and F. Tramontano, *Associated ZH production at hadron colliders: The fully differential NNLO QCD calculation*, Phys. Lett. B **740** (2015) 51, arXiv:1407.4747 [hep-ph].

[44] G. Bevilacqua, M. Czakon, M. Garzelli, A. van Hameren, A. Kardos, et al., *HELAC-NLO*, Comput. Phys. Commun. **184** (2013) 986, arXiv:1110.1499 [hep-ph].

[45] M. Garzelli, A. Kardos, C. G. Papadopoulos, and Z. Trocsanyi, *Standard Model Higgs boson production in association with a top anti-top pair at NLO with parton showering*, arXiv:1108.0387 [hep-ph].

[46] F. Maltoni and T. Stelzer, *MadEvent: Automatic event generation with MadGraph*, JHEP **0302** (2003) 027, arXiv:hep-ph/0208156 [hep-ph].

[47] D. de Florian, G. Ferrera, M. Grazzini, and D. Tommasini, *Higgs boson production at the LHC: transverse momentum resummation effects in the H –> 2gamma, H –> WW –> lnulnu and H –> ZZ –> 4l decay modes*, JHEP **1206** (2012) 132, arXiv:1203.6321 [hep-ph].

[48] M. Grazzini and H. Sargsyan, *Heavy-quark mass effects in Higgs boson production at the LHC*, JHEP **1309** (2013) 129, arXiv:1306.4581 [hep-ph].

[49] J. M. Campbell, R. K. Ellis, and G. Zanderighi, *Next-to-Leading order Higgs + 2 jet production via gluon fusion*, JHEP **10** (2006) 028, arXiv:hep-ph/0608194 [hep-ph].

[50] F. M. B. Hespel and E. Vryonidou, *Higgs and Z boson associated production via gluon fusion in the SM and the 2HDM*, JHEP **1506** (2015) 065, arXiv:1503.01656 [hep-ph].

[51] ATLAS Collaboration, *Measurement of Higgs boson production in the diphoton decay channel in pp collisions at center-of-mass energies of 7 and 8 TeV with the ATLAS detector*, Phys. Rev. **D90** (2014) 112015, arXiv:1408.7084 [hep-ex].

[52] CMS Collaboration, *Observation of the diphoton decay of the 125 GeV Higgs boson and measurement of its properties*, Eur. Phys. J. C **74** (2014) 3076, arXiv:1407.0558 [hep-ex].

[53] ATLAS Collaboration, *Measurements of Higgs boson production and couplings in the four-lepton channel in pp collisions at center-of-mass energies of 7 and 8 TeV with the ATLAS detector*, Phys. Rev. **D91** (2015) 012006, arXiv:1408.5191 [hep-ex].

[54] CMS Collaboration, *Measurement of the properties of a Higgs boson in the four-lepton final state*, Phys. Rev. D **89** (2014) 092007, arXiv:1312.5353 [hep-ex].

[55] ATLAS Collaboration, *Observation and measurement of Higgs boson decays to WW^* with the ATLAS detector*, Phys. Rev. **D92** (2015) 012006, arXiv:1412.2641 [hep-ex].

[56] ATLAS Collaboration, *Study of the Higgs boson decaying to WW* produced in association with a weak boson with the ATLAS detector at the LHC*, JHEP **1508** (2015) 137, arXiv:1506.06641 [hep-ph].

[57] CMS Collaboration, *Measurement of Higgs boson production and properties in the WW decay channel with leptonic final states*, JHEP **01** (2014) 096, arXiv:1312.1129 [hep-ex].

[58] ATLAS Collaboration, *Evidence for the Higgs-boson Yukawa coupling to tau leptons with the ATLAS detector*, arXiv:1501.04943 [hep-ex].

[59] CMS Collaboration, *Evidence for the 125 GeV Higgs boson decaying to a pair of τ leptons*, JHEP **05** (2014) 104, arXiv:1401.5041 [hep-ex].

[60] ATLAS Collaboration, *Search for the Standard Model Higgs boson decay to $\mu^+\mu^-$ with the ATLAS detector*, Phys. Lett. **B738** (2014) 68, arXiv:1406.7663 [hep-ex].

[61] CMS Collaboration, *Search for a standard model-like Higgs boson in the $\mu^+\mu^-$ and e^+e^- decay channels at the LHC*, Phys. Lett. **B** (2015) , arXiv:1410.6679 [hep-ex].

[62] ATLAS Collaboration, *Search for the Standard Model Higgs boson produced in association with top quarks and decaying into $b\bar{b}$ in pp collisions at $\sqrt{s} = 8$ TeV with the ATLAS detector*, Eur. Phys. J. C **75** (2015) 349, arXiv:1503.05066 [hep-ex].

[63] ATLAS Collaboration, *Search for the associated production of the Higgs boson with a top quark pair in multi-lepton final states with the ATLAS detector*, ATLAS-CONF-2015-007 (2015).

[64] CMS Collaboration, *Search for the standard model Higgs boson produced in association with a top-quark pair in pp collisions at the LHC*, JHEP **1305** (2013) 145, arXiv:1303.0763 [hep-ex].

[65] CMS Collaboration, *Search for the associated production of the Higgs boson with a top-quark pair*, JHEP **09** (2014) 087, arXiv:1408.1682 [hep-ex].

[66] ATLAS Collaboration, *Search for Higgs boson decays to a photon and a Z boson in pp collisions at $\sqrt{s}$=7 and 8 TeV with the ATLAS detector*, Phys. Lett. **B732** (2014) 8, arXiv:1402.3051 [hep-ex].

[67] CMS Collaboration, *Search for a Higgs boson decaying into a Z and a photon in pp collisions at $\sqrt{s}$ = 7 and 8 TeV*, Phys. Lett. **B726** (2013) 587–609, arXiv:1307.5515 [hep-ex].

[68] ATLAS Collaboration, *Search for Invisible Decays of a Higgs Boson Produced in Association with a Z Boson in ATLAS*, Phys. Rev. Lett. **112** (2014) 201802, arXiv:1402.3244 [hep-ex].

[69] ATLAS Collaboration, *Search for invisible decays of the Higgs boson produced in association with a hadronically decaying vector boson in pp collisions at $\sqrt{s}$ = 8 TeV with the ATLAS detector*, Eur. Phys. J. **C75** no. 7, (2015) 337, arXiv:1504.04324 [hep-ex].

[70] CMS Collaboration, *Search for invisible decays of Higgs bosons in the vector boson fusion and associated ZH production modes*, Eur. Phys. J. **C74** (2014) 2980, arXiv:1404.1344 [hep-ex].

[71] CMS Collaboration, *Search for the standard model Higgs boson produced through vector boson fusion and decaying to* $\mathrm{b\bar{b}}$, arXiv:1506.01010 [hep-ex].

[72] ATLAS and CMS Collaborations, *Procedure for the LHC Higgs boson search combination in Summer 2011*, ATL-PHYS-PUB-2011-011, CERN-CMS-NOTE-2011-005 (2011), http://cdsweb.cern.ch/record/1375842.

[73] W. Verkerke and D. P. Kirkby, *The RooFit toolkit for data modeling*, eConf **C0303241** (2003) MOLT007, [,186(2003)], arXiv:physics/0306116 [physics].

[74] L. Moneta, K. Belasco, K. S. Cranmer, S. Kreiss, A. Lazzaro, D. Piparo, G. Schott, W. Verkerke, and M. Wolf, *The RooStats Project*, PoS **ACAT2010** (2010) 057, arXiv:1009.1003 [physics.data-an].

[75] ROOT, K. Cranmer, G. Lewis, L. Moneta, A. Shibata, and W. Verkerke, *HistFactory: A tool for creating statistical models for use with RooFit and RooStats*,.

[76] G. Cowan, K. Cranmer, E. Gross, and O. Vitells, *Asymptotic formulae for likelihood-based tests of new physics*, Eur. Phys. J. **C71** (2011) 1554, arXiv:1007.1727 [physics.data-an].

[77] G. J. Feldman and R. D. Cousins, *Unified approach to the classical statistical analysis of small signals*, Phys. Rev. D **57** (1998) 3873, arXiv:physics/9711021 [physics.data-an].

[78] I. W. Stewart and F. J. Tackmann, *Theory Uncertainties for Higgs and Other Searches Using Jet Bins*, Phys. Rev. **D85** (2012) 034011, arXiv:1107.2117 [hep-ph].

[79] A. Banfi, G. P. Salam, and G. Zanderighi, *NLL+NNLO predictions for jet-veto efficiencies in Higgs-boson and Drell-Yan production*, JHEP **06** (2012) 159, arXiv:1203.5773 [hep-ph].

[80] A. Banfi, P. F. Monni, G. P. Salam, and G. Zanderighi, *Higgs and Z-boson production with a jet veto*, Phys. Rev. Lett. **109** (2012) 202001, arXiv:1206.4998 [hep-ph].

[81] T. Lee, *A Theory of Spontaneous T Violation*, Phys. Rev. **D8** (1973) 1226.

[82] S. Dimopoulos and H. Georgi, *Softly Broken Supersymmetry and SU(5)*, Nucl. Phys. B **193** (1981) 150.

Appendix

A. Generic models with breakdown of systematic uncertainties

The results of the generic rate model with $H \to ZZ$ as a reference are shown in Table 17. A similar model, with $H \to WW$ as reference, are shown in Table 18 and illustrated in Fig. 26.

Table 17: Best-fit values of $\sigma(gg \to H \to ZZ)$, $\sigma_i/\sigma_{\mathrm{ggF}}$ and BR^f/BR^{ZZ} from the combined analysis of the $\sqrt{s}$ = 7 and 8 TeV data. The cross-section ratios are given for $\sqrt{s}$ = 8 TeV, assuming the SM values for $\sigma_i(7\ \mathrm{TeV})/\sigma_i(8\ \mathrm{TeV})$. The results are shown for the ATLAS+CMS combination and also separately for each experiment, together with their total uncertainties and their breakdown into the four components described in the text. The expected total uncertainties on the measurements are also shown (in parentheses). The SM predictions [27] are also shown with their total uncertainties.

Parameter	SM prediction	Best-fit value	Uncertainty Stat	Expt	Thbgd	Thsig
		ATLAS+CMS				
$\sigma(gg \to H \to ZZ)$ (pb)	0.513 ±0.057	$0.58^{+0.11}_{-0.10}$ $\left(^{+0.11}_{-0.10}\right)$	$^{+0.11}_{-0.10}$ $\left(^{+0.11}_{-0.09}\right)$	$^{+0.02}_{-0.02}$ $\left(^{+0.02}_{-0.02}\right)$	$^{+0.01}_{-0.01}$ $\left(^{+0.01}_{-0.01}\right)$	$^{+0.01}_{-0.01}$ $\left(^{+0.01}_{-0.01}\right)$
$\sigma_{\mathrm{VBF}}/\sigma_{\mathrm{ggF}}$	0.082 ±0.009	$0.11^{+0.03}_{-0.03}$ $\left(^{+0.03}_{-0.02}\right)$	$^{+0.03}_{-0.02}$ $\left(^{+0.02}_{-0.02}\right)$	$^{+0.01}_{-0.01}$ $\left(^{+0.01}_{-0.01}\right)$	$^{+0.01}_{-0.00}$ $\left(^{+0.00}_{-0.00}\right)$	$^{+0.01}_{-0.01}$ $\left(^{+0.01}_{-0.01}\right)$
$\sigma_{WH}/\sigma_{\mathrm{ggF}}$	0.037 ±0.004	$0.03^{+0.03}_{-0.03}$ $\left(^{+0.02}_{-0.02}\right)$	$^{+0.02}_{-0.02}$ $\left(^{+0.02}_{-0.02}\right)$	$^{+0.01}_{-0.01}$ $\left(^{+0.01}_{-0.01}\right)$	$^{+0.01}_{-0.01}$ $\left(^{+0.01}_{-0.00}\right)$	$^{+0.00}_{-0.00}$ $\left(^{+0.00}_{-0.00}\right)$
$\sigma_{ZH}/\sigma_{\mathrm{ggF}}$	0.022 ±0.002	$0.07^{+0.04}_{-0.03}$ $\left(^{+0.02}_{-0.01}\right)$	$^{+0.03}_{-0.03}$ $\left(^{+0.01}_{-0.01}\right)$	$^{+0.02}_{-0.01}$ $\left(^{+0.01}_{-0.00}\right)$	$^{+0.01}_{-0.01}$ $\left(^{+0.01}_{-0.00}\right)$	$^{+0.01}_{-0.00}$ $\left(^{+0.00}_{-0.00}\right)$
$\sigma_{ttH}/\sigma_{\mathrm{ggF}}$	0.0067 ±0.0010	$0.022^{+0.007}_{-0.006}$ $\left(^{+0.004}_{-0.004}\right)$	$^{+0.005}_{-0.005}$ $\left(^{+0.003}_{-0.003}\right)$	$^{+0.003}_{-0.002}$ $\left(^{+0.002}_{-0.001}\right)$	$^{+0.002}_{-0.002}$ $\left(^{+0.002}_{-0.002}\right)$	$^{+0.001}_{-0.001}$ $\left(^{+0.001}_{-0.000}\right)$
$\mathrm{BR}^{WW}/\mathrm{BR}^{ZZ}$	8.10 ± < 0.01	$6.8^{+1.7}_{-1.3}$ $\left(^{+2.2}_{-1.7}\right)$	$^{+1.5}_{-1.2}$ $\left(^{+2.0}_{-1.6}\right)$	$^{+0.5}_{-0.3}$ $\left(^{+0.7}_{-0.5}\right)$	$^{+0.4}_{-0.3}$ $\left(^{+0.5}_{-0.4}\right)$	$^{+0.3}_{-0.2}$ $\left(^{+0.3}_{-0.2}\right)$
$\mathrm{BR}^{\gamma\gamma}/\mathrm{BR}^{ZZ}$	0.085 ±0.001	$0.069^{+0.018}_{-0.015}$ $\left(^{+0.025}_{-0.019}\right)$	$^{+0.018}_{-0.014}$ $\left(^{+0.024}_{-0.019}\right)$	$^{+0.003}_{-0.002}$ $\left(^{+0.005}_{-0.004}\right)$	$^{+0.002}_{-0.001}$ $\left(^{+0.002}_{-0.001}\right)$	$^{+0.002}_{-0.002}$ $\left(^{+0.003}_{-0.002}\right)$
$\mathrm{BR}^{\tau\tau}/\mathrm{BR}^{ZZ}$	2.36 ±0.05	$1.8^{+0.6}_{-0.5}$ $\left(^{+0.9}_{-0.7}\right)$	$^{+0.5}_{-0.4}$ $\left(^{+0.8}_{-0.6}\right)$	$^{+0.3}_{-0.2}$ $\left(^{+0.5}_{-0.3}\right)$	$^{+0.1}_{-0.0}$ $\left(^{+0.1}_{-0.1}\right)$	$^{+0.1}_{-0.0}$ $\left(^{+0.1}_{-0.1}\right)$
$\mathrm{BR}^{bb}/\mathrm{BR}^{ZZ}$	21.6 ±1.0	$4.2^{+4.6}_{-2.6}$ $\left(^{+16.9}_{-9.1}\right)$	$^{+2.8}_{-2.0}$ $\left(^{+13.9}_{-7.9}\right)$	$^{+2.5}_{-1.1}$ $\left(^{+6.3}_{-2.8}\right)$	$^{+2.5}_{-1.2}$ $\left(^{+6.8}_{-3.3}\right)$	$^{+0.4}_{-0.2}$ $\left(^{+2.0}_{-0.9}\right)$

Parameter	Best-fit value	Uncertainty Stat	Expt	Thbgd	Thsig
	ATLAS				
$\sigma(gg \to H \to ZZ)$ (pb)	$0.76^{+0.19}_{-0.17}$ $\left(^{+0.16}_{-0.14}\right)$	$^{+0.19}_{-0.16}$ $\left(^{+0.16}_{-0.13}\right)$	$^{+0.04}_{-0.03}$ $\left(^{+0.03}_{-0.02}\right)$	$^{+0.03}_{-0.02}$ $\left(^{+0.02}_{-0.02}\right)$	$^{+0.01}_{-0.01}$ $\left(^{+0.01}_{-0.01}\right)$
$\sigma_{\mathrm{VBF}}/\sigma_{\mathrm{ggF}}$	$0.08^{+0.03}_{-0.03}$ $\left(^{+0.04}_{-0.03}\right)$	$^{+0.03}_{-0.02}$ $\left(^{+0.04}_{-0.03}\right)$	$^{+0.01}_{-0.01}$ $\left(^{+0.02}_{-0.01}\right)$	$^{+0.01}_{-0.00}$ $\left(^{+0.01}_{-0.01}\right)$	$^{+0.01}_{-0.01}$ $\left(^{+0.01}_{-0.01}\right)$
$\sigma_{WH}/\sigma_{\mathrm{ggF}}$	$0.05^{+0.04}_{-0.03}$ $\left(^{+0.03}_{-0.02}\right)$	$^{+0.03}_{-0.02}$ $\left(^{+0.03}_{-0.02}\right)$	$^{+0.01}_{-0.01}$ $\left(^{+0.01}_{-0.01}\right)$	$^{+0.01}_{-0.01}$ $\left(^{+0.01}_{-0.01}\right)$	$^{+0.01}_{-0.00}$ $\left(^{+0.00}_{-0.00}\right)$
$\sigma_{ZH}/\sigma_{\mathrm{ggF}}$	$0.01^{+0.03}_{-0.01}$ $\left(^{+0.03}_{-0.01}\right)$	$^{+0.02}_{-0.01}$ $\left(^{+0.02}_{-0.01}\right)$	$^{+0.01}_{-0.01}$ $\left(^{+0.01}_{-0.00}\right)$	$^{+0.01}_{-0.00}$ $\left(^{+0.01}_{-0.00}\right)$	$^{+0.00}_{-0.00}$ $\left(^{+0.00}_{-0.00}\right)$
$\sigma_{ttH}/\sigma_{\mathrm{ggF}}$	$0.013^{+0.007}_{-0.005}$ $\left(^{+0.006}_{-0.004}\right)$	$^{+0.005}_{-0.004}$ $\left(^{+0.005}_{-0.004}\right)$	$^{+0.003}_{-0.002}$ $\left(^{+0.003}_{-0.002}\right)$	$^{+0.002}_{-0.002}$ $\left(^{+0.003}_{-0.002}\right)$	$^{+0.001}_{-0.001}$ $\left(^{+0.001}_{-0.000}\right)$
$\mathrm{BR}^{WW}/\mathrm{BR}^{ZZ}$	$6.5^{+2.2}_{-1.6}$ $\left(^{+3.5}_{-2.4}\right)$	$^{+2.0}_{-1.5}$ $\left(^{+3.3}_{-2.2}\right)$	$^{+0.6}_{-0.5}$ $\left(^{+0.9}_{-0.6}\right)$	$^{+0.5}_{-0.4}$ $\left(^{+0.8}_{-0.6}\right)$	$^{+0.3}_{-0.2}$ $\left(^{+0.4}_{-0.3}\right)$
$\mathrm{BR}^{\gamma\gamma}/\mathrm{BR}^{ZZ}$	$0.063^{+0.024}_{-0.018}$ $\left(^{+0.040}_{-0.027}\right)$	$^{+0.023}_{-0.017}$ $\left(^{+0.039}_{-0.027}\right)$	$^{+0.007}_{-0.004}$ $\left(^{+0.009}_{-0.005}\right)$	$^{+0.003}_{-0.002}$ $\left(^{+0.005}_{-0.002}\right)$	$^{+0.003}_{-0.002}$ $\left(^{+0.004}_{-0.003}\right)$
$\mathrm{BR}^{\tau\tau}/\mathrm{BR}^{ZZ}$	$2.2^{+1.1}_{-0.8}$ $\left(^{+1.5}_{-1.0}\right)$	$^{+0.9}_{-0.6}$ $\left(^{+1.3}_{-0.9}\right)$	$^{+0.5}_{-0.4}$ $\left(^{+0.8}_{-0.4}\right)$	$^{+0.2}_{-0.1}$ $\left(^{+0.2}_{-0.1}\right)$	$^{+0.2}_{-0.1}$ $\left(^{+0.2}_{-0.1}\right)$
$\mathrm{BR}^{bb}/\mathrm{BR}^{ZZ}$	$9.7^{+10.2}_{-5.8}$ $\left(^{+29.4}_{-11.8}\right)$	$^{+7.4}_{-4.4}$ $\left(^{+24.3}_{-10.5}\right)$	$^{+4.5}_{-2.6}$ $\left(^{+11.0}_{-3.3}\right)$	$^{+5.2}_{-2.7}$ $\left(^{+11.9}_{-4.0}\right)$	$^{+1.3}_{-0.5}$ $\left(^{+3.9}_{-1.2}\right)$

Parameter	Best-fit value	Uncertainty Stat	Expt	Thbgd	Thsig
	CMS				
$\sigma(gg \to H \to ZZ)$ (pb)	$0.44^{+0.14}_{-0.11}$ $\left(^{+0.15}_{-0.13}\right)$	$^{+0.13}_{-0.11}$ $\left(^{+0.15}_{-0.13}\right)$	$^{+0.04}_{-0.03}$ $\left(^{+0.03}_{-0.02}\right)$	$^{+0.01}_{-0.01}$ $\left(^{+0.00}_{-0.00}\right)$	$^{+0.02}_{-0.01}$ $\left(^{+0.02}_{-0.01}\right)$
$\sigma_{\mathrm{VBF}}/\sigma_{\mathrm{ggF}}$	$0.14^{+0.07}_{-0.05}$ $\left(^{+0.04}_{-0.03}\right)$	$^{+0.06}_{-0.05}$ $\left(^{+0.04}_{-0.03}\right)$	$^{+0.03}_{-0.02}$ $\left(^{+0.02}_{-0.01}\right)$	$^{+0.01}_{-0.01}$ $\left(^{+0.01}_{-0.00}\right)$	$^{+0.02}_{-0.01}$ $\left(^{+0.01}_{-0.01}\right)$
$\sigma_{WH}/\sigma_{\mathrm{ggF}}$	$0.01^{+0.04}_{-0.04}$ $\left(^{+0.03}_{-0.02}\right)$	$^{+0.04}_{-0.03}$ $\left(^{+0.03}_{-0.02}\right)$	$^{+0.02}_{-0.02}$ $\left(^{+0.01}_{-0.01}\right)$	$^{+0.01}_{-0.01}$ $\left(^{+0.01}_{-0.01}\right)$	$^{+0.00}_{-0.00}$ $\left(^{+0.00}_{-0.00}\right)$
$\sigma_{ZH}/\sigma_{\mathrm{ggF}}$	$0.13^{+0.08}_{-0.05}$ $\left(^{+0.02}_{-0.01}\right)$	$^{+0.06}_{-0.05}$ $\left(^{+0.02}_{-0.01}\right)$	$^{+0.04}_{-0.02}$ $\left(^{+0.01}_{-0.00}\right)$	$^{+0.02}_{-0.01}$ $\left(^{+0.01}_{-0.00}\right)$	$^{+0.01}_{-0.01}$ $\left(^{+0.00}_{-0.00}\right)$
$\sigma_{ttH}/\sigma_{\mathrm{ggF}}$	$0.034^{+0.016}_{-0.012}$ $\left(^{+0.007}_{-0.005}\right)$	$^{+0.012}_{-0.010}$ $\left(^{+0.005}_{-0.004}\right)$	$^{+0.009}_{-0.005}$ $\left(^{+0.003}_{-0.002}\right)$	$^{+0.005}_{-0.004}$ $\left(^{+0.003}_{-0.003}\right)$	$^{+0.003}_{-0.001}$ $\left(^{+0.001}_{-0.000}\right)$
$\mathrm{BR}^{WW}/\mathrm{BR}^{ZZ}$	$7.2^{+2.9}_{-2.1}$ $\left(^{+3.2}_{-2.2}\right)$	$^{+2.6}_{-1.8}$ $\left(^{+2.9}_{-2.0}\right)$	$^{+1.0}_{-0.7}$ $\left(^{+1.1}_{-0.8}\right)$	$^{+0.7}_{-0.5}$ $\left(^{+0.7}_{-0.5}\right)$	$^{+0.4}_{-0.3}$ $\left(^{+0.5}_{-0.4}\right)$
$\mathrm{BR}^{\gamma\gamma}/\mathrm{BR}^{ZZ}$	$0.079^{+0.033}_{-0.023}$ $\left(^{+0.035}_{-0.025}\right)$	$^{+0.032}_{-0.023}$ $\left(^{+0.034}_{-0.024}\right)$	$^{+0.008}_{-0.005}$ $\left(^{+0.007}_{-0.004}\right)$	$^{+0.003}_{-0.002}$ $\left(^{+0.002}_{-0.001}\right)$	$^{+0.004}_{-0.003}$ $\left(^{+0.004}_{-0.003}\right)$
$\mathrm{BR}^{\tau\tau}/\mathrm{BR}^{ZZ}$	$1.6^{+0.9}_{-0.6}$ $\left(^{+1.2}_{-0.9}\right)$	$^{+0.8}_{-0.5}$ $\left(^{+1.0}_{-0.7}\right)$	$^{+0.4}_{-0.3}$ $\left(^{+0.7}_{-0.4}\right)$	$^{+0.1}_{-0.0}$ $\left(^{+0.0}_{-0.0}\right)$	$^{+0.1}_{-0.0}$ $\left(^{+0.1}_{-0.1}\right)$
$\mathrm{BR}^{bb}/\mathrm{BR}^{ZZ}$	$3.7^{+4.1}_{-2.4}$ $\left(^{+29.4}_{-11.9}\right)$	$^{+3.1}_{-1.9}$ $\left(^{+23.4}_{-10.4}\right)$	$^{+1.9}_{-1.4}$ $\left(^{+12.6}_{-3.8}\right)$	$^{+1.9}_{-0.6}$ $\left(^{+12.2}_{-4.4}\right)$	$^{+0.4}_{-0.1}$ $\left(^{+2.6}_{-0.9}\right)$

Table 18: Best-fit values of $\sigma(gg \to H \to WW)$, $\sigma_i/\sigma_{\text{ggF}}$ and BR^f/BR^{WW} from the combined analysis of the $\sqrt{s}$ = 7 and 8 TeV data. The cross-section ratios are given for $\sqrt{s}$ = 8 TeV, assuming the SM values for $\sigma_i(7\ \text{TeV})/\sigma_i(8\ \text{TeV})$. The results are shown for the ATLAS+CMS combination and also separately for each experiment, together with their total uncertainties and their breakdown into the four components described in the text. The expected total uncertainties on the measurements are also shown (in parentheses). The SM predictions [27] are also shown with their total uncertainties.

Parameter	SM prediction	ATLAS+CMS Best-fit value	ATLAS+CMS Uncertainty Stat	ATLAS+CMS Uncertainty Expt	ATLAS+CMS Uncertainty Thbgd	ATLAS+CMS Uncertainty Thsig
$\sigma(gg \to H \to WW)$ (pb)	4.15 ±0.47	$3.97^{+0.63}_{-0.60}$ $\left(^{+0.65}_{-0.62}\right)$	$^{+0.46}_{-0.45}$ $\left(^{+0.47}_{-0.46}\right)$	$^{+0.32}_{-0.29}$ $\left(^{+0.33}_{-0.30}\right)$	$^{+0.24}_{-0.23}$ $\left(^{+0.26}_{-0.25}\right)$	$^{+0.16}_{-0.12}$ $\left(^{+0.16}_{-0.12}\right)$
$\sigma_{\text{VBF}}/\sigma_{\text{ggF}}$	0.082 ±0.009	$0.11^{+0.03}_{-0.03}$ $\left(^{+0.03}_{-0.02}\right)$	$^{+0.03}_{-0.02}$ $\left(^{+0.02}_{-0.02}\right)$	$^{+0.01}_{-0.01}$ $\left(^{+0.01}_{-0.01}\right)$	$^{+0.01}_{-0.00}$ $\left(^{+0.01}_{-0.00}\right)$	$^{+0.01}_{-0.01}$ $\left(^{+0.01}_{-0.01}\right)$
$\sigma_{WH}/\sigma_{\text{ggF}}$	0.037 ±0.004	$0.03^{+0.03}_{-0.03}$ $\left(^{+0.02}_{-0.02}\right)$	$^{+0.02}_{-0.02}$ $\left(^{+0.02}_{-0.02}\right)$	$^{+0.01}_{-0.01}$ $\left(^{+0.01}_{-0.01}\right)$	$^{+0.01}_{-0.01}$ $\left(^{+0.01}_{-0.00}\right)$	$^{+0.00}_{-0.00}$ $\left(^{+0.00}_{-0.00}\right)$
$\sigma_{ZH}/\sigma_{\text{ggF}}$	0.022 ±0.002	$0.07^{+0.04}_{-0.03}$ $\left(^{+0.02}_{-0.01}\right)$	$^{+0.03}_{-0.03}$ $\left(^{+0.01}_{-0.01}\right)$	$^{+0.02}_{-0.01}$ $\left(^{+0.01}_{-0.00}\right)$	$^{+0.01}_{-0.01}$ $\left(^{+0.01}_{-0.00}\right)$	$^{+0.01}_{-0.00}$ $\left(^{+0.00}_{-0.00}\right)$
$\sigma_{ttH}/\sigma_{\text{ggF}}$	0.0067 ±0.0010	$0.022^{+0.007}_{-0.006}$ $\left(^{+0.004}_{-0.004}\right)$	$^{+0.005}_{-0.005}$ $\left(^{+0.003}_{-0.003}\right)$	$^{+0.003}_{-0.003}$ $\left(^{+0.002}_{-0.001}\right)$	$^{+0.002}_{-0.002}$ $\left(^{+0.002}_{-0.002}\right)$	$^{+0.001}_{-0.001}$ $\left(^{+0.000}_{-0.000}\right)$
$\text{BR}^{ZZ}/\text{BR}^{WW}$	0.124 ± < 0.001	$0.148^{+0.036}_{-0.030}$ $\left(^{+0.033}_{-0.027}\right)$	$^{+0.032}_{-0.027}$ $\left(^{+0.029}_{-0.025}\right)$	$^{+0.013}_{-0.009}$ $\left(^{+0.011}_{-0.007}\right)$	$^{+0.009}_{-0.006}$ $\left(^{+0.009}_{-0.006}\right)$	$^{+0.006}_{-0.004}$ $\left(^{+0.005}_{-0.003}\right)$
$\text{BR}^{\gamma\gamma}/\text{BR}^{WW}$	0.0106 ±0.0001	$0.0103^{+0.0023}_{-0.0019}$ $\left(^{+0.0025}_{-0.0021}\right)$	$^{+0.0020}_{-0.0018}$ $\left(^{+0.0021}_{-0.0019}\right)$	$^{+0.0009}_{-0.0006}$ $\left(^{+0.0009}_{-0.0006}\right)$	$^{+0.0006}_{-0.0004}$ $\left(^{+0.0007}_{-0.0005}\right)$	$^{+0.0005}_{-0.0003}$ $\left(^{+0.0005}_{-0.0003}\right)$
$\text{BR}^{\tau\tau}/\text{BR}^{WW}$	0.292 ±0.006	$0.263^{+0.079}_{-0.064}$ $\left(^{+0.094}_{-0.076}\right)$	$^{+0.062}_{-0.053}$ $\left(^{+0.071}_{-0.061}\right)$	$^{+0.045}_{-0.034}$ $\left(^{+0.057}_{-0.043}\right)$	$^{+0.016}_{-0.010}$ $\left(^{+0.019}_{-0.012}\right)$	$^{+0.011}_{-0.007}$ $\left(^{+0.015}_{-0.009}\right)$
$\text{BR}^{bb}/\text{BR}^{WW}$	2.66 ±0.12	$0.62^{+0.66}_{-0.39}$ $\left(^{+2.01}_{-1.08}\right)$	$^{+0.40}_{-0.29}$ $\left(^{+1.63}_{-0.93}\right)$	$^{+0.37}_{-0.17}$ $\left(^{+0.78}_{-0.36}\right)$	$^{+0.37}_{-0.19}$ $\left(^{+0.84}_{-0.42}\right)$	$^{+0.05}_{-0.03}$ $\left(^{+0.22}_{-0.10}\right)$

Parameter	ATLAS Best-fit value	ATLAS Uncertainty Stat	ATLAS Uncertainty Expt	ATLAS Uncertainty Thbgd	ATLAS Uncertainty Thsig
$\sigma(gg \to H \to WW)$ (pb)	$4.96^{+0.96}_{-0.90}$ $\left(^{+0.94}_{-0.88}\right)$	$^{+0.73}_{-0.71}$ $\left(^{+0.73}_{-0.70}\right)$	$^{+0.43}_{-0.39}$ $\left(^{+0.41}_{-0.36}\right)$	$^{+0.37}_{-0.35}$ $\left(^{+0.39}_{-0.36}\right)$	$^{+0.24}_{-0.18}$ $\left(^{+0.21}_{-0.14}\right)$
$\sigma_{\text{VBF}}/\sigma_{\text{ggF}}$	$0.08^{+0.03}_{-0.03}$ $\left(^{+0.04}_{-0.03}\right)$	$^{+0.03}_{-0.02}$ $\left(^{+0.04}_{-0.03}\right)$	$^{+0.01}_{-0.01}$ $\left(^{+0.02}_{-0.01}\right)$	$^{+0.01}_{-0.00}$ $\left(^{+0.01}_{-0.01}\right)$	$^{+0.01}_{-0.01}$ $\left(^{+0.01}_{-0.01}\right)$
$\sigma_{WH}/\sigma_{\text{ggF}}$	$0.05^{+0.04}_{-0.03}$ $\left(^{+0.03}_{-0.02}\right)$	$^{+0.03}_{-0.02}$ $\left(^{+0.03}_{-0.02}\right)$	$^{+0.01}_{-0.01}$ $\left(^{+0.01}_{-0.01}\right)$	$^{+0.01}_{-0.01}$ $\left(^{+0.01}_{-0.01}\right)$	$^{+0.01}_{-0.00}$ $\left(^{+0.00}_{-0.00}\right)$
$\sigma_{ZH}/\sigma_{\text{ggF}}$	$0.01^{+0.03}_{-0.02}$ $\left(^{+0.03}_{-0.01}\right)$	$^{+0.02}_{-0.01}$ $\left(^{+0.02}_{-0.01}\right)$	$^{+0.01}_{-0.00}$ $\left(^{+0.01}_{-0.00}\right)$	$^{+0.01}_{-0.00}$ $\left(^{+0.01}_{-0.00}\right)$	$^{+0.00}_{-0.00}$ $\left(^{+0.00}_{-0.00}\right)$
$\sigma_{ttH}/\sigma_{\text{ggF}}$	$0.013^{+0.007}_{-0.005}$ $\left(^{+0.006}_{-0.005}\right)$	$^{+0.005}_{-0.004}$ $\left(^{+0.005}_{-0.004}\right)$	$^{+0.003}_{-0.002}$ $\left(^{+0.003}_{-0.002}\right)$	$^{+0.002}_{-0.002}$ $\left(^{+0.003}_{-0.002}\right)$	$^{+0.001}_{-0.001}$ $\left(^{+0.001}_{-0.000}\right)$
$\text{BR}^{ZZ}/\text{BR}^{WW}$	$0.154^{+0.050}_{-0.039}$ $\left(^{+0.050}_{-0.037}\right)$	$^{+0.045}_{-0.036}$ $\left(^{+0.045}_{-0.036}\right)$	$^{+0.016}_{-0.010}$ $\left(^{+0.015}_{-0.008}\right)$	$^{+0.014}_{-0.008}$ $\left(^{+0.014}_{-0.008}\right)$	$^{+0.007}_{-0.005}$ $\left(^{+0.006}_{-0.004}\right)$
$\text{BR}^{\gamma\gamma}/\text{BR}^{WW}$	$0.0097^{+0.0031}_{-0.0025}$ $\left(^{+0.0037}_{-0.0029}\right)$	$^{+0.0026}_{-0.0023}$ $\left(^{+0.0032}_{-0.0027}\right)$	$^{+0.0013}_{-0.0008}$ $\left(^{+0.0014}_{-0.0008}\right)$	$^{+0.0008}_{-0.0005}$ $\left(^{+0.0011}_{-0.0006}\right)$	$^{+0.0006}_{-0.0004}$ $\left(^{+0.0007}_{-0.0005}\right)$
$\text{BR}^{\tau\tau}/\text{BR}^{WW}$	$0.336^{+0.141}_{-0.105}$ $\left(^{+0.153}_{-0.109}\right)$	$^{+0.108}_{-0.086}$ $\left(^{+0.118}_{-0.090}\right)$	$^{+0.082}_{-0.056}$ $\left(^{+0.087}_{-0.057}\right)$	$^{+0.030}_{-0.017}$ $\left(^{+0.032}_{-0.017}\right)$	$^{+0.028}_{-0.015}$ $\left(^{+0.029}_{-0.014}\right)$
$\text{BR}^{bb}/\text{BR}^{WW}$	$1.48^{+1.54}_{-0.89}$ $\left(^{+3.49}_{-1.38}\right)$	$^{+1.06}_{-0.66}$ $\left(^{+2.83}_{-1.20}\right)$	$^{+0.72}_{-0.40}$ $\left(^{+1.36}_{-0.42}\right)$	$^{+0.81}_{-0.43}$ $\left(^{+1.45}_{-0.52}\right)$	$^{+0.20}_{-0.09}$ $\left(^{+0.45}_{-0.14}\right)$

Parameter	CMS Best-fit value	CMS Uncertainty Stat	CMS Uncertainty Expt	CMS Uncertainty Thbgd	CMS Uncertainty Thsig
$\sigma(gg \to H \to WW)$ (pb)	$3.15^{+0.83}_{-0.76}$ $\left(^{+0.92}_{-0.85}\right)$	$^{+0.60}_{-0.58}$ $\left(^{+0.63}_{-0.62}\right)$	$^{+0.45}_{-0.39}$ $\left(^{+0.51}_{-0.45}\right)$	$^{+0.30}_{-0.28}$ $\left(^{+0.36}_{-0.33}\right)$	$^{+0.19}_{-0.13}$ $\left(^{+0.24}_{-0.18}\right)$
$\sigma_{\text{VBF}}/\sigma_{\text{ggF}}$	$0.14^{+0.07}_{-0.05}$ $\left(^{+0.04}_{-0.03}\right)$	$^{+0.06}_{-0.05}$ $\left(^{+0.04}_{-0.03}\right)$	$^{+0.03}_{-0.02}$ $\left(^{+0.02}_{-0.01}\right)$	$^{+0.01}_{-0.01}$ $\left(^{+0.01}_{-0.00}\right)$	$^{+0.02}_{-0.01}$ $\left(^{+0.01}_{-0.01}\right)$
$\sigma_{WH}/\sigma_{\text{ggF}}$	$0.01^{+0.04}_{-0.04}$ $\left(^{+0.03}_{-0.02}\right)$	$^{+0.04}_{-0.03}$ $\left(^{+0.03}_{-0.02}\right)$	$^{+0.02}_{-0.02}$ $\left(^{+0.01}_{-0.01}\right)$	$^{+0.01}_{-0.01}$ $\left(^{+0.01}_{-0.01}\right)$	$^{+0.00}_{-0.00}$ $\left(^{+0.00}_{-0.00}\right)$
$\sigma_{ZH}/\sigma_{\text{ggF}}$	$0.13^{+0.08}_{-0.05}$ $\left(^{+0.02}_{-0.01}\right)$	$^{+0.06}_{-0.05}$ $\left(^{+0.02}_{-0.01}\right)$	$^{+0.04}_{-0.02}$ $\left(^{+0.01}_{-0.00}\right)$	$^{+0.02}_{-0.01}$ $\left(^{+0.01}_{-0.00}\right)$	$^{+0.01}_{-0.00}$ $\left(^{+0.00}_{-0.00}\right)$
$\sigma_{ttH}/\sigma_{\text{ggF}}$	$0.034^{+0.016}_{-0.012}$ $\left(^{+0.007}_{-0.005}\right)$	$^{+0.012}_{-0.010}$ $\left(^{+0.005}_{-0.004}\right)$	$^{+0.009}_{-0.005}$ $\left(^{+0.003}_{-0.002}\right)$	$^{+0.005}_{-0.004}$ $\left(^{+0.003}_{-0.003}\right)$	$^{+0.003}_{-0.001}$ $\left(^{+0.001}_{-0.000}\right)$
$\text{BR}^{ZZ}/\text{BR}^{WW}$	$0.140^{+0.057}_{-0.041}$ $\left(^{+0.048}_{-0.036}\right)$	$^{+0.049}_{-0.038}$ $\left(^{+0.042}_{-0.033}\right)$	$^{+0.023}_{-0.012}$ $\left(^{+0.019}_{-0.010}\right)$	$^{+0.016}_{-0.008}$ $\left(^{+0.013}_{-0.007}\right)$	$^{+0.009}_{-0.006}$ $\left(^{+0.009}_{-0.005}\right)$
$\text{BR}^{\gamma\gamma}/\text{BR}^{WW}$	$0.0111^{+0.0040}_{-0.0029}$ $\left(^{+0.0036}_{-0.0027}\right)$	$^{+0.0033}_{-0.0027}$ $\left(^{+0.0030}_{-0.0025}\right)$	$^{+0.0018}_{-0.0010}$ $\left(^{+0.0015}_{-0.0008}\right)$	$^{+0.0011}_{-0.0006}$ $\left(^{+0.0010}_{-0.0005}\right)$	$^{+0.0006}_{-0.0004}$ $\left(^{+0.0007}_{-0.0005}\right)$
$\text{BR}^{\tau\tau}/\text{BR}^{WW}$	$0.219^{+0.115}_{-0.081}$ $\left(^{+0.132}_{-0.100}\right)$	$^{+0.090}_{-0.070}$ $\left(^{+0.095}_{-0.080}\right)$	$^{+0.066}_{-0.039}$ $\left(^{+0.084}_{-0.058}\right)$	$^{+0.024}_{-0.011}$ $\left(^{+0.029}_{-0.014}\right)$	$^{+0.012}_{-0.006}$ $\left(^{+0.020}_{-0.011}\right)$
$\text{BR}^{bb}/\text{BR}^{WW}$	$0.52^{+0.54}_{-0.34}$ $\left(^{+3.56}_{-1.46}\right)$	$^{+0.39}_{-0.27}$ $\left(^{+2.78}_{-1.25}\right)$	$^{+0.25}_{-0.15}$ $\left(^{+1.57}_{-0.49}\right)$	$^{+0.27}_{-0.14}$ $\left(^{+1.55}_{-0.58}\right)$	$^{+0.04}_{-0.01}$ $\left(^{+0.26}_{-0.10}\right)$

Table 19: Best-fit values of $\kappa_{gZ} = \kappa_{g} \cdot \kappa_{Z}/\kappa_{H}$ and of the ratios of coupling modifiers, as defined in the most generic model described in the context of the κ framework, from the combined analysis of the $\sqrt{s} = 7$ and 8 TeV data. The results are shown for the ATLAS+CMS combination and also separately for each experiment, together with their total uncertainties and their breakdown into the four components described in the text. The total uncertainties on λ_{WZ} and λ_{tg}, for which a negative solution is allowed, are calculated around the overall best-fit value, while the uncertainty breakdown is performed in the positive range. The full ATLAS+CMS 68% CL limits are $\lambda_{tg} = [-2.00, -1.55] \cup [1.47, 2.08]$ and $\lambda_{WZ} = [-0.97, -0.82] \cup [0.80, 0.98]$.

Parameter	Best-fit	Uncertainty				Best-fit	Uncertainty				Best-fit	Uncertainty			
	value	Stat	Expt	Thbgd	Thsig	value	Stat	Expt	Thbgd	Thsig	value	Stat	Expt	Thbgd	Thsig
	ATLAS+CMS					ATLAS					CMS				
$\kappa_{gZ} = \kappa_g \cdot \kappa_Z/\kappa_H$	$1.10^{+0.11}_{-0.11}$ $\left(^{+0.11}_{-0.11}\right)$	$^{+0.09}_{-0.09}$ $\left(^{+0.09}_{-0.09}\right)$	$^{+0.03}_{-0.02}$ $\left(^{+0.02}_{-0.02}\right)$	$^{+0.01}_{-0.01}$ $\left(^{+0.01}_{-0.01}\right)$	$^{+0.06}_{-0.05}$ $\left(^{+0.06}_{-0.05}\right)$	$1.20^{+0.16}_{-0.15}$ $\left(^{+0.16}_{-0.15}\right)$	$^{+0.14}_{-0.14}$ $\left(^{+0.14}_{-0.13}\right)$	$^{+0.01}_{-0.02}$ $\left(^{+0.03}_{-0.03}\right)$	$^{+0.02}_{-0.02}$ $\left(^{+0.02}_{-0.02}\right)$	$^{+0.07}_{-0.06}$ $\left(^{+0.06}_{-0.05}\right)$	$0.99^{+0.14}_{-0.13}$ $\left(^{+0.15}_{-0.14}\right)$	$^{+0.12}_{-0.12}$ $\left(^{+0.13}_{-0.12}\right)$	$^{+0.04}_{-0.03}$ $\left(^{+0.03}_{-0.03}\right)$	$^{+0.01}_{-0.01}$ $\left(^{+0.01}_{-0.01}\right)$	$^{+0.06}_{-0.05}$ $\left(^{+0.06}_{-0.05}\right)$
$\lambda_{Zg} = \kappa_Z/\kappa_g$	$1.26^{+0.23}_{-0.19}$ $\left(^{+0.20}_{-0.17}\right)$	$^{+0.18}_{-0.16}$ $\left(^{+0.15}_{-0.14}\right)$	$^{+0.09}_{-0.07}$ $\left(^{+0.08}_{-0.06}\right)$	$^{+0.06}_{-0.05}$ $\left(^{+0.05}_{-0.04}\right)$	$^{+0.09}_{-0.08}$ $\left(^{+0.08}_{-0.07}\right)$	$1.06^{+0.26}_{-0.21}$ $\left(^{+0.28}_{-0.23}\right)$	$^{+0.21}_{-0.18}$ $\left(^{+0.23}_{-0.20}\right)$	$^{+0.08}_{-0.06}$ $\left(^{+0.10}_{-0.07}\right)$	$^{+0.08}_{-0.06}$ $\left(^{+0.09}_{-0.06}\right)$	$^{+0.09}_{-0.07}$ $\left(^{+0.09}_{-0.07}\right)$	$1.47^{+0.44}_{-0.34}$ $\left(^{+0.27}_{-0.23}\right)$	$^{+0.34}_{-0.28}$ $\left(^{+0.22}_{-0.19}\right)$	$^{+0.22}_{-0.14}$ $\left(^{+0.12}_{-0.09}\right)$	$^{+0.13}_{-0.08}$ $\left(^{+0.07}_{-0.05}\right)$	$^{+0.13}_{-0.10}$ $\left(^{+0.09}_{-0.07}\right)$
$\lambda_{tg} = \kappa_t/\kappa_g$	$1.76^{+0.32}_{-0.29}$ $\left(^{+0.29}_{-0.39}\right)$	$^{+0.21}_{-0.20}$ $\left(^{+0.20}_{-0.21}\right)$	$^{+0.12}_{-0.11}$ $\left(^{+0.11}_{-0.12}\right)$	$^{+0.09}_{-0.09}$ $\left(^{+0.14}_{-0.19}\right)$	$^{+0.18}_{-0.13}$ $\left(^{+0.11}_{-0.08}\right)$	$1.39^{+0.34}_{-0.33}$ $\left(^{+0.38}_{-0.54}\right)$	$^{+0.25}_{-0.24}$ $\left(^{+0.28}_{-0.28}\right)$	$^{+0.12}_{-0.13}$ $\left(^{+0.14}_{-0.19}\right)$	$^{+0.12}_{-0.14}$ $\left(^{+0.18}_{-0.26}\right)$	$^{+0.15}_{-0.10}$ $\left(^{+0.12}_{-0.07}\right)$	$-2.25^{+0.51}_{-0.55}$ $\left(^{+0.42}_{-0.64}\right)$	$^{+0.39}_{-0.36}$ $\left(^{+0.31}_{-0.33}\right)$	$^{+0.26}_{-0.19}$ $\left(^{+0.16}_{-0.21}\right)$	$^{+0.15}_{-0.14}$ $\left(^{+0.21}_{-0.40}\right)$	$^{+0.25}_{-0.18}$ $\left(^{+0.13}_{-0.07}\right)$
$\lambda_{WZ} = \kappa_W/\kappa_Z$	$0.89^{+0.10}_{-0.09}$ $\left(^{+0.12}_{-0.10}\right)$	$^{+0.09}_{-0.08}$ $\left(^{+0.11}_{-0.09}\right)$	$^{+0.03}_{-0.03}$ $\left(^{+0.04}_{-0.03}\right)$	$^{+0.02}_{-0.02}$ $\left(^{+0.03}_{-0.03}\right)$	$^{+0.02}_{-0.01}$ $\left(^{+0.02}_{-0.01}\right)$	$0.92^{+0.14}_{-0.12}$ $\left(^{+0.18}_{-0.15}\right)$	$^{+0.13}_{-0.11}$ $\left(^{+0.16}_{-0.13}\right)$	$^{+0.03}_{-0.03}$ $\left(^{+0.05}_{-0.04}\right)$	$^{+0.03}_{-0.03}$ $\left(^{+0.04}_{-0.04}\right)$	$^{+0.02}_{-0.02}$ $\left(^{+0.02}_{-0.02}\right)$	$-0.85^{+0.13}_{-0.15}$ $\left(^{+0.17}_{-0.14}\right)$	$^{+0.13}_{-0.11}$ $\left(^{+0.15}_{-0.13}\right)$	$^{+0.05}_{-0.05}$ $\left(^{+0.06}_{-0.05}\right)$	$^{+0.04}_{-0.03}$ $\left(^{+0.03}_{-0.03}\right)$	$^{+0.02}_{-0.02}$ $\left(^{+0.03}_{-0.02}\right)$
$\lambda_{\gamma Z} = \kappa_\gamma/\kappa_Z$	$0.89^{+0.11}_{-0.10}$ $\left(^{+0.13}_{-0.12}\right)$	$^{+0.11}_{-0.09}$ $\left(^{+0.13}_{-0.11}\right)$	$^{+0.03}_{-0.02}$ $\left(^{+0.03}_{-0.02}\right)$	$^{+0.01}_{-0.01}$ $\left(^{+0.02}_{-0.01}\right)$	$^{+0.02}_{-0.02}$ $\left(^{+0.02}_{-0.02}\right)$	$0.88^{+0.16}_{-0.14}$ $\left(^{+0.20}_{-0.17}\right)$	$^{+0.15}_{-0.13}$ $\left(^{+0.19}_{-0.17}\right)$	$^{+0.03}_{-0.03}$ $\left(^{+0.05}_{-0.04}\right)$	$^{+0.02}_{-0.02}$ $\left(^{+0.03}_{-0.02}\right)$	$^{+0.02}_{-0.02}$ $\left(^{+0.02}_{-0.02}\right)$	$0.91^{+0.17}_{-0.14}$ $\left(^{+0.18}_{-0.16}\right)$	$^{+0.16}_{-0.13}$ $\left(^{+0.17}_{-0.15}\right)$	$^{+0.04}_{-0.03}$ $\left(^{+0.04}_{-0.03}\right)$	$^{+0.02}_{-0.02}$ $\left(^{+0.01}_{-0.01}\right)$	$^{+0.02}_{-0.02}$ $\left(^{+0.03}_{-0.02}\right)$
$\lambda_{\tau Z} = \kappa_\tau/\kappa_Z$	$0.85^{+0.14}_{-0.12}$ $\left(^{+0.17}_{-0.15}\right)$	$^{+0.12}_{-0.10}$ $\left(^{+0.14}_{-0.13}\right)$	$^{+0.07}_{-0.06}$ $\left(^{+0.09}_{-0.08}\right)$	$^{+0.02}_{-0.02}$ $\left(^{+0.02}_{-0.02}\right)$	$^{+0.02}_{-0.02}$ $\left(^{+0.03}_{-0.02}\right)$	$0.97^{+0.22}_{-0.18}$ $\left(^{+0.27}_{-0.23}\right)$	$^{+0.18}_{-0.15}$ $\left(^{+0.23}_{-0.19}\right)$	$^{+0.09}_{-0.08}$ $\left(^{+0.13}_{-0.11}\right)$	$^{+0.04}_{-0.03}$ $\left(^{+0.04}_{-0.03}\right)$	$^{+0.03}_{-0.02}$ $\left(^{+0.04}_{-0.02}\right)$	$0.78^{+0.20}_{-0.17}$ $\left(^{+0.23}_{-0.20}\right)$	$^{+0.16}_{-0.15}$ $\left(^{+0.19}_{-0.17}\right)$	$^{+0.10}_{-0.08}$ $\left(^{+0.12}_{-0.11}\right)$	$^{+0.02}_{-0.02}$ $\left(^{+0.02}_{-0.01}\right)$	$^{+0.02}_{-0.02}$ $\left(^{+0.03}_{-0.02}\right)$
$\lambda_{bZ} = \kappa_b/\kappa_Z$	$0.56^{+0.18}_{-0.18}$ $\left(^{+0.25}_{-0.22}\right)$	$^{+0.12}_{-0.11}$ $\left(^{+0.21}_{-0.18}\right)$	$^{+0.07}_{-0.07}$ $\left(^{+0.09}_{-0.08}\right)$	$^{+0.07}_{-0.08}$ $\left(^{+0.08}_{-0.07}\right)$	$^{+0.03}_{-0.02}$ $\left(^{+0.06}_{-0.04}\right)$	$0.61^{+0.24}_{-0.24}$ $\left(^{+0.36}_{-0.29}\right)$	$^{+0.20}_{-0.18}$ $\left(^{+0.31}_{-0.24}\right)$	$^{+0.09}_{-0.10}$ $\left(^{+0.13}_{-0.10}\right)$	$^{+0.10}_{-0.11}$ $\left(^{+0.11}_{-0.09}\right)$	$^{+0.04}_{-0.02}$ $\left(^{+0.08}_{-0.05}\right)$	$0.47^{+0.26}_{-0.17}$ $\left(^{+0.38}_{-0.37}\right)$	$^{+0.17}_{-0.15}$ $\left(^{+0.32}_{-0.25}\right)$	$^{+0.09}_{-0.09}$ $\left(^{+0.15}_{-0.12}\right)$	$^{+0.11}_{-0.13}$ $\left(^{+0.11}_{-0.11}\right)$	$^{+0.04}_{-0.03}$ $\left(^{+0.08}_{-0.05}\right)$

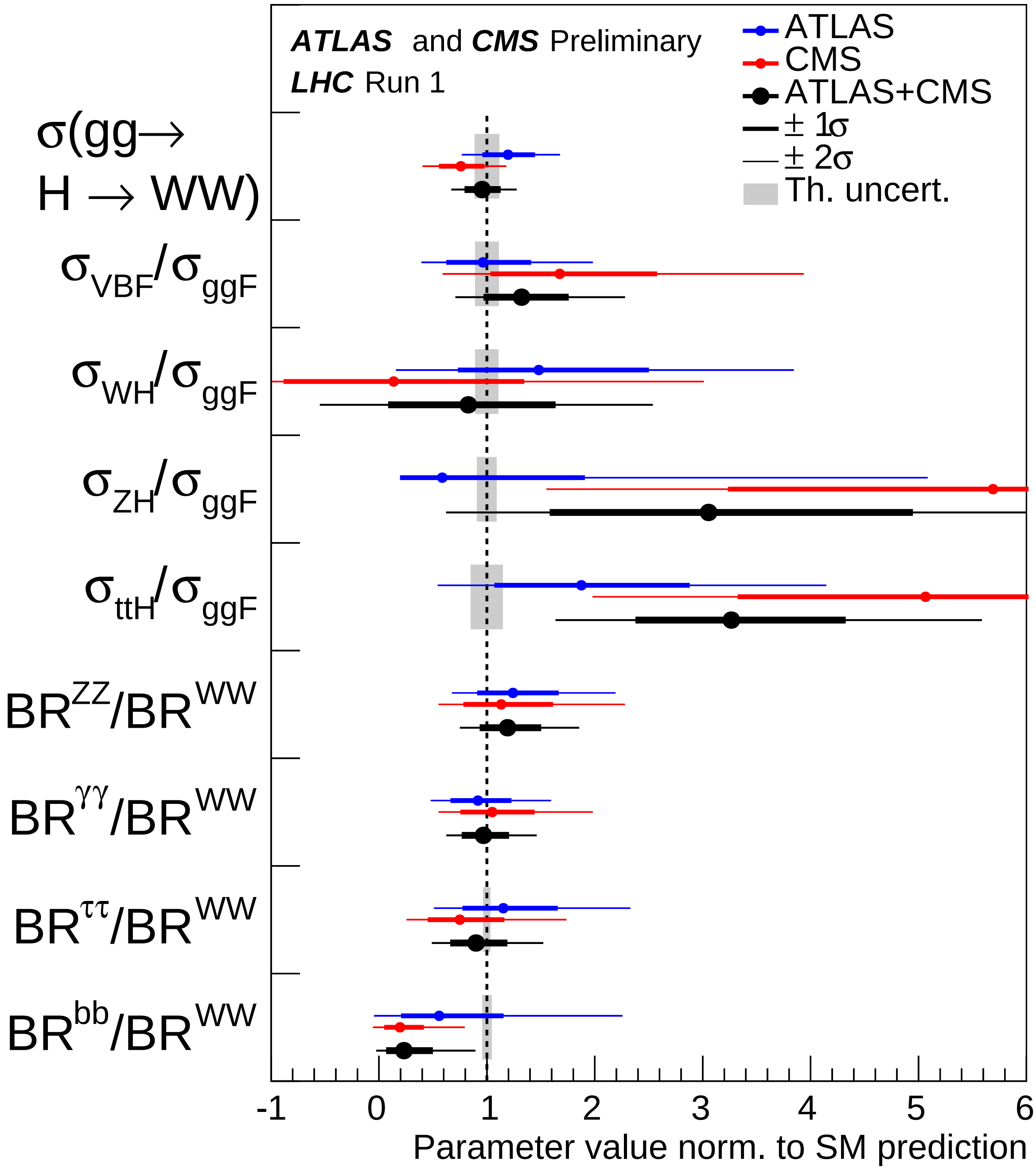

Figure 26: Best-fit values of the $\sigma(gg \to H \to WW)$ cross section and of ratios of cross sections and branching ratios, as obtained from the generic parameterisation described in Section 4.1 and as tabulated in Table 18 for the combination of ATLAS and CMS measurements. Also shown for completeness are the results for each experiment. The error bars indicate the 1σ (thick lines) and 2σ (thin lines) intervals. In this figure, the fit results are normalised to the SM predictions for the various parameters and the shaded bands indicate the theory uncertainties on these predictions.

B. Reduced coupling modifiers

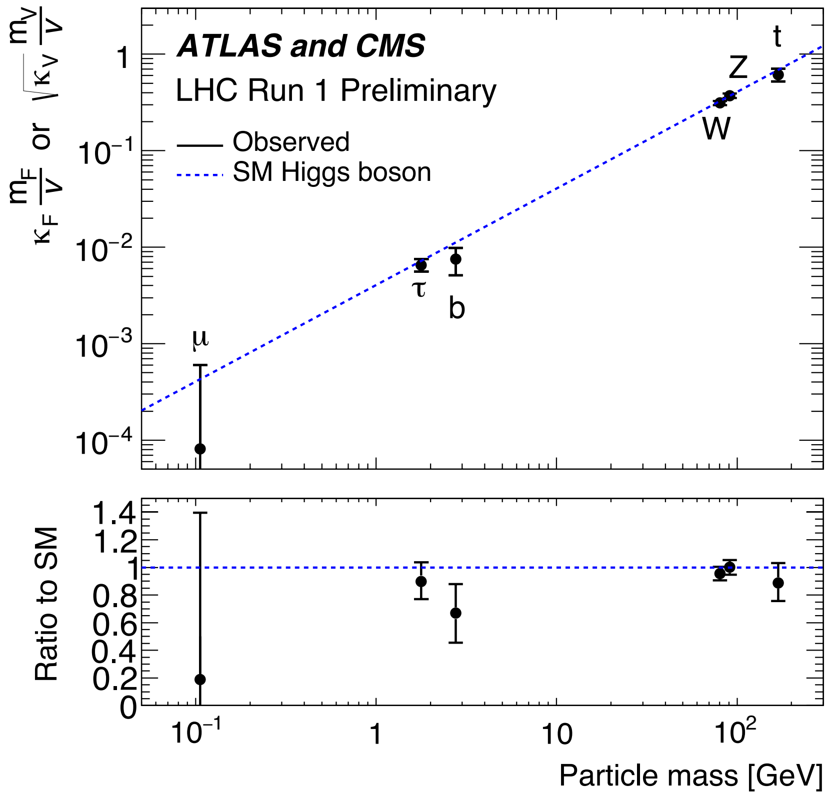

Figure 27: Fit results for the combination of ATLAS and CMS in the case of the parameterisation with reduced coupling modifiers $y_{V,i} = \sqrt{\kappa_{V,i} \frac{g_{V,i}}{2v}} = \sqrt{\kappa_{V,i}} \frac{m_{V,i}}{v}$ for the weak vector bosons, and $y_{F,i} = \kappa_{F,i} \frac{g_{F,i}}{\sqrt{2}} = \kappa_{F,i} \frac{m_{F,i}}{v}$ for the fermions, as a function of the particle mass. The dashed line indicates the predicted dependence on the particle mass for the SM Higgs boson. The bottom panel shows the ratios of the reduced coupling modifiers to the SM predictions with their total uncertainties as a function of the particle mass.

C. Boson- and fermion-mediated production processes

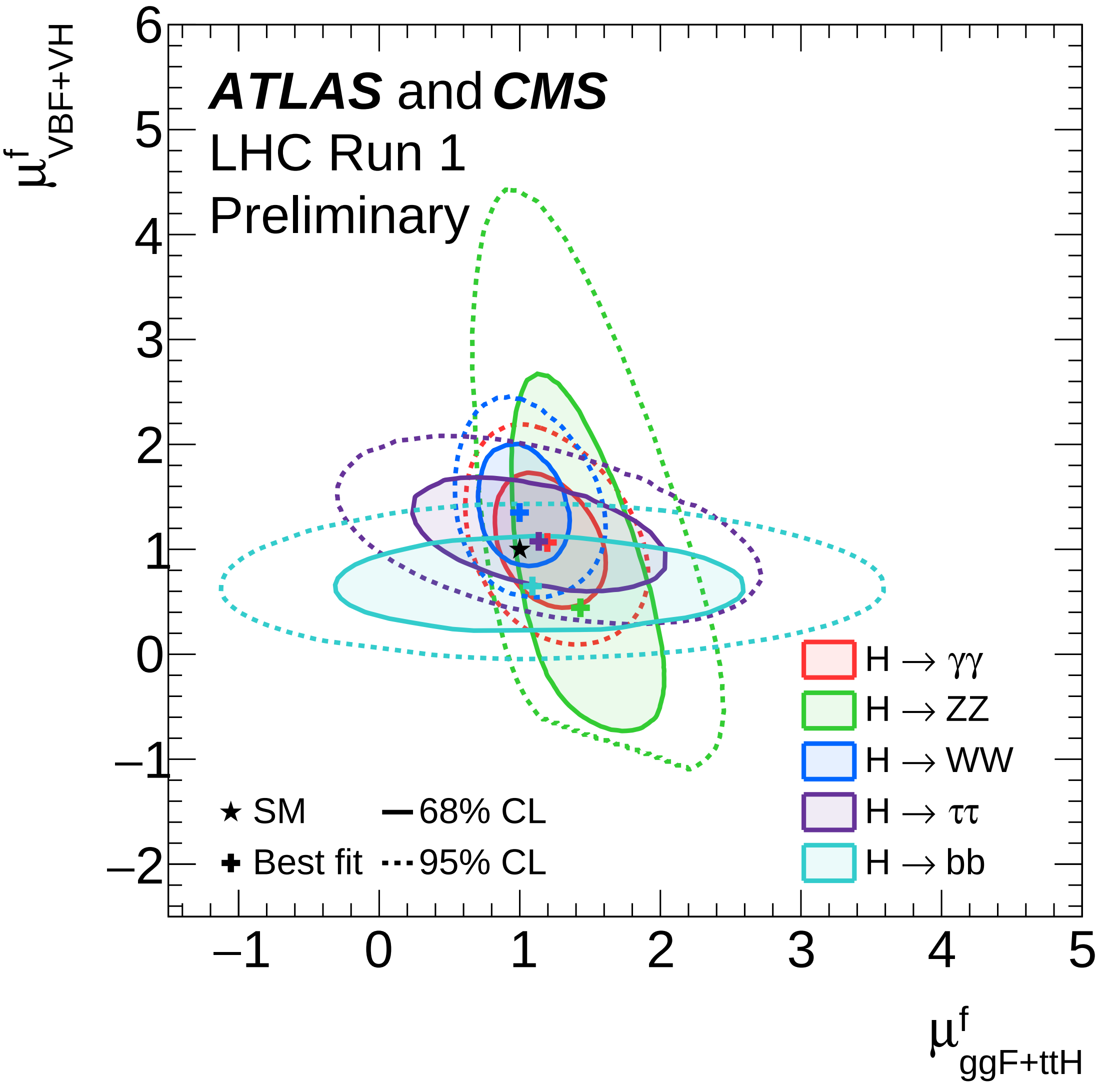

Figure 28: Likelihood contours in the ($\mu^f_{ggF+ttH}$, μ^f_{VBF+VH}) plane for the ATLAS+CMS combination, shown for the five decay channels, $H \to ZZ$, $H \to WW$, $H \to \gamma\gamma$, $H \to \tau\tau$, and $H \to bb$. The results are shown as 68% (full) and 95% (dashed) CL contours, together with the best-fit values to the data and the SM expectation.

D. Compatibility of combined fit results with SM

Table 20: Compatibility with the SM prediction of fit results as a whole under the asymptotic approximation. For each model, the unconditional best-fit is compared with the conditional fit where all parameters are set to their SM values. The conversion from $-2 \ln \Lambda$ to the quoted p-value is performed assuming a two-sided distribution with the specified number of degrees of freedom (DoF). Note that the quoted p-values are partially correlated between the different models.

Model	p-value	DoF	Parameters
Global signal strength	34%	1	μ
Production processes	24%	5	μ_{ggF}, μ_{VBF}, μ_{WH}, μ_{ZH}, μ_{ttH}
Decay modes	60%	5	$\mu^{\gamma\gamma}$, μ^{ZZ}, μ^{WW}, $\mu^{\tau\tau}$, $\mu^{b\bar{b}}$
μ_V and μ_F per decay	88%	10	$\mu_V^{\gamma\gamma}$, μ_V^{ZZ}, μ_V^{WW}, $\mu_V^{\tau\tau}$, $\mu_V^{b\bar{b}}$, $\mu_F^{\gamma\gamma}$, μ_F^{ZZ}, μ_F^{WW}, $\mu_F^{\tau\tau}$, $\mu_F^{b\bar{b}}$
μ_V/μ_F ratio	72%	6	μ_V/μ_F, $\mu_F^{\gamma\gamma}$, μ_F^{ZZ}, μ_F^{WW}, $\mu_F^{\tau\tau}$, $\mu_F^{b\bar{b}}$
Ratios of σ and BR relative to $\sigma(gg \to H \to ZZ)$	16%	9	$\sigma(gg \to H \to ZZ)$, $\sigma_{\text{VBF}}/\sigma_{\text{ggF}}$, $\sigma_{WH}/\sigma_{\text{ggF}}$, $\sigma_{ZH}/\sigma_{\text{ggF}}$, $\sigma_{ttH}/\sigma_{\text{ggF}}$, $\text{BR}^{WW}/\text{BR}^{ZZ}$, $\text{BR}^{\gamma\gamma}/\text{BR}^{ZZ}$, $\text{BR}^{\tau\tau}/\text{BR}^{ZZ}$, $\text{BR}^{b\bar{b}}/\text{BR}^{ZZ}$
Ratios of σ and BR relative to $\sigma(gg \to H \to WW)$	16%	9	$\sigma(gg \to H \to WW)$, $\sigma_{\text{VBF}}/\sigma_{\text{ggF}}$, $\sigma_{WH}/\sigma_{\text{ggF}}$, $\sigma_{ZH}/\sigma_{\text{ggF}}$, $\sigma_{ttH}/\sigma_{\text{ggF}}$, $\text{BR}^{ZZ}/\text{BR}^{WW}$, $\text{BR}^{\gamma\gamma}/\text{BR}^{WW}$, $\text{BR}^{\tau\tau}/\text{BR}^{WW}$, $\text{BR}^{b\bar{b}}/\text{BR}^{WW}$
Coupling ratios	13%	7	κ_{gZ}, λ_{Zg}, λ_{tg}, λ_{WZ}, $\lambda_{\gamma Z}$, $\lambda_{\tau Z}$, λ_{bZ}
Couplings, SM loops	65%	6	κ_Z, κ_W, κ_t, κ_τ, κ_b, κ_μ
Couplings, BSM loops	11%	7	κ_Z, κ_W, κ_t, κ_τ, κ_b, κ_g, κ_γ
BSM loops only	82%	2	κ_g, κ_γ
Up vs down couplings	67%	3	λ_{du}, λ_{Vu}, κ_{uu}
Lepton vs quark couplings	78%	3	λ_{lq}, λ_{Vq}, κ_{qq}
Fermion and vector couplings	59%	2	κ_V, κ_F